Numerical and experimental research of wave interaction with a porous breakwater

Master Thesis
A basis for numerical modelling of the notional permeability P

by
Bart Mellink
(1230166)

Section of Enviromental Fluid Mechanics
Faculty of civil engineering and geosciences
TU Delft
2012

Numerical and experimental research of wave interaction with a porous breakwater

MSC THESIS
A basis for numerical modelling of the notional permeability P

by
Bart Mellink
(1230166)

Master of Science Thesis,
Delft, November 2012

Graduation Comittee:

Prof. dr. ir. W.S.J. Uijttewaal	Environmental Fluid Mechanics
ir. J. van den Bos	Hydraulic Engineering
ir. B van den Berg	Hydraulic Engineering
dr. ir. M. Zijlema	Environmental Fluid Mechanics

Faculty of Civil Engineering and Geosciences
TU Delft
2012

Preface

This research was carried out in order to obtain the degree of Master of Science at Delft University of Technology. The experimental research took place at the Environmental Mechanics Fluid Laboratory of the Faculty of Civil Engineering .
My master thesis was very varied, it consisted out of experimental research, analytical research and numerical research. It was a great challenge to explore a road which has never been explored before and combine a wide set of skills obtained during my study.
First of all I wish to thank my graduation committee for their supervision and guidance during my master thesis. I am grateful for the advices and supervision from Jeroen van den Bos, Wim Uijttewaal, Bert van den Berg and Marcel Zijlema. I am very grateful that Marcel van Gent helped me sorting out the reasons behind the numerical results. Furthermore I wish to thank the lab personnel for helping me with my work in the laboratory. Sander de Vree helped me a great deal with setting up the experiment and assisting me with analysing my data. Hans Tas and Jaap van Duin supported me with all kinds of practical issues. I also wish to thank Pieter Smit for his help with my boundary conditions in SWASH and Ikha Magdalena and Guglielmo Stecca for helping me discovering Latex.

Finally, I wish to thank my family for their support throughout my entire study.

Bart Mellink

Delft, November 2012

Abstract

The design formula for rubble mound breakwaters by Van der Meer has an unclear Notional Permeability term. This term causes a lot of confusion for designers. In the past many people have tried to derive a better formulation for that term by experimental and analytical research. The goal of this study is to obtain a better formulation along a numerical way. This study explores the numerical possibilities and tries to define which direction has to be taken in future research.

A very simplified case is taken with a vertical homogeneous breakwater (blocks) which interact with monochromatic waves. In total six different blocks are made of epoxy and elastocoast. Only 4 out of the 6 blocks were tested. It is possible to derive the porous fluid constants of the blocks experimentally such that it can be used for computations.

These tests have been done in the large flume of the Environmental Fluid Mechanics Laboratory of the TU Delft. Two types of data were collected: pore pressures and water levels in front and behind the block. The water levels seemed to be the most reliable data. The main deficit of the setup was the wave absorber at the end of the flume. The wave absorber is not able to sufficiently absorb long waves. So the dataset had to be corrected for that effect. Eventually a dataset is created which is in line with earlier experiments.

Results were compared with an analytical solution and the numerical SWASH model. Comparisons with the analytical solution showed a reasonable fit without any calibration. The SWASH model showed in first instance large deviations with the experimental dataset, after calibrating the turbulent flow resistance (β), it was possible to generate a decent fit.The reason behind the need for an increased β is not clear. The used β constants are 6-10 times higher than the measured β constants. The most likely explanation is an error in the transition between the water and the porous medium. During the experiment discontinuities can occur on this border while SWASH uses an continuity requirement.

Numerical tests were performed on some multi-layered combinations of the different blocks in order to derive an "Vertical P" value in a similar way as Van der Meer prescribes. The results showed, nevertheless, quite some different patterns as the computations done by Van der Meer. However, the method shows the possibility of numerically calculating a notional permeability.

Keywords: *partial reflection and transmission, porous flow, notional permeability, Van der Meer formula, SWASH model.*

Contents

List of Figures

List of Symbols

α	Laminar friction constant (-)
α_R	Slope of the breakwater (-)
β	Stationary turbulent friction constant (-)
β_{NS}	Nonstationary turbulent friction constant (-)
Δ	Relative density (-)
δ	Damping coefficient in pore attenuation formula(-)
η	Instantaneous water level (m)
γ	Non dimensional constant for nonstationary forchheimer formula(-)
$\hat{U}$	Amplitude of velocity (m/s)
λ	Scaling factor (-)
ν	Kinematic Viscosity, taken as 1.1×10^{-6} (m^2/s)
ω	Radian frequency (1/s)
ρ_w	Density of water (kg/m^3)
$\vec{G}$	Gravitation Vector (g_x, g_y, g_z) (m/s^2)
$\vec{u}$	Velocity vector(u,v,w) (m/s)
ξ	Irribarren number (-)
a	Dimensional coefficient in Forchheimer equation (s/m)
a_δ	Constant for damping coefficient (-)
A_c	Non-dimensional number for acceleration for a porous medium (-)
b	Dimensional coefficient in Forchheimer equation (s^2/m^2)
c	Dimensional coefficient in Forchheimer equation (s^2/m)
c	Wave celerity (m/s)
C_m	Added Mass coefficient (-)

d_p	Pore size (m)
d_{n50}	Median nominal stone diameter (m)
f	Non-dimensional friction factor to account for porous resistance (-)
f_l	Laminar friction term for porous flow (m/s^2)
f_t	Turbulent friction term for porous flow (m/s^2)
g	Gravitational constant (m/s^2)
h	Instantaneous water depth (m)
H_s	Significant Wave Height (m)
H_{inc}	Incoming wave height (m)
H_{ref}	Reflected wave height (m)
I	Pressure gradient (-)
k	Darcy's Permeability Constant (s/m)
k'	Porous wave number (1/m)
KC	Keuler-Carpenter Number (-)
L	Wave length (m)
l	Length of porous structure (m)
L'	Porous wave length (m)
N	Number of waves during storm (-)
n	Porosity (-)
P	Notional Permeability (-)
p	Pressure (N/m^2)
$p_{0,max}$	Maximal reference pressure (N/m^2)
p_{atm}	Atmospherical pressure (N/m^2)
R	Reflection Coefficient(-)
R_H	Healy Reflection Coefficient(-)
Re_d	Reynolds number related to grain size (-)
Re_p	Reynolds number related to pore size (-)
S	Damage factor (-)
S_f	Non-dimensional Factor to account for unsteady motion (-)

s_p	Wave steepness (-)
T	Transmission Coefficient(-)
T_p	Peak period (s)
u	Velocity in x-direction (m/s)
u_f	Filter velocity (m/s)
u_{char}	Characteristic filter velocity averaged over time space (m/s)
v	Velocity in y-direction (m/s)
V_p	Total volume of pores in a sample (m^3)
V_t	Total volume of sample (m^3)
w	Velocity in z-direction (m/s)

Chapter 1

Introduction

This study is done in order to improve design formula's for rubble mound breakwaters. These are used worldwide in order to protect vessels and facilities inside ports, protect beaches against erosion or anything else which needs protection against wave action. Figure 1.1 shows an example of how a small harbour can be protected by breakwaters. Breakwaters can be made in many different ways but this study will focus on the rubble mound breakwaters. Rubble mound breakwaters typically consists of large amounts of gravel, quarry run or large concrete blocks. An essential question when designing such a structure is which stone is heavy enough in order to keep the damage level within tolerable amounts with an expected wave climate. That this question is not always fully answered can be seen in Figure 1.2.

Figure 1.1: Breakwater protecting small harbor, Capri Harbor, Italy

The general layout of a rubble mound breakwater is a multi-layered structure. The outside is an armour layer which consists of large rocks, followed by a filter layer and thereafter the structures core material. The layers are designed in order to create granular filters and prevent the washing out of smaller material. These structures need to survive high peak pressures during wave action.

Figure 1.2: Example of damaged breakwater, Asparuhovo breakwater, Bulgaria

All design formula's developed by researchers approached the design problem by making scale models in order to find empirical relationships between stability of the stones and all influential parameters.

1.1 Problem Description

The design of rubble mound breakwaters is mostly done by two types of formulas, the formulas of Van der Meer (1988) and the Hudson formula. This study will focus on the Van der Meer formulas. The advantage of the Van der Meer formula is that it covers more terms (wave period, damage level, notional permeability and storm duration) and can predict the required stone size more accurate for different situations than the Hudson formula. It must be noted that the breaker type determines the kind of formula that is required. The breaker type is defined by the Irribarren number:

$$\xi = \frac{\tan\alpha}{\sqrt{\frac{H}{L_0}}} \tag{1.1}$$

where α is the slope of the bathymetry and L_0 is the deep water wave length. The Van der Meer formula is developed by doing large series of scale tests and empirically derived relationships between stability and hydraulic conditions. The empirical character of the formulas can easily be recognized by the usage of powers of P like 0.13 and 0.18. The Van der Meer formula depends on the Irribarren number:
For plunging breakers ($\xi = 0.5 - 1.5$):

$$\frac{H_{sc}}{\Delta d_{n50}} = 6.2P^{0.18}\left(\frac{S}{\sqrt{N}}\right)^{0.2}\xi^{-0.5} \tag{1.2}$$

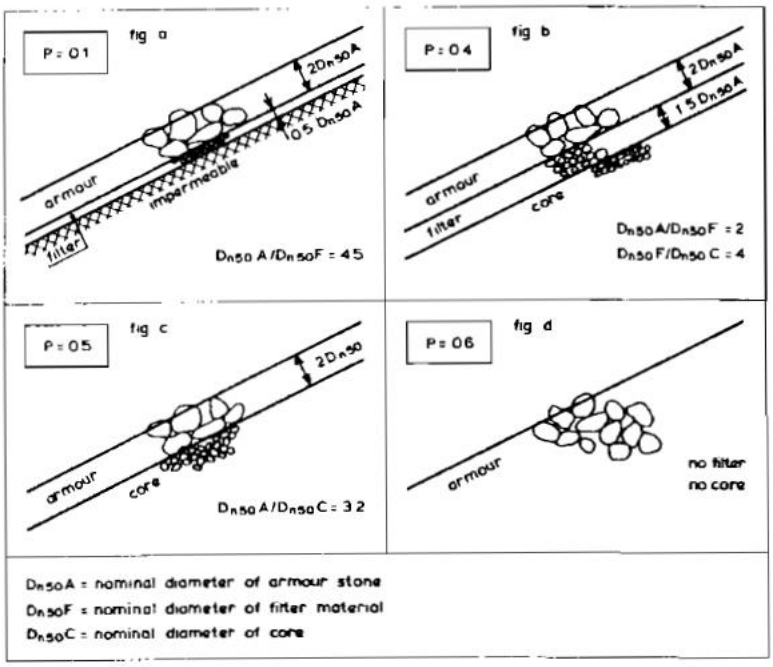

Figure 1.3: Various P factors for different structures according to Van der Meer (1988)

For surging breakers ($\xi = 5$):

$$\frac{H_{sc}}{\Delta d_{n50}} = 1.0P^{-0.13}\left(\frac{S}{\sqrt{N}}\right)^{0.2}\xi^{P}\sqrt{\cot\alpha_R} \tag{1.3}$$

where P is the notional permeability, S is a damage factor, ξ is the Irribarren number, H_{sc} is the significant wave height, δ is the relative density, d_{n50} is the median nominal stone diameter and N is the number of waves during a storm. The permeability of a structure depends on the build up and influences the amount of dissipation and the pressure build up. The formula of Van der Meer (Equations 1.2 and 1.3) has a notional permeability term P which is related to the build up of the structure as shown in Figure 1.3. It is defined as a non-dimensional constant which should give the notional permeability of a structure on a scale from P=0.1 (Impermeable core) till P=0.6 (Homogeneous Structure). The task of a designer is to compare the drawn structure with the sketches from Figure 1.3. This results in a lot of uncertainty for structures which do not match any of the pictures drawn. Another point of criticism is the limited physical and theoretical background for the P factor.

This has led to two directions of research in the past in order to find a more convenient description of the P term. Kik (2011) and Kluwen (2012) tested different configurations of structures and tried to derive empirically additional P values. Jumelet (2010) made a mathematical model where the notional permeability was linked with the amount of run-up on the structure. This model was experimentally tested by van Broekhoven (2011). One of his conclusions of the experimental research to proof this relation was that there was no link between run-up and permeability. The present research is done to explore a

third method for determining the notional permeability, a numerical method.

Van der Meer (1988) describes a method to determine the P factor numerically. In order to do this he describes the dissipation which is defined as the amount of water entering the core of the structure during one wave cycle per meter width. This dissipation is characteristic for the notional permeability. The dissipation for a homogenous structure (P=0.6) is then seen as maximum and the relative dissipation in comparison with that maximum is introduced.

The relative dissipation for different wave conditions and different structures (P=0.6, P=0.5 and P=0.1) can be numerically computed. This results in a graph like Figure 1.4. By calculating the relative dissipation of the structure with an unknown P factor and comparing the results with the created graph a P factor can be determined. As such it should be possible to numerically determine the P value.

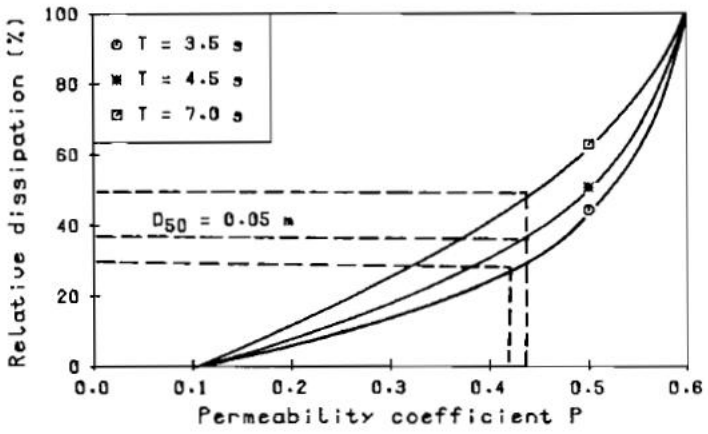

Figure 1.4: Numerical method for determining P factor, Van der Meer (1988)

However, there is one problem: How to calculate the relative dissipation? A numerical method is needed that is capable of simulating the wave interaction with a porous structure like a breakwater. This study will investigate if it is possible by means of a numerical method, to calculate the relative dissipation into the core for a given structure. The numerical packages available are already capable of calculating with porosity, however the main question is how accurate they are and how valid the used theory is of these packages.

1.2 Goal Description

The general goal is to make a numerical model which is capable of predicting hydraulic conditions in a breakwater structure. The hypothesis is that the P factor from the Van der Meer formula can possibly be determined more accurately if we are able to numerically compute correctly the wave interaction with different porosities.

In order to get that knowledge several steps have to be taken:

- Test and validate a model which can predict porous flow in a very simplified breakwater structure.
- Test and validate the model for more complex structures (different slopes, different layers, irregular waves)
- Test and validate the model to be able to determine P values. Possibly compare results with full scale breakwater measurements.

The goal of this study is to reach the first step. With the help of known theoretical relationships a numerical model needs to be validated which is capable of predicting the hydraulic conditions for a simplified structure.

1.3 Research Question

The main research question is:

Is it possible to numerically simulate the wave interaction with a simplified setup of a breakwater?

In addition there are also some sub questions:

- *Looking at the options of pressure sensors and wave gauges for collecting data from the experiment, what is the most reliable method for validating a numerical model?*
- *Are classical theoretical relationships valid to describe porous flow for this case?*
- *Does this method have potential to grow into a stability predicting model?*

1.4 Research Scope

To answer these questions a simplified test case will be used which is simple enough to compare on a 1:1 scale experimental, mathematical and numerical data. This simplified test case is sketched in Figure 1.5.

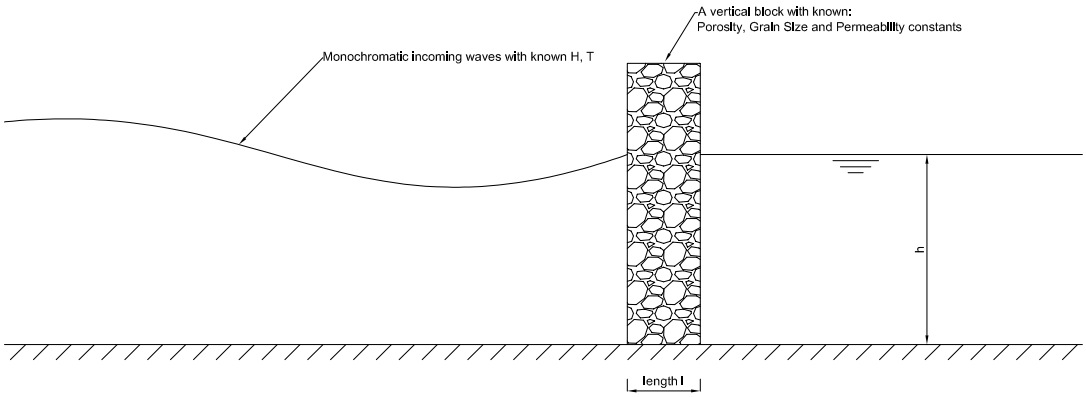

Figure 1.5: Sketch of the simplified test case

This study investigates the interaction of monochromatic waves with a homogeneous porous structure with a vertical interface. This will simplify the modelling since it allows a clear separation between a porous domain and a non-porous domain. Also the up- and downrush and the resulting in- and outflow into the structure will be less complex. The differences between a real breakwater and the proposed model are described in Table 1.1.

Real life breakwater	**Simplified Test case**
Irregular waves with a spectrum and random direction	Normal incident monochromatic waves
Up- and downrush onto breakwater face	Vertical up- and downrush
Transport of water through the front face of breakwater and infiltration from runup	Only water transport through front face of breakwater
Turbulent non steady flow through the porous breakwater	No difference
Air entrainment	No Air entrainment
Complex geometry of the breakwater (different porous layers, berms)	Vertical breakwater with homogeneous porous structure.
Very large scale with high Reynolds numbers	Laboratory scale with significant lower Reynolds numbers.

Table 1.1: Differences between full scale breakwater and the case investigated in this research

The test case is experimentally tested in the Environmental Fluid Mechanics Laboratory of the TU Delft for different wave cases and for four different type of blocks. The blocks differ in both grain size and length. The blocks are made out of stones glued together with elastocoast and epoxy in order to guarantee the exact same porous structure for every single test. One of the advantages of these types of block is that it is possible to determine all the porous characteristics needed for all calculations.

As described earlier the goal is to:

- understand the behaviour of this test case
- use it to calibrate and validate a numerical model in comparison with experimental data
- investigate whether such a model has predictive capabilities

The numerical Part is done with the SWASH model which is recently extended into covering porous flow. In order to test the numerical outcome a third comparison is made with an analytical solution.

The report starts with a literature review in Chapter 2. In Chapter 3 the experimental setup is explained in detail. Chapter 4 discusses the experimental results and Chapter 5 compares the experimental results with an analytical solution. In Chapter 6 the numerical simulations with the SWASH model are discussed. Chapter 7 consists out of the conclusions and recommendations.

Chapter 2

Literature Review

This chapter describes the literature relevant for this study. Fluid dynamics can roughly be divided into a non-porous section which is described in Section 2.1 and a porous section which is described in Section 2.2. The remainder of this chapter describes how the test case can be solved mathematically (Section 2.3) as well as methods to scale the test cases (Section 2.4). Section 2.5 goes briefly through some statistical methods, while Section 2.6 discusses an earlier case with a similar setup.

2.1 Fluid Mechanics

Fluid dynamics describe fluid motion based on the conservation laws of momentum and mass. By analysing the mass balance over an infinitely small cubic element the continuity equation for an incompressible fluid can be derived:

$$\nabla \cdot \vec{u} = 0 \tag{2.1}$$

With $\vec{u}$ the flow velocity in x,y and z direction. Doing a similar analysis for the momentum balance results in the Navier-Stokes equation:

$$\frac{D\vec{u}}{Dt} = -\frac{1}{\rho_w}\nabla p + \nu\nabla^2\vec{u} + \vec{G} \tag{2.2}$$

The left hand side is the total derivative of the velocity vector $\vec{u}$. The first term on the right hand side represents the pressure gradient, while the second term represents the viscous stresses and the third term represents the gravitational vector. The Coriolis force is neglected.

One of the main problems of solving the Navier-Stokes equations is that the computational power of modern computers is not capable of directly solving the equations in a reasonable time. So in order to solve problems, assumptions and simplifications have to be made. In the next section some of the derivations and assumptions are explained. In order to understand the behaviour of different solution methods it is crucial to understand which simplifications are made.

2.1.1 Hydrostatic Shallow Water Equations

The derivation for the Shallow Water Equations is based on the method described by Vreugdenhil (1994). Only difference is the viscous stress terms in Equation 2.2 are left out in this case. This is legitimate since the experimental setup deals with very turbulent flows with high Reynolds numbers. Also a constant density, salinity and atmospheric pressure is assumed. This creates the Euler equation:

$$\frac{D\vec{u}}{Dt} = -\frac{1}{\rho_w}\nabla p + \vec{G} \tag{2.3}$$

Written out in three directions in Cartesian coordinates:

$$\frac{\partial u}{\partial x} + \frac{\partial v}{\partial y} + \frac{\partial w}{\partial z} = 0 \tag{2.4}$$

$$\frac{\partial u}{\partial t} + u\frac{\partial u}{\partial x} + v\frac{\partial u}{\partial y} + w\frac{\partial u}{\partial z} = -\frac{1}{\rho_w}\frac{\partial p}{\partial x} \tag{2.5}$$

$$\frac{\partial v}{\partial t} + u\frac{\partial v}{\partial x} + v\frac{\partial v}{\partial y} + w\frac{\partial v}{\partial z} = -\frac{1}{\rho_w}\frac{\partial p}{\partial y} \tag{2.6}$$

$$\frac{\partial w}{\partial t} + u\frac{\partial w}{\partial x} + v\frac{\partial w}{\partial y} + w\frac{\partial w}{\partial z} = -\frac{1}{\rho_w}\frac{\partial p}{\partial z} - g \tag{2.7}$$

In Figure 2.1 the free surface η and the flat bottom d are defined. The depth is defined as $h = \eta - z_b$.

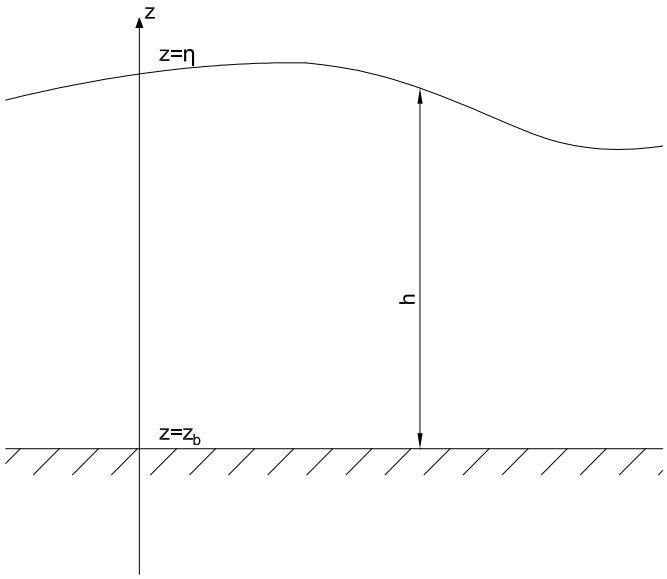

Figure 2.1: Definition bottom and free surface

These four PDE's can be solved with the help of dynamic and kinematic boundary conditions. First of all water can not go through the bottom or exit the free surface. This results in two kinematic boundary conditions:

$$w = 0 \text{ at } \mathrm{z} = \mathrm{z_b} \tag{2.8}$$

$$\frac{\partial \eta}{\partial t} + u\frac{\partial \eta}{\partial x} + v\frac{\partial \eta}{\partial y} - w = 0 \text{ at } \mathrm{z} = \eta \tag{2.9}$$

At the bottom there is a "no slip" condition stating the velocity is 0. Also the free surface has the requirement of having the atmospheric pressure. This results in two dynamic boundary conditions:

$$u = v = 0 \text{ at } \mathrm{z} = \mathrm{z_b} \tag{2.10}$$

$$p = p_{atm} \text{ at } \mathrm{z} = \eta \tag{2.11}$$

The most important assumption of the shallow water equations is that horizontal scales are significantly larger than vertical scales. Horizontal scales are in the order of the wave length, while vertical scales are in the order of the water depth. As a consequence $\frac{\partial w}{\partial x}$ and $\frac{\partial w}{\partial y}$ are small. Assuming that all vertical accelerations are small compared to the gravitational acceleration, Equation 2.7 can be rewritten as:

$$\frac{\partial p}{\partial z} = -\rho_w g \tag{2.12}$$

Using the dynamic boundary condition of the free surface (Equation 2.11) the pressure distribution can be integrated over the depth. This results in a hydrostatic vertical pressure distribution. The pressure can be written as a function of the depth:

$$p = \rho_w g\,(\eta - z) + p_{atm} \tag{2.13}$$

Then, by assuming that all pressures are hydrostatic, the pressure gradients in Equations 2.6 and 2.7 could be written as:

$$\frac{\partial p}{\partial x} = \rho_w g \frac{\partial \eta}{\partial x} \tag{2.14}$$

$$\frac{\partial p}{\partial y} = \rho_w g \frac{\partial \eta}{\partial y} \tag{2.15}$$

Substituting these Equations into Equation 2.5 and 2.6 leads to the three dimensional shallow water equations in combination with Equation 2.4:

$$\frac{\partial u}{\partial t} + u\frac{\partial u}{\partial x} + v\frac{\partial u}{\partial y} + w\frac{\partial u}{\partial z} = -g\frac{\partial \eta}{\partial x} \tag{2.16}$$

$$\frac{\partial v}{\partial t} + u\frac{\partial v}{\partial x} + v\frac{\partial v}{\partial y} + w\frac{\partial v}{\partial z} = -g\frac{\partial \eta}{\partial y} \tag{2.17}$$

The two dimensional shallow water equations are obtained by integrating the equations over the depth. This results in the shallow water equations with the depth averaged velocities $\bar{u}$ and $\bar{v}$.

$$\frac{\partial \eta}{\partial t} + \frac{\partial h\bar{u}}{\partial x} + \frac{\partial h\bar{v}}{\partial y} = 0 \tag{2.18}$$

$$\frac{\partial \bar{u}}{\partial t} + \bar{u}\frac{\partial \bar{u}}{\partial x} + \bar{v}\frac{\partial \bar{u}}{\partial y} = -g\frac{\partial \eta}{\partial x} \tag{2.19}$$

$$\frac{\partial \bar{v}}{\partial t} + \bar{u}\frac{\partial \bar{v}}{\partial x} + \bar{v}\frac{\partial \bar{v}}{\partial y} = -g\frac{\partial \eta}{\partial y} \tag{2.20}$$

In addition, these equations can be simplified by writing them only for the longitudinal direction and by neglecting all terms in y direction. Also, for very small waves, the advection term ($\bar{u}\frac{\partial \bar{u}}{\partial x}$) could be neglected. This results in the long wave theory which is applied in the analytical model described in Chapter 5

$$\frac{\partial \eta}{\partial t} + h\frac{\partial \bar{u}}{\partial x} = 0 \tag{2.21}$$

$$\frac{\partial \bar{u}}{\partial t} + g\frac{\partial \eta}{\partial x} = 0 \tag{2.22}$$

2.1.2 Non-Hydrostatic Shallow Water Equations

For short waves the hydrostatic theory is not valid. The derivation is based on Stelling and Zijlema (2003) and Zijlema et al. (2011). The non-hydrostatic equations are similar to the hydrostatic equations with the difference of adding a non-hydrostatic term q to the pressure distribution of Equation 2.13. The pressure can be divided in a hydrostatic part and a non-hydrostatic part, by assuming zero atmospheric pressure this leads to:

$$p = g(\eta - z) + q = p_h + q \tag{2.23}$$

Adding the extra term to Equations 2.16 and 2.17 leads to the following equations.

$$\frac{\partial u}{\partial t} + u\frac{\partial u}{\partial x} + v\frac{\partial u}{\partial y} + w\frac{\partial u}{\partial z} = -g\frac{\partial \eta}{\partial x} - \frac{\partial q}{\partial x} \tag{2.24}$$

$$\frac{\partial v}{\partial t} + u\frac{\partial v}{\partial x} + v\frac{\partial v}{\partial y} + w\frac{\partial v}{\partial z} = -g\frac{\partial \eta}{\partial y} - \frac{\partial q}{\partial y} \tag{2.25}$$

Integrating these equations similar as done with Equations 2.18, 2.19 and 2.20 results in the non-hydrostatic 2D shallow water equations:

$$\frac{\partial \eta}{\partial t} + \frac{\partial h\bar{u}}{\partial x} + \frac{\partial h\bar{v}}{\partial y} = 0 \tag{2.26}$$

$$\frac{\partial \bar{u}}{\partial t} + \bar{u}\frac{\partial \bar{u}}{\partial x} + \bar{v}\frac{\partial \bar{u}}{\partial y} = -g\frac{\partial \eta}{\partial x} - \frac{1}{h}\int_{z_b}^{\eta}\frac{\partial q}{\partial x}\mathrm{d}z \tag{2.27}$$

$$\frac{\partial \bar{v}}{\partial t} + \bar{u}\frac{\partial \bar{v}}{\partial x} + \bar{v}\frac{\partial \bar{v}}{\partial y} = -g\frac{\partial \eta}{\partial y} - \frac{1}{h}\int_{z_b}^{\eta}\frac{\partial q}{\partial y}\mathrm{d}z \tag{2.28}$$

These equations are used by the SWASH model in Chapter 6. SWASH has additional friction and viscous stress terms.

2.2 Porous flow

The main difference between free surface flow and porous flow is the presence of grains and voids. The effect of grains on the flow could be described as a resistance to the flow that dissipates energy. The complex structure of pores and voids make that not every individual flow pattern can be solved. In order to describe the porous flow, the filter velocity is introduced. This is the actual pore velocity averaged over the pores. It is defined as:

$$u_f = nu \left(n = \frac{V_p}{V_t} \right) \tag{2.29}$$

Here u is given by the actual velocity in the pores and u_f is the velocity averaged over the pores. V_p is the pore volume and V_t is the total volume of the sample. In the beginning most research in porous flow has been done to find relations for groundwater flow. Darcy solved flow problems in a homogenous porous medium for laminar groundwater flow. He discovered a linear relationship between the filter velocity and the pressure gradient:

$$u_f = kI \tag{2.30}$$

k is here a permeability constant and I is given by:

$$I = -\frac{1}{\rho_w g}\frac{\partial p}{\partial x} \tag{2.31}$$

Forchheimer (1901) added a quadratic term to the Darcy law and proposed the following formula:

$$I = au_f + bu_f|u_f| \tag{2.32}$$

In the Forchheimer equation the pressure gradient has a linear and a non-linear term. The linear term is associated with the laminar flow part and the non-linear term with the turbulent part of the flow. The porous flow characteristics depend on the Reynolds number related to the pore sizes d_p and pore velocities u.

$$Re_p = \frac{ud_p}{\nu} \tag{2.33}$$

Dybbs and Edwards (1984) described different flow regimes depending on the Re_p number based on experimental results. They stated that:

"(I) The Darcy or creeping flow regime where the flow is dominated by viscous forces and the exact nature of the velocity distribution is determined by local geometry. This type of flow occurs at $Re_p < 1$. At $Re_p \approx 1$, boundary layers begin to develop near the solid boundaries of the pores."

"(II) The inertial flow regime. This initiates at Re_p between 1 and 10 where the boundary layers become more pronounced and an inertial core appears. The developing of these core flows outside the boundary layers is the reason for the non-linear relationship between pressure drop and flow rate. As the Reynolds number increases the core flows enlarge in size and their influence becomes more and more significant on the overall flow picture.

This steady non-linear laminar flow regime persists to a $Re_p \approx 150$."

"(III) An unsteady laminar flow regime in the Reynolds number range of 150 to 300. At a $Re_p \approx 150$, the first evidence of unsteady flow is observed in the form of laminar wake oscillations in the pores. These oscillations take the form of travelling waves characterised by distinct periods, amplitudes and growth rates. In this flow regime, these oscillations exhibit preferred frequencies that seem to correspond to specific growth rates. Vortices form at $Re_p \gg 250$ and persist to $Re_p \approx 300$."

"(IV) A highly unsteady and chaotic flow regime for $Re_p > 300$, qualitatively resembling turbulent flow."

In literature the different flow regimes are generally described as:

1. The Darcy flow regime
2. The Forchheimer flow regime
3. Transitional flow regime
4. The fully turbulent flow regime

Due to the differences in the different flow regimes there are also different constants in the Forchheimer formula. Note that for the fully turbulent flow (IV) the first term has no physical meaning and is purely used for curve fitting.

Type	**Name**	$\boldsymbol{Re_p}$	**Formula**
(I)	Darcy flow regime	$\mathrm{Re}_p <$ 1-10	$I = au_f$
(II)	The Forchheimer flow regime	1-10 $< \mathrm{Re}_p <$ 150	$I = au_f + bu_f^2$
(IV)	Fully turbulent flow	300 $< \mathrm{Re}_p$	$I = (au_f) + bu_f^2$

Table 2.1: Classification of different porous flow regimes

The Reynolds number based on pore sizes is different than the Reynolds number based on grain size. The Reynolds number used in the rest of the document is:

$$Re_d = \frac{u_f d_{n50}}{\nu} \tag{2.34}$$

Bakker (1989) described how the Reynolds number based on grain sizes is roughly 1.5 times as large as the Re_p since the filter velocity is 0.3-0.4 times the pore velocity and the grain diameter is 4 a 5 times the pore diameter. The Reynolds numbers in real life breakwaters are in the order of 10^6 in the armour layer. In laboratories it is impossible to reach these magnitudes.

2.2.1 Derivation Forchheimer formula based on Navier Stokes Equation

There are many different formulations for the constant a and b in the Forchheimer formula. The formulation which is directly derived from the Navier-Stokes equation is used in this thesis. This derivation is described by Burcharth and Andersen (1995).

$$\frac{D\vec{u}}{Dt} = -\frac{1}{\rho_w}\nabla p + \nu\nabla^2\vec{u} + \vec{G} \tag{2.35}$$

Using the following assumptions on Equation 2.2 it is possibly to derive a simplification:

1. Only one dimensional flow in x direction is considered
2. The hydraulic pressure gradient can be written as $I = -\frac{1}{\rho_w g}\frac{\partial p}{\partial x}$
3. Only consider pressure driven flow so the gravitational term could be written in the pressure term
4. Only consider stationary flow so $\frac{\partial u}{\partial t} = 0$

Equation 2.2 could then be written as:

$$I = \frac{\nu}{g}\left(\frac{\partial^2 u}{\partial x^2}\right) + \frac{u}{g}\frac{\partial u}{\partial x} \tag{2.36}$$

If u_k and D are used as a characteristic speed and length parameter, and by using the non dimensional constants α and β, the equation could then be written as:

$$I = \alpha\frac{\nu}{g}\frac{u_k}{D^2} + \beta\frac{1}{g}\frac{{u_k}^2}{D} \tag{2.37}$$

By substituting u_k with u_f/n - where u_f is a filter velocity and n is the porosity - and also substituting D with the hydraulic radius R (defined as the ratio of pore volume over pore surface area, $R = \frac{n}{1-n}\frac{d_{n50}}{6}$ for spheres), this results in:

$$I = \alpha\frac{(1-n)^2}{n^3}\frac{\nu}{g{d_{n50}}^2}u_f + \beta\frac{(1-n)}{n^3}\frac{1}{gd_{n50}}{u_f}^2 \tag{2.38}$$

Note that the Forchheimer coefficients a and b in Equation 2.32 are now defined by a formula with a new coefficient α and β as in Equation 2.38. In order to solve the equations, the values for α and β have to be determined. These constants have to be experimentally determined and are only applicable for a certain flow regime.

2.2.2 Non Stationary Flow

The Forchheimer Equation describes a stationary flow. For non-stationary flow the equation needs an extra time dependent term. Polubarinova-Kocina (1952) extended the Forcheimer equation as follows:

$$I = au_f + b{u_f}^2 + c\frac{\partial u_f}{\partial t} \tag{2.39}$$

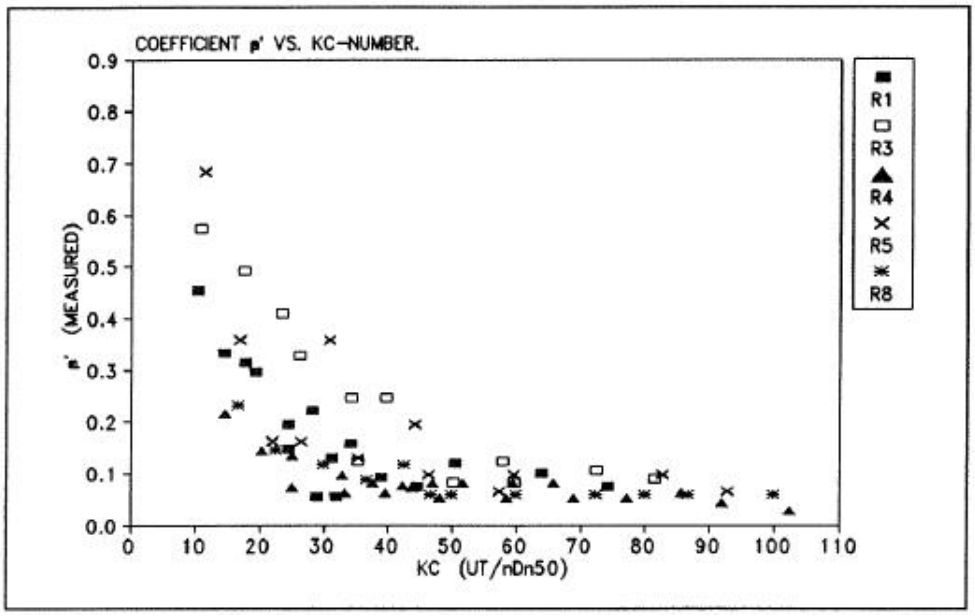

Figure 2.2: Different values for the β constant depending on the KC number by Van Gent (1993)

Here c is a dimensional coefficient (s^2/m). The c term describes the effect of inertia for non-stationary flow. Van Gent (1992) wrote about the principle of added mass. In order to accelerate a certain volume of water in a porous medium there is extra momentum needed compared to a non-porous medium.

Van Gent (1993) concluded, on the basis of experimental research, that the parameters of the stationary Forchheimer formula (α ,β) are not equal for the non-stationary formula. For determining the difference of the Forchheimer constants between stationary and non-stationary cases Van Gent (1993) produced Figure 2.2 where the measured β is plotted against the KC number. It can be concluded that for lower KC numbers the β is significantly higher than for higher KC numbers. The KC number can be seen as the magnitude of the convective acceleration term over the local acceleration term:

$$KC = \frac{\hat{U}T_p}{nd_{n50}} \tag{2.40}$$

This number determines how "stationary" the flow is. As T=∞ for stationary flow KC=∞ as well. Van Gent argued that the non-stationary quadratic constant β was made out of a stationary term β and a non stationary term β_{NS}. By stating that the β term appeared to be constant for very high KC numbers (stationary flow) he developed a relation based on curve fitting for the non-stationary β_{NS} term depending on the stationary β term.

$$\beta_{NS} = \beta\left(1 + \frac{7.5}{KC}\right) \tag{2.41}$$

Determining the correct contribution of the a, b and c term for non-stationary situations has been proven to be difficult. Experiments have been carried out where different samples were tested with a known oscillatory pressure created by a piston. The difficulty is

splitting the signal to recover the magnitude per term. Van Gent (1993) describes how the problem can be solved by first measuring the sample in a stationary situations and assuming that the α values are the same for a non-stationary situation. Then it is possible to determine the contribution of the turbulent friction term by analysing $au_f + bu_f^2$ at the points of $u_f = u_{f,max}$ since the $\frac{\partial u_f}{\partial t}$ term is zero at those points. By iteratively correcting the resulted formula to fit the measurements, the c term can be determined.

Burcharth and Andersen (1995) derived the following equation for the c term:

$$c = \frac{1 + C_m \frac{1-n}{n}}{g} \tag{2.42}$$

Where C_m is a term which represents the added mass. Anderson (1994) came with the following expression for C_m:

$$C_m = 1.5 + 12(1 - n) \tag{2.43}$$

It must be noted that this relationship was established from a limited amount of experiments.

After a theoretical analysis Van Gent (1992) derived an alternative formulation for the c term, namely:

$$c = \frac{1 + \gamma \frac{1-n}{n}}{ng} \tag{2.44}$$

He relates the c value with a so called acceleration number A_c given by:

$$A_c = \frac{\hat{U}}{nTg} \tag{2.45}$$

By curve fitting with experimental data, the following expression is derived for c:

$$c = \frac{1 + \frac{1-n}{n}\left(0.85 - \frac{0.015}{A_c}\right)}{ng} \; for \; A_c > \frac{0.015}{\frac{n}{1-n} + 0.85} \tag{2.46}$$

The large amount of different formulations with many different terms show how little is known about this inertia term.

2.2.3 Measured Forchheimer constants in previous research

In Appendix A a is given of all the experimentally determined values for the α and β constants. These measurements are all done with a turbulent stationary setup. In order to use them in non-stationary environments, they should be converted with Equation 2.41. The results of the blocks used in this experiment, as derived by Zeelenberg and Koote (2012) are also included.

A wide range of β values are found for irregular rocks. They range from values of 0.55 till 11. The most values are in the order of 2-3. The results obtained by Zeelenberg and Koote (2012) are a bit low with values of 1.1-1.7. The explanation given by Van Gent (1993) is

that the difference could be the result of different orientations of the stones during the different experiments. The flow resistance is depending on the projected area perpendicular to the flow direction. If the stones have an aspect ratio which is not similar to 1 and the side with the largest projected area is perpendicular to the mean flow, the outcome will be different from the case where the smallest projected area is perpendicular to the mean flow.

According to Burcharth and Andersen (1995), the coefficients of the Forchheimer formula in the fully turbulent regime are considered to be independent of the Reynolds number. It is proven that for fully turbulent flow up to Reynolds numbers of 10^4 the β is constant and it is assumed to be constant for higher Reynolds numbers.

2.2.4 Relative importance of the various terms in Forchheimer equation

The extended Forchheimer Equation 2.39 has three terms, a laminar resistance, a turbulent resistance and the effects of inertia. The relative importance of the various terms of the Forchheimer formula can be estimated with two non-dimensional parameters. The magnitude of the turbulent resistance over the laminar resistance is linear with the Reynolds number. Also the magnitude of the turbulent resistance over the inertia effects is linear with the Keuler Carpenter number.

$$Re = \frac{convective\ acceleration}{viscous\ forces} = \frac{u\frac{\partial u}{\partial x}}{\nu\frac{\partial^2 u}{\partial x^2}} = \frac{U\frac{U}{D}}{\nu\frac{U}{D^2}} = \frac{u_f d_{n50}}{\nu}$$

$$KC = \frac{convective\ acceleration}{local\ acceleration} = \frac{u\frac{\partial u}{\partial x}}{\frac{\partial u}{\partial t}} = \frac{U\frac{U}{D}}{\frac{U}{T}} = \frac{\hat{U}T_p}{nd_{n50}}$$

In Figure 2.3 the different flow regimes are presented graphically depending on the Reynolds number and the Keuler Carpenter number.

Troch (2000) investigated the relative importance of the various terms for turbulent flow. He did this by taking standard values for all flow parameters based on averages from literature on irregular rock. For this case a similar calculation can be made to predict the relative importance of the Forchheimer terms. In Table 2.2 the values used for this calculation are shown based on Zeelenberg and Koote (2012):

Constant	**Value**	**Unit**
α	1020	(-)
β_{NS}	2.90	(-)
n	0.46	(-)
d_{n50}	0.039	(m)

Table 2.2: Porous variables used for test case

The water is given an acceleration from 0 up to 0.17 m/s (characteristic velocity) during 1.5 s (half of the period). The characteristic velocity is taken from the analytical model discussed in Chapter 5. This way the arbitrary function V could be defined:

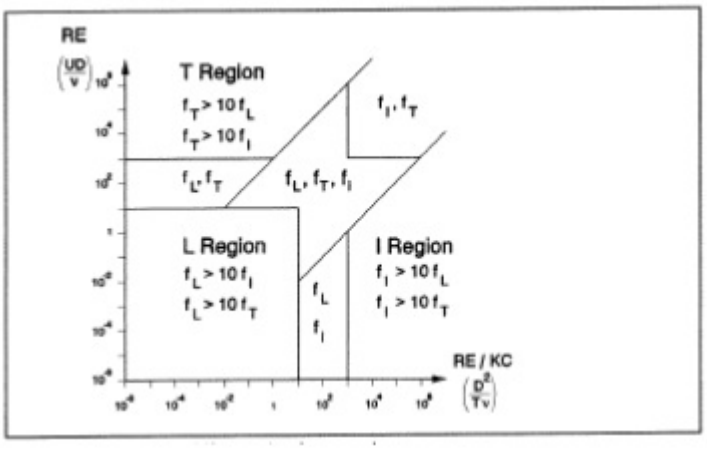

Figure 2.3: Classification of the importance of the various terms according to Gu and Wang (1991)

$$V(t) = \frac{0.10}{2}\left(1 - \cos\frac{\pi}{1.5}\,t\right) \tag{2.47}$$

With a wave period of 3 s and the characteristic speed of 0.17 m/s the A_c value can be calculated with Equation 2.45. Using A_c=0.0063 in Equation 2.46 results in a value of c=0.33.

The results are plotted in Figure 2.4 and 2.5. The relative importance of the turbulent term bV^2 is clearly visible. The turbulent term is clearly dominant over the laminar term. The inertia term does not seem to be of influence when one looks at the difference between the computations done with and without the intertia term. It results in a small phase and amplitude difference compared to the estimate of taking only the laminar and turbulent terms ($I = aV + bV^2$). Based on this case the decision is made to neglect the non-stationary term in further analyses.

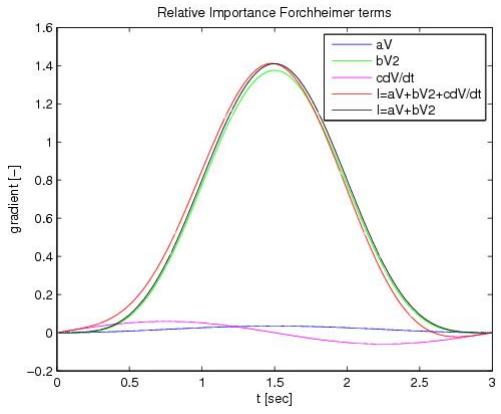

Figure 2.4: Comparison of magnitude of different Forchheimer terms for example case

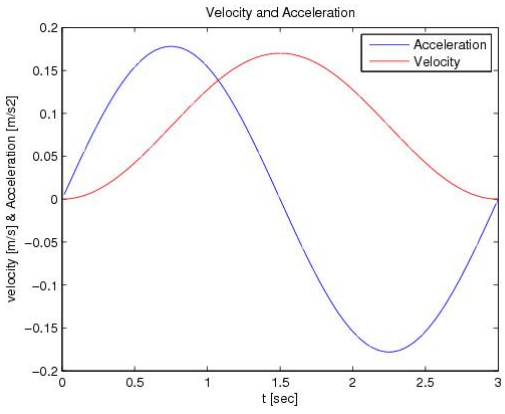

Figure 2.5: The velocity and acceleration of the water

2.2.5 Pore pressure attenuation

The formula's for pore pressure attenuation are used for predicting the flow inside a porous structure and are therefore very useful for scaling purposes. The model uses a linearised friction term and neglects the viscous terms from the momentum balance equations. In appendix B a derivation is given of the model described by Biésel (1950).

Based on this theoretical model, Oumeraci and Partenscky (1990) derived an exponential decay function, being:

$$p\left(x\right) = p_0 e^{-\delta \frac{2\pi}{L'} x} \tag{2.48}$$

The situation is sketched in Figure 2.6. Where x is the distance from the interface of core and filter layer and p_0 is the reference pressure at this interface. For the case of a homogenous porous block a different referent system needs to be used. δ is the damping coefficient and L' is the wave length in the core. ($L' = \frac{L}{\sqrt{1.4}}$). L is the incident wave height.

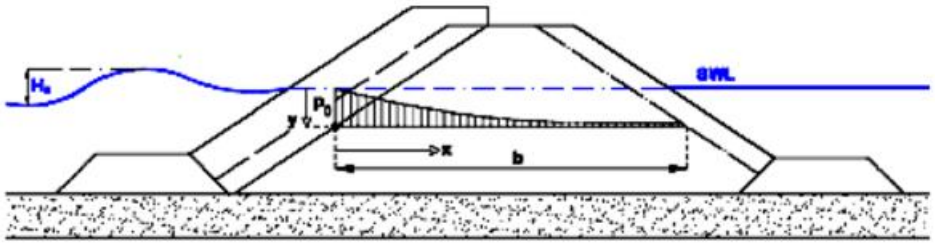

Figure 2.6: Situation sketch pressure attenuation Troch (2000)

The damping coefficient according to Burcharth et al. (1999) is:

$$\delta = a_\delta \frac{\sqrt{n} L^2}{H_s l} \tag{2.49}$$

where n is the porosity, l is the width of the core and H_s and L_p are the height and length of the wave. The coefficient a_δ is a result of linear regression analysis. Troch (2000) reported a value of $a_\delta = 0.014$.

He draws two conclusions regarding the damping coefficient:

1. The damping coefficient decreases for increased depth below the SWL
2. The damping coefficient increases for increased wave period.

Based on these two conclusions Troch (2000) rewrites the formula for the damping coefficient. The l term can be seen as a term to account for the reduced damping in the vertical direction as the width of the core for a sloped breakwater increases with the depth:

$$\delta = a_\delta \frac{\sqrt{n} L^2}{H_s l} = a_\delta \frac{\sqrt{n} L}{s_p l} \tag{2.50}$$

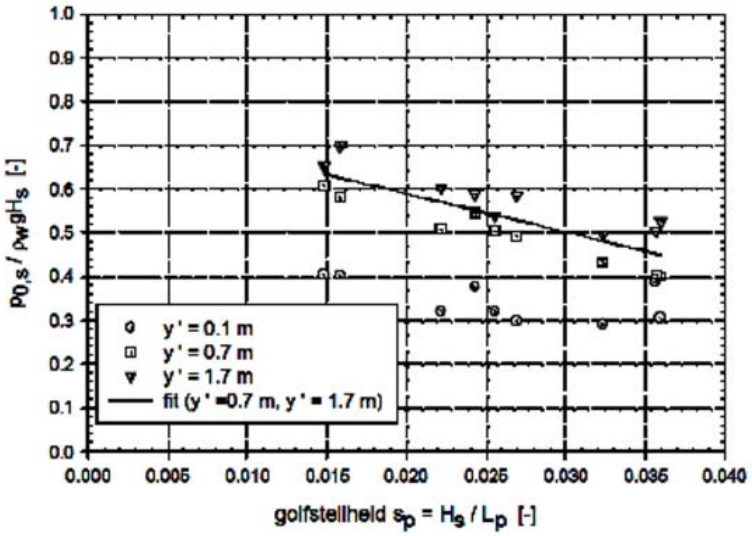

Figure 2.7: Maximal reference pressure, Troch (2000)

The wave height was removed and the wave steepness s_p is introduced to better reflect the dependency of the damping coefficient on the wave period.

Troch (2000) analysed the relation of wave height and maximum pressure between the filter and core. He measured the maximal reference pressure and plotted it against the wave steepness as can be seen in Figure 2.7. He concluded that the maximal reference pressure was roughly constant and 0.55 of the hydrostatic wave pressure. In Burcharth et al. (1999) the maximum reference pressure is described as:

$$p_{0,max} = \frac{\rho_w g H_s}{2} \tag{2.51}$$

Furthermore, the formula for the pore pressure at a given time/space neglecting internal setup according to Burcharth et al. (1999) is:

$$p\left(x,t\right) = \rho_w g \frac{H_s}{2} e^{-\delta \frac{2\pi}{L'} x} cos\left(\frac{2\pi}{L'}x + \frac{2\pi}{T_p}t\right) \tag{2.52}$$

To determine the pore velocities the equation 2.52 can be transformed into:

$$I_x = \frac{1}{\rho_w g}\frac{dp(x,t)}{dx} = -\frac{\pi H_s}{L'} e^{-\delta \frac{2\pi}{L'} x}\left[\delta \cos\left(\frac{2\pi}{L'}x + \frac{2\pi}{T_p}t\right) + \sin\left(\frac{2\pi}{L'}x + \frac{2\pi}{T_p}t\right)\right] \tag{2.53}$$

By stating that the pressure gradients have to be equal to the pressure gradient of the Forchheimer formula, the filter velocities can be determined as follows:

$$I_x = \alpha \frac{(1-n)^2}{n^3}\frac{\nu}{g{d_{n50}}^2} u_f + \beta \frac{(1-n)}{n^3}\frac{1}{g d_{n50}} u_f^2 \tag{2.54}$$

Burcharth et al. (1999) suggested for scaling core materials to determine an characteristic filter velocity. This way it is possible to account for the unsteady motion by averaging the

filter velocities in time and space. A properly scaled core is then obtained by scaling the characteristic filter velocity according to the Froude scaling laws.

2.3 Analytical Solution with a Harmonic method

One of the advantages of working with a simplified test setup is that it is possible to produce an analytical solution. The mathematical solution of the simplified test case could be made based on a harmonic method. This model is developed by the "*Staatscomissie Lorentz*" in order to predict the effects on the Waddenzee by closing the Zuiderzee using the Afsluitdijk. Madsen and White (1976) described a solution for a similar case as the test case for this study.

The method solves the problem as set out in Figure 2.8 with complex harmonics and a linearised friction factor based on the Forchheimer formula. The solution consists out of a reflected and transmitted wave which are exponentially damped in their direction.

If one recalls equations 2.18, 2.19 and 2.20, one could derive the long wave equations by writing the system in one dimension and neglecting the advection term. The governing equations outside the structure are the long wave equations earlier derived. These equations are hydrostatic, have no advection term, have no viscous terms and only solve the problem in one direction.

$$\frac{\partial \eta}{\partial t} + h\frac{\partial u}{\partial x} = 0 \tag{2.55}$$

$$\frac{\partial u}{\partial t} + g\frac{\partial \eta}{\partial x} = 0 \tag{2.56}$$

Equation 2.55 is the continuity equation and Equation 2.56 is the momentum balance equation. In these equations η is the free surface elevation relative to the still water level. h is the water depth, u is the velocity and g is the gravitational constant.

For the porous part, the linearised governing equations are:

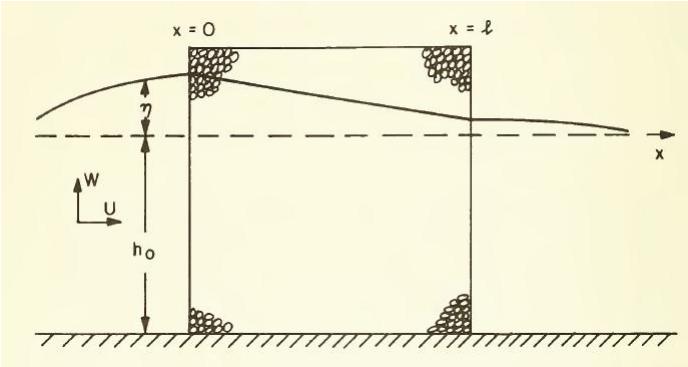

Figure 2.8: Definition sketch from Madsen and White (1976)

$$n\frac{\partial \eta}{\partial t} + h\frac{\partial u}{\partial x} = 0 \tag{2.57}$$

$$\frac{S}{n}\frac{\partial u}{\partial t} + g\frac{\partial \eta}{\partial x} + f\frac{\omega}{n} = 0 \tag{2.58}$$

Here the ω is the radian frequency, S is a factor expressing the effect of unsteady motion and f is a non-dimensional friction factor which covers the effect of porous resistance. This friction term can be related to the Forchheimer formula as follows:

$$f\frac{\omega}{n} = \alpha + \beta|u_f| \tag{2.59}$$

This equation can be linearised by stating:

$$f\frac{\omega}{n} = \alpha + \frac{8}{3\pi}\beta|\hat{u}| \tag{2.60}$$

Here $\hat{u}$ is the horizontal velocity amplitude inside the structure.
Because of the linearised equations it is possible to look for a periodic solution with radian frequency ω. The system can be solved by taking:

$$\eta = Real\{\zeta\,(x)\,e^{i\omega t}\} \tag{2.61}$$

$$u = Real\{u\,(x)\,e^{i\omega t}\} \tag{2.62}$$

Eventually after applying algebraic manipulations described in Madsen and White (1976), it is possible to derive an analytical expressions for the complex amplitude of the reflected and transmitted wave:

$$\frac{a_t}{a_i} = \frac{4\epsilon}{(1+\epsilon)^2\,e^{ikl} - (1-\epsilon)^2\,e^{-ikl}} \tag{2.63}$$

$$\frac{a_t}{a_i} = \frac{\left(1-\epsilon^2\right)\left(e^{ikl} - e^{-ikl}\right)}{(1+\epsilon)^2\,e^{ikl} - (1-\epsilon)^2\,e^{-ikl}} \tag{2.64}$$

where ϵ is given by:

$$\epsilon = \frac{n}{\sqrt{S - if}} \tag{2.65}$$

a_t is the complex transmitted amplitude, a_i is the complex incoming amplitude, a_r is the complex reflected amplitude, k is the complex wave number, l is the length of the block, f is the linearised friction factor and n is the porosity. This results in a Reflection coefficient and Transmission coefficient:

$$R = \frac{|a_r|}{a_i} \tag{2.66}$$

$$T = \frac{|a_t|}{a_i} \tag{2.67}$$

This makes it possible to compare the experimental results with an analytical solution.

2.4 Scaling problems

One of the major problems of scaled models are scaling problems. The behaviour of a fluid might be different on a different scale. This study will compare experimental and numerical simulations on a 1:1 scale but there is still some sort of scaling needed in order to certify that the scale model is a representation of the real life situations of a breakwater under wave attack. Also the Forchheimer formulations make a clear distinction between different flow regimes. Scaling can be used to make sure that the investigated domain is turbulent enough to apply for the fully turbulent flow regime. This means $Re_d > 450$. Also the experimental Reynolds number preferably needs to be of the same order as the Reynolds number used in the experiments of Zeelenberg and Koote (2012) to determine the Forchheimer constants.

2.4.1 Froude Scaling Laws

The Froude relationship describes the relation between inertial and gravitational forces in a fluid:

$$Fr = \frac{u}{\sqrt{gh}} \tag{2.68}$$

In order to scale according to the Froude law, the Froude number needs to be identical in model and prototype. This can be done by defining the relation between the characteristic length scale in model and prototype as the scaling factor λ. According to this relation the other scales can be determined by:

Length scale: $L_p/L_m = \lambda$
Velocity scale: $V_p/V_m = \sqrt{\lambda}$
Time scale: $t_p/t_m = \sqrt{\lambda}$
Force scale: $F_p/F_m = \lambda^3$
If these rules are applied on the Forchheimer equation and n, ν and g are equal in Prototype and Model:

$$I = \alpha \frac{(1-n)^2}{n^3} \frac{\nu}{g d_{n50}^2} u_f + \beta \frac{(1-n)}{n^3} \frac{1}{g d_{n50}} u_f^2 \tag{2.69}$$

The laminar term in that case can be scaled with U/D^2 and the turbulent term can be scaled with U^2/D. This results in the following scale factors:
Laminar scale (First term): $\sqrt{\lambda}/\lambda^2 = \lambda^{-3/2}$
Turbulent scale (Second term): $\left(\sqrt{\lambda}\right)^2/\lambda = 1$
These scales conflict, so both fluid characters can't be modelled correctly at the same time. However as earlier discovered, turbulent terms are more important in this case.

For scaling the grain sizes of the core, filter and armour layer the method described by Burcharth earlier is the best method since it scales the porous velocities. By ensuring the experiment is carried out in the fully turbulent regime, scaling problems are minimized.

2.4.2 Air Entrainment

Besides the turbulent scaling problems there are also other possible scaling problems. During wave breaking it is possible for air bubbles to enter the water. They are easily recognisable by the white foam that is on top of breaking waves. On a laboratory scale some air bubbles are also expected as a result of the wave action on a porous structure. The typical size of air bubbles is in the range of 20-30 μm. This size and it's effects give a possible scaling problem.

The air entrainment will create a water air mixture which has some consequences for the traditional formulas. As a result, the water is not fully incompressible any more. For example, the density ratio of air and water is 1/800 and the compressibility ratio of air and water is 20000/1. The air-water mixture will give a sort of "cushioning effect" for the high peak loads. The maximum pressure will be reduced with an increase of air voids in the water.

Bubbles in the water will eventually reach the free surface and disappear. There is a significant difference between bubbles in salt and fresh water. Slauenwhite and Johnson (1999) found that there are 4-5 times more bubbles in salt water than fresh water. Furthermore, they discovered that the bubbles tend to have a smaller diameter in salt water.

Because of the compressibility of air-water mixtures, the results as obtained on laboratory scale can differ from the real scale. Bullock et al. (2001) compared the results of laboratory (1:25 Froude scaled) and prototype results. They found that waves generated 10% more impact pressure on laboratory scale than on prototype scale.

As air entrainment complicates the equations greatly the effect is left out in this report. Nevertheless, one should keep in mind that it is an important effect which can play a role when the model is scaled up to real life sizes.

2.4.3 Surface Tension

An even smaller scaling effect is the influence of surface tension. Surface tension can cause some scale effects on non-breaking waves in laboratory, but this will only be the case for very small steep waves. In Tirindelli and Lamberti (2000) it can be read that only wave heights below 2 cm and periods below 0.3 seconds will create situations where the surface tension plays a significant role according to Hughes (1993). This is why surface tension is not considered to influence any results in this study.

In Figure 2.9 indicates that in situations with weak surface tension jets of water are allowed to exit the surface, which in turn creates extra air bubbles and droplets. While in situations with strong surface tension capillary waves will form no droplets or bubbles will.

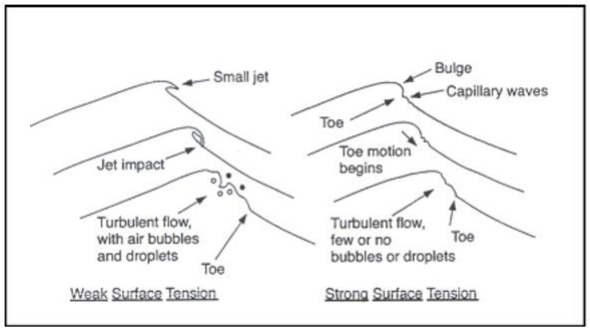

Figure 2.9: Difference between strong surface tension and weak surface tension on breaking waves Tirindelli and Lamberti (2000)

2.5 Statistical Methods

Two methods are used to compare numerical and analytical computations with experimental observed values; the Root Mean Square Error (RMSE) and the relative bias. The RMSE is as the name indicates the root mean square error but normalized by the mean observed value. It is a method to determine the order of spread in the results, and is defined by:

$$RMSE = \frac{\sqrt{\frac{1}{N}\sum_{i=1}^{N}(y_i - x_i)^2}}{\frac{1}{N}\sum_{i=1}^{N}|x_i|} \tag{2.70}$$

Where N is the number of observation, y_i is the predicted value and x_i is the observed value. The RMSE is always positive.

The second method is the calculation of the relative bias. The relative bias shows the systematic error between predictions and observations normalized by the observations. The relative bias can be positive (overestimation of predictions) and negative (underestimation of predictions), and is defined as:

$$Bias = \frac{\sum_{i=1}^{N}(y_i - x_i)}{\sum_{i=1}^{N} x_i} \tag{2.71}$$

2.6 Previous research

Keulegan (1973) investigated a similar test case, but unfortunately the dataset is not publicly accessible. However, the dataset is used by Madsen and Warren (1984) to compare their numerical computations. As a result the only method to obtain the necessary data is by extracting the data from the graphs published by Madsen and Warren (1984), as can be seen in Figures 2.11 and 2.12.

The setup used by Keulegan (1973) is drawn in Figure 2.10. Madsen and Warren (1984) retrieved that the water depth used by Keulegan is 0.30m. Combining this fact with the knowledge that the wave steepness was H/L=0.1 the wave period can be derived as 1.86s.

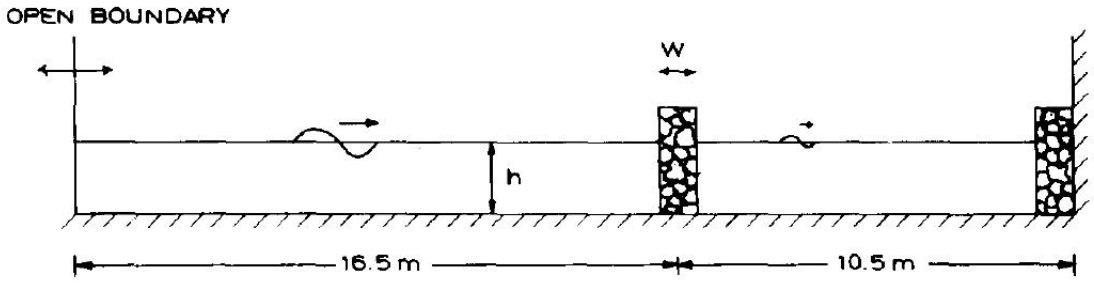

Figure 2.10: Setup used by Keulegan for experimental research on reflection and transmission Madsen and Warren (1984)

There are two different cases, one has a width of 0.15m and one has a width of 0.30m. Both use grain sizes of 0.025m and porosity of 0.46.

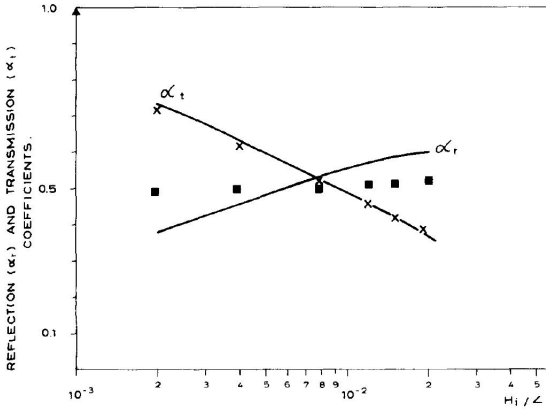

Figure 2.11: Width=0.15m. Comparison of computed results (solid line) by Madsen and White (1976) and experimental data from Keulegan (1973) where crosses are transmission coefficient and squares are reflection coefficients

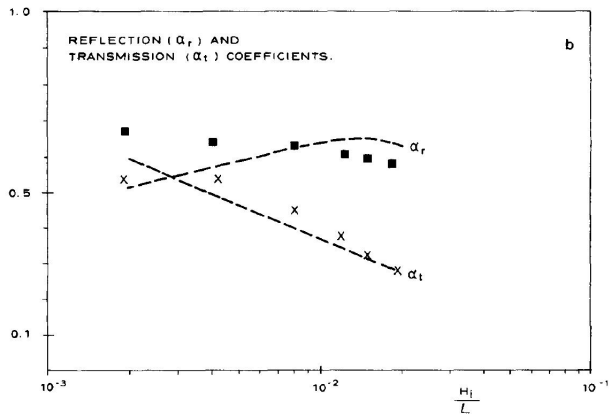

Figure 2.12: Width=0.30m. Comparison of computed results (solid line) by Madsen and White (1976) and experimental data from Keulegan (1973) where crosses are transmission coefficient and squares are reflection coefficients

Based on Figures 2.11 and 2.12, Tables 2.3 and 2.4 are created as estimate of the results.

H/L (-)	**R (-)**	**T (-)**
2×10^{-3}	0.49	0.71
4×10^{-3}	0.5	0.61
8×10^{-3}	0.5	0.51
1.3×10^{-2}	0.51	0.47
1.7×10^{-2}	0.51	0.42
2×10^{-2}	0.52	0.38

Table 2.3: Reflection and transmission measured by Keulegan (1973) for a block width of 0.15m

H/L (-)	**R (-)**	**T (-)**
2×10^{-3}	0.58	0.53
4×10^{-3}	0.56	0.53
8×10^{-3}	0.55	0.47
1.3×10^{-2}	0.52	0.44
1.7×10^{-2}	0.51	0.32
2×10^{-2}	0.49	0.28

Table 2.4: Reflection and transmission measured by Keulegan (1973) for a block width of 0.30m

Chapter 3

Experimental Research

The experiment is designed to get data on the process of wave interaction with a vertical porous structure. As described in the introduction a simplified setup will be used. The objective is to use standardized samples with known characteristics such that they can easily be reproduced on a 1:1 scale in other models. Four different blocks, with different porosity and grain size, will be tested with a wide variety of wave conditions. Furthermore, there are two kind of sensors, wave gauges which can analyse the reflection and pressure sensors which can measure pore pressures.

3.1 Experimental Setup

The experiments are carried out in the large flume of Environmental Fluid Mechanics Laboratory of the TU Delft. The length of the flume is roughly 38m. The testing blocks are placed in the flume at 28 meters from the wavemaker. A sketch of the setup is included in Figure 3.1.

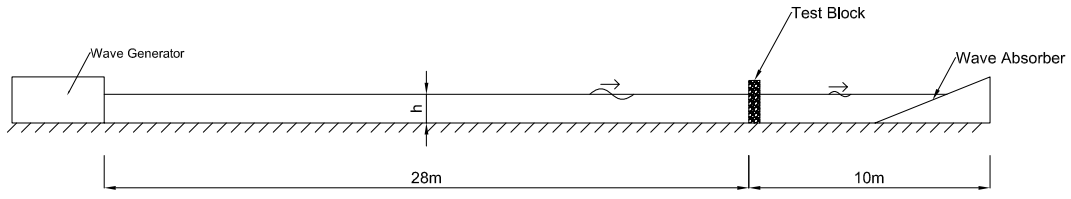

Figure 3.1: Sketch of experimental setup

The wavemaker is capable of creating monochromatic waves where the user should choose the period, waveheight and water depth. It uses an automated reflection compensator in order to minimize wave reflections created from the wave board. As a result, it is ensured that the incoming signal is the desired wave signal at all times.

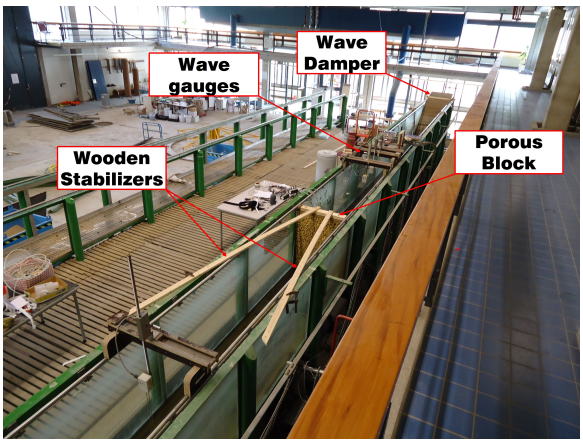

Figure 3.2: Overview end of the flume

Figure 3.2 shows an overview of the end of the flume. The tested block needs to be put firmly in place in order to prevent it from starting to resonate or displace due to the wave action. This is done by two wooden bars. These are also visible in Figure 3.4, where the front view of the block is visible. In Figure 3.3 the wave absorber at the end of the flume can be seen. This structure is placed on approximately a 1:3 slope and has to damp the waves coming through the structure and prevent them from reflecting back to the structure.

Figure 3.3: Wave Absorber at the end of the flume

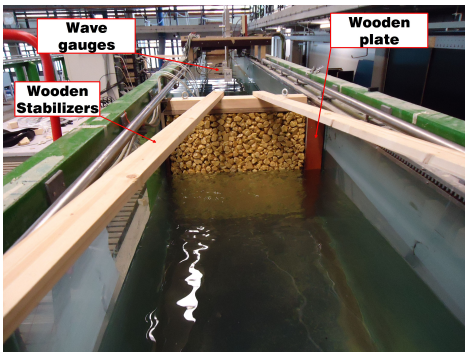

Figure 3.4: Front view of the setup, note the wooden plate on right side

3.2 Description of the blocks

The blocks were made by (Zeelenberg and Koote (2012)). They constructed the blocks with three different types of irregular stones. In total they made six blocks with elastocoast and six smaller samples for testing porosity and permeability of different configurations. The blocks are made by filling wooden moulds with stones. The stones are mixed in a concrete mixer with elastocoast or epoxy before they were placed in the moulds. By removing the plate on the back of the mould a permeable block is created. The blocks have a width of 725 mm and a height of 925 mm. The width is a bit smaller than the width of

	Material	**Thickness** (mm)	d_{n50} (m)	**n** (-)	**k** (m/s)	α (-)	β (-)	Re_d (-)
1	Yellow sun limestone 8-11 mm	39	0.007	0.386	0.065	700	1.1	220
2	Yellow sun limestone 20-40 mm	88	0.020	0.405	0.136	1200 (est.)	1.25 (est.)	2100
3	Yellow sun limestone 20-40 mm	132	0.020	0.423	0.131	1200	1.25	2700
4	Norwergian >40 mm	80	0.039	0.41	0.154	1900	1.7	6000
5	Norwergian >40 mm	160	0.039	0.466	0.214	1150	1.6	7850
6	Norwergian >40 mm	240	0.039	0.46	0.213	1020	1.45	8300

Table 3.1: Description of the blocks based on Zeelenberg and Koote (2012)

the wave flume because of the rail installed on top of the flume. In Figure 3.4 a front view of the structure in the flume can be seen. This also shows one of the major setbacks of the setup, the wooden plate on the right of the structure. This fully blocks the incoming waves. In total 11 cm out of the 80 cm width of the flume is fully blocked.

For all stone classes a sieve analysis was made. The permeability tests on the smaller samples were performed in a water tank with a special setup. By creating a fixed water level difference between two water tanks which are connected through the tested sample it is possible to calculate the static constants for the Forchheimer formula with flow meters. This was done five times per sample and the averaged results are presented. The porosity was measured by comparing the weight of a dry block and a block filled with water. In Table 3.1 a summary of the most important information per block can be found based on the report of Zeelenberg and Koote (2012) (permeability results of sample 2 are estimated).

For block number 2 the permeability results are estimated since the authors report that they cannot find a solution to the equations for those cases. Block number 6 is made with epoxy instead of elastocoast. It is assumed that epoxy makes no difference with elastocoast for flow properties. In general the constants for blocks with similar grain size are quite similar. Only block 4 is a bit different then block 5 and block 6. The porosity of block 5 and 6 are very high according to Van Gent (2012). Porosities outside the range of 0.35-0.45 are physically not realistic according to Van Gent (2012). A possible reason could be that for larger stone sizes the influence of the edges gets larger. Compared to a normal porous structure the edges have some larger pores since certain stones could not be placed. The porosity measured for the small samples with stones might be significantly different than the larger blocks.

The general idea behind the different blocks is that block 4, 5 and 6 function as armour layer, while block 2 and 3 function as filter layer and block 1 is a core layer. Only blocks 2,3,5 and 6 will be tested.

3.3 Scaling

As discussed in Section 2.4 some scaling is needed in order to test the blocks within the right wave regime and with the right amount of turbulence. The scaling method used will be the method of Burcharth (see Section 2.2.5 and 2.4.1). In order to end up with useful data a full scale example is chosen on which the scaling laws are applied for creating a similar flow regime. Preferably, the created flow regime should match the Reynolds numbers used for determining the α and β constants.

The base scale is based on an example from Schiereck (2004), a summary is given in Table 3.2.

Variable	**Value**
H_s	2 m
$\cot\alpha$	3 (-)
P	0.5 (-)
T_m	6 s
N	3000 (-)
d_{n50}	0.625 m (300-1000 kg)
Δ	1.65 (-)
S	2 (-)

Table 3.2: Variables for a fictive breakwater used for scaling purposes

In order to transform this example into a model scale vertical breakwater some data can be removed. Only the incoming wave data and the size of the grains will be used. A fictive filter layer and core layer are determined based on standard filter rules to create an imaginary breakwater as sketched in Figure 3.5.

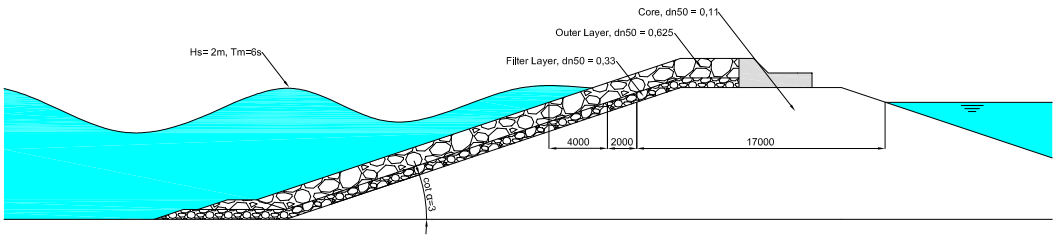

Figure 3.5: Fictive structure for scaling purposes

According to the relation between the d_{n50} of the example and the biggest d_{n50} of the blocks, a general scale of 1:16 for the experiment is determined.

The method of Burcharth requires a characteristic filter velocity which needs to be scaled with the Froude scaling laws. The characteristic filter velocity can be calculated with Equations 2.53 and 2.54, by averaging several data points in time and space. In this case the filter velocities are determined at 5 steps (0 till 0.5T) till half the wave period for x=0, x=l/4 and x=l/2. Where l is the width of the structure. By averaging all the results, a characteristic value for the filter velocity (u_{char}) can be used to determine the Reynolds number.

	Full scale				**Model scale** (1:16)			
	H_s	T_p	u_{char}	Re_d	H_s	T_p	u_{char}	Re_d
"Fictive Outer Layer"	2	6	0.33	210000	0.125	1.5	0.09	3600
"Filter layer"	2	6	0.33	110000	0.125	1.5	0.08	1600
"Core"	2	6	0.09	38000	0.125	1.5	0.09	650

Table 3.3: Comparison of characteristic velocities on base scale and model scale

In Table 3.3 the characteristic velocities are summarised. This table indicates that characteristic velocities on full scale are roughly $\sqrt{16} = 4$ times the model scale. This suggest that they are Froude scaled according to Burcharth et al. (1999). In addition, the Reynolds numbers are sufficiently high ($Re_d > 450$) to apply for the fully turbulent flow regime. However, for this experiment minor scale effects are not a big issue, since the numerical and physical scale is 1:1. The only thing which has to be assured is that the flow through the pores is fully turbulent (instead of laminar) to make the Forchheimer model applicable.

The placement of sensors in the structure is done in order to capture the main processes, so the process with the smallest scale is therefore leading. The most important scale in this case is the length scale of the exponential decay, since the length scale of the wave length is significantly larger. However, this is also the most uncertain scale. In literature, practical values are reported ranging from 0.5 till 5 by Troch (2000) for the damping coefficient δ in Equation 2.48.

	$\boldsymbol{\delta}$ (-)	$\boldsymbol{L_{1/2}}$(m)
Minimum damping factor	0.5	0.53
Current damping factor	2.5	0.1
Maximum damping factor	5	0.05

Table 3.4: Influence of damping factor on the length scale of the exponential decay

The water depth needs to be chosen such that the waves are non breaking during the experiment. The minimum water depth for non-breaking waves is roughly 2 times the wave height. For this experiment 5 times the wave height is chosen, which comes down to h=0.65 m.

The base values for the wave height and period (0.125m and 1.5s) are expanded into a measuring range. This is done on basis of a JONSWAP spectrum, which dictates that

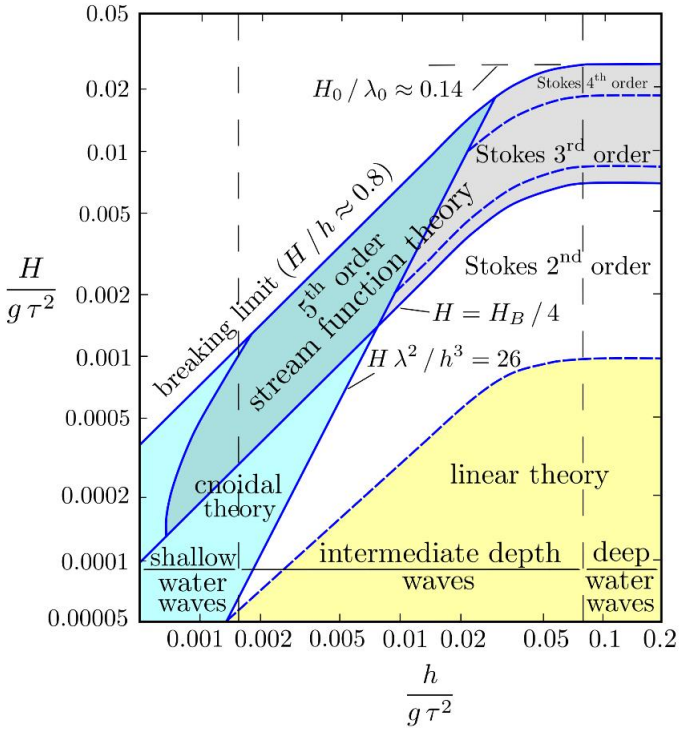

Figure 3.6: Applicability of linear wave theory according to Le Mehauté (1976)

wave periods would vary between 1.0 s and 3.0 s. Wave height are chosen with increments of 0.025m, from 0.075m till 0.150m.

Although the intention is to have regular linear waves, in practice most of the waves are non-linear. They are not a perfect sinusoid but have small crests and long troughs. In Figure 3.6 the different wave regions according to Le Mehauté (1976) are drawn. The wave cases used in this research are in the stokes 2nd order region, stokes 3rd order and 5th order stream function theory. This means that none of the waves can be fully described with linear wave theory.

3.4 Setup of sensors

Due to practical considerations, measuring velocities or water levels inside a porous structure is difficult. The sensors available are rather large, large holes need to be drilled to fit them in the samples. The sensors will have a relatively large size compared to the typical pore and grain size. This will influence the measurements. It is therefore much more convenient to extract data with sensors outside the structure. For that reasons two types of sensors are chosen:

- Differential Pressure Sensors
- Wave Gauges

In order to prevent confusion the sensors that are placed outside the flume are called sensors, the tubes of ∅ 6mm are connected to the pores in the block are named sensor tubes and the pores where the pressures are measured are named sensorpoints. The pressure difference sensors , see Figure 3.7 compare the pressure on the left and right side of the sensor and produce a tiny voltage which is amplified till a voltage between -10V and +10V. This voltage can be registered by the computer. The range is about ±35 cm static water pressure. The wave gauges can be seen in Figure 3.8. They measure the conductivity depending on the water level and give a signal ranging between -10V and +10V. Wave gauges are placed in groups of three, while only two are necessary in order to decompose the wave signal. Placing 3 sensors gives however more flexibility and makes it more easy to compare the different results. The wave gauges should have a spacing of roughly 1/4 of the wavelength. More information on the sensors can be found in Appendix C.

All sensors need to be calibrated individually. This is done by creating series of fixed water level differences and measuring the corresponding response in volts. The sensors possess a linear relation between pressure/water level and voltage.

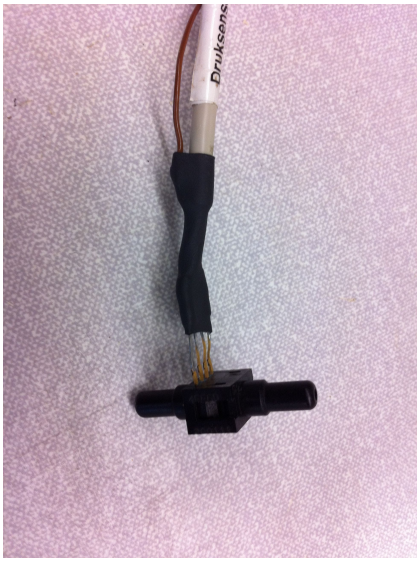

Figure 3.7: Differential Pressure Sensor, type RS 24 PCE (range 0.5psi)

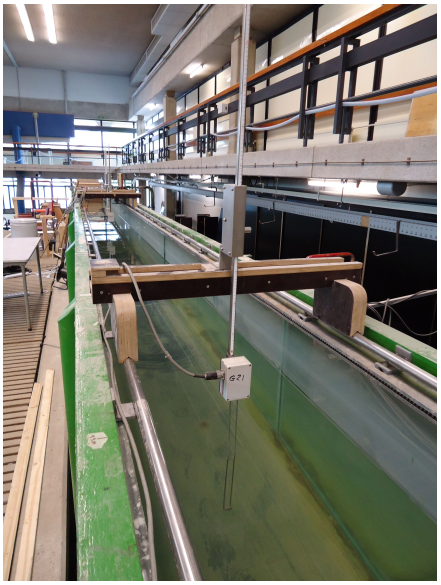

Figure 3.8: Wave Gauges

Figure 3.7 and 3.8 shows both sensors. In Figure 3.9 a sketch is drawn for the total setup. Wave gauges in front and at the back of the structure measure the water levels, and pressure sensors are connected with ∅ 6 mm sensortubes.

An important, and sometimes frustrating, problem of the pressure sensors is the necessity of having a closed system without any air bubbles. This in order to assume that the pressure difference cannot be absorbed in the system itself before it reaches the sensors. If the wave hits the sensorpoints there is a small delay before the pressure signal reaches the electronic pressure sensors. This delay is however negligible low (order of milliseconds).

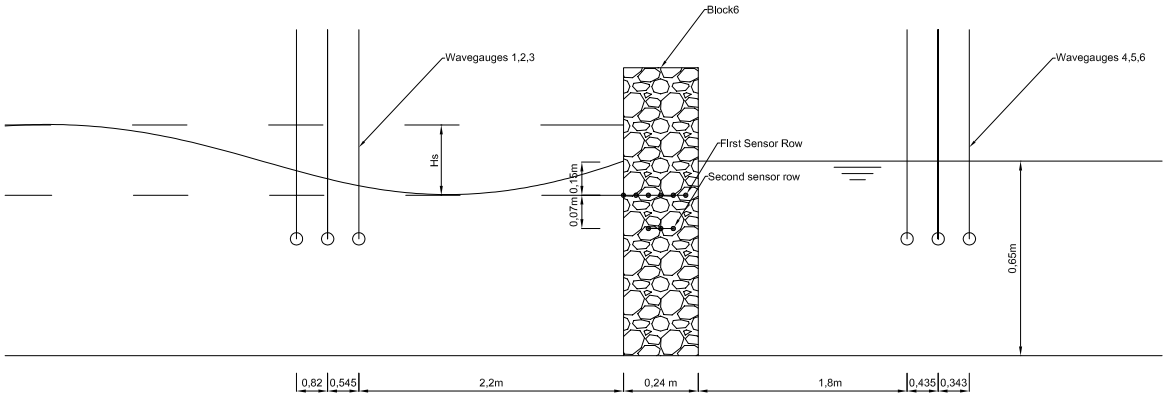

Figure 3.9: Detail of sensor setup

The exponential decay model is a one dimensional solution (only x direction), it suggests that the decay factor is constant over the depth. Troch (2000) concluded out of small scale physical experiments, that this isn't true. The depth of measurement influences the damping. That's why it's interesting to measure the pressure at various depths. The depth of the placement is limited by the SWL and the wave height. In order to make sure that under no condition the top of the tube will become dry, a minimal depth of 0.7 times the wave height below the SWL should be used. For that reason the first row of sensorspoints is at 50 cm depth and the second row at 43 cm depth.

The sensorpoints are placed in such a way that the damping process (smallest scale) can be measured. However, it also needs to be physically possible to fit the sensors tubes inside the block. This is why an offset in the order of 4 cm is used between the different sensorpoints. For all samples a sensorlocation at the outer side and inner side of the block is placed. The placement method of all sensors is summarised in Table 3.5.

Block	**Thickness**	**Nr of sensors**	**Placement Method**	**Appendix**
Block 2	88 mm	2 outer, 1 internal	Drilling holes	Appendix D.1
Block 3	132 mm	2 outer, 2 internal	Drilling holes	Appendix D.2
Block 5	160 mm	1 outer, 6 internal	Tubes can be inserted through the pores	Appendix D.3
Block 6	240 mm	2 outer, 5 internal	Tubes can be inserted through the pores	Appendix D.4

Table 3.5: Placement method of the sensors for the different blocks

With two sensorspoints outside the structure the reference water levels can be measured. These sensorpoints have a pressure equal to the SWL. Combining this data with the internal sensorpoints, a reconstruction can be made of the water levels and pressures through the sample.

The sensors tubes are tiny tubes in the order of 6 mm and are made out of hard plastic to prevent pressure loss by stretching of the tubes. For the blocks with a smaller d_{n50} (blocks 2 and 3) the placement of the sensor tubes was done by drilling in the monster from the front of the structure. The drilling was done by a diamond drill to prevent damaging the surrounding structure. For blocks 5 and 6 it was possible to enter the pores with the tubes without drilling.

Unfortunately the placement of the sensors and the sensors itself always influence the measurements. Also the location of the sensor in the porous flow field influences the measured pressures. The entrance can be blocked by a big stone, giving different results than when the entrance was a relatively large pore. The direction of the sensorpoints in relation to the mean flow influences the measured pressures, though this effect is totally random because the geometry of the pores is random.

3.5 Total Measurement Plan

The results of the first tests showed that in a short time a stable pattern of reflection and transmission is created. Most tests are done for a total period of 1.5 min till 3 mins. As the forcing by the wavemaker is done for every test the same, and the structure is in a fixed position, repetition tests are not necessary. Nevertheless, they were carried out at the start of the project and showed, no difference as expected.

The total range of measurements is:

Variable	**Range**
Dn50	0.020-0.039 m
Hs	0.025-0.150 m
Tp	1-6 s
y' (height of measurement below SWL)	15-22 cm
Thickness	88-240 mm

Table 3.6: Total measurement range

In Appendix E the full table of measurements can be seen. Per block a 4x4 matrix is tested with varying wave height and period. In addition to the 64 tests, 2 extra tests are performed in order to clarify some questions which raised from the first set of tests.

- How large is the influence of the wave reflection from the end of the flume?
- How does the trend continue for cases with a lower wave steepness?

For the first question it is required to investigate the reflection of waves from the wave damper on the end of the flume. For this test a small wave train is created with the

wavemaker and it can be examined how much reflection is visible from the end of the flume. The wavemaker can not make single waves and always needs to make a few smaller waves before it can make the desired wave, so by letting it generate for 2-3 wave periods the wave train can be created. Four tests were performed with period ranging from 1.0 s till 3.0 s and a wave height of 0.125 m. These tests are done with a structure and without a structure in the flume.

The second set of tests includes tests to see how the trend outside the measured domain continues. Since most of the measurements will be done for quite steep waves with a steepness of 1% till 6% it is interesting to see the behaviour in a different wave region. The extra tests are test numbers 65 till number 72 in Appendix E.

Chapter 4

Experimental Results

This chapter discusses the results from the experiments. The chapter is divided into two sections. First the general observations are discussed in Section 4.1. Then in Section 4.2 the results of the pressure sensors are discussed and finally Section 4.3 discusses the results from the wave gauges.

4.1 Observations

Figure 4.1: Peak of the wave in front of the block, note the water level difference over the block.

Figure 4.2: Trough of the wave in front of the block, note the water level difference over the block.

In Figure 4.1 the peak of the waves is on the location of the block. A water level difference is created over the block since the water level in the block and behind the block can't rise as fast as in front of the block. The level difference causes a pressure difference which pushes the water through the block. In Figure 4.2 the next moment can be seen, now the trough is in front of the block, again the water level in the block and behind the block can't follow the quick motion and a water level difference is created. This causes a flow back in the direction of the wavemaker. The waves cause an oscillatory flow inside the block compensating for the water level differences.

In Figure 4.3 the air bubbles at the back of the block can be seen. The pores in the wave

Figure 4.3: Top view of the back of the block

zone are continuously wetted and dried. Part of the air gets trapped in the flow and is pushed out with the flow.

Another observation is that the wave pattern in front of the block evolves into a regular standing wave pattern as expected. In some very steep wave cases however a standing wave pattern perpendicular to the main wave direction was seen because of a slight asymmetry in the setup.

4.2 Pressure Sensor Results

For comparison purpose one wave case will be picked out in order to analyze the results. This will be the case with a wave height of 0.125 m and a period of 2 s.

4.2.1 Raw Data of Pressure Sensors

In Figure 4.4 the results for one wave period are shown. At first glance, this is a rather chaotic picture. In order to capture all processes, the sampling frequency was increased after the first test from 100 to 2000 Hz. At the start of the measurement the noise is really low (order 0.5 mm). When the first waves start to interact with the structure, all kinds of extra harmonics are introduced. These extra harmonics have a different frequency than the standard background noise frequency. The most plausible explanation is resonance of waves inside the pores. Because every pore has a different geometry all pores will give a different signal.

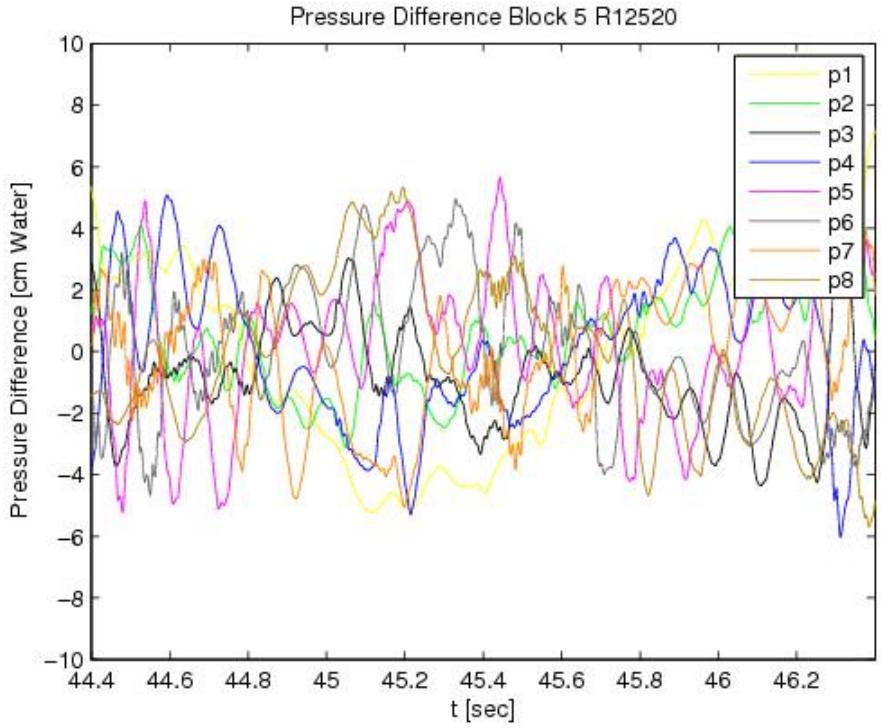

Figure 4.4: Raw Data of 8 pressure sensors for one wave period for block5. P1 till P8 represent 8 different sensors, P1 is connected with outside reference level while P2 till P8 are internal connected.

4.2.2 Filtered Data

The resonance of waves inside the pores is not of particular interest for this study. Therefore the harmonics with a different period than the wave period need to be filtered out of the signal. This is done by a so-called Butterworth filter with a passband and a stopband. It has the following characteristics for the case of a wave period of 2s:

- Fpass= 0.5 Hz, the frequency of the main harmonic
- Fstop= 1 Hz, twice the frequency of the main harmonic
- Apass = 0.5 dB
- Astop= 12 dB

For different wave periods only the Fpass and Fstop will be changed as described, so for a wave period of 3 s the Fpass will become 0.333 Hz and the Fstop will become 0.666 Hz. The data has for every wave period a different phase difference. An artificial delay is introduced to prevent phase differences, the results are shown in the Figures 4.5 to 4.12 for all eight pressure difference sensors. Comparing the filtered data in Figure 4.5 with Figures 4.6 to 4.12 shows clearly that one of the problems causing the noise are the sensors that compare the pressure difference between two oscillating pores. The data in

Figure 4.5 is far more regular because it only measures the pressure difference between one oscillating pore and the external SWL. Overall, the filter performs reasonably well and it clearly distinct the first harmonic oscillation.

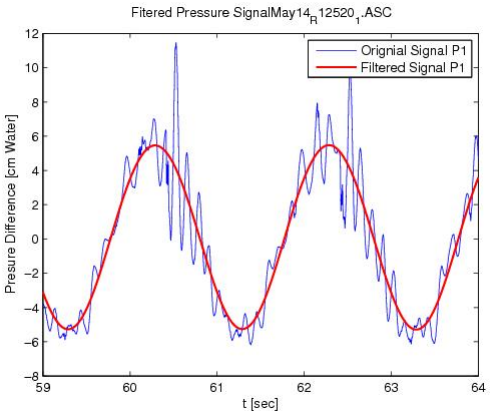

Figure 4.5: Filter comparison sensor 1

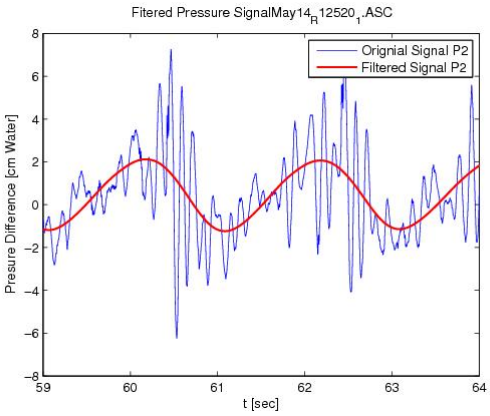

Figure 4.6: Filter comparison sensor 2

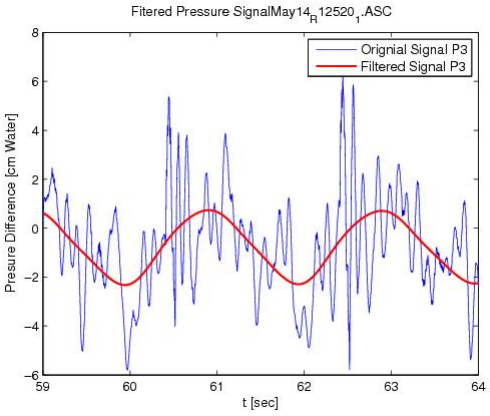

Figure 4.7: Filter comparison sensor 3

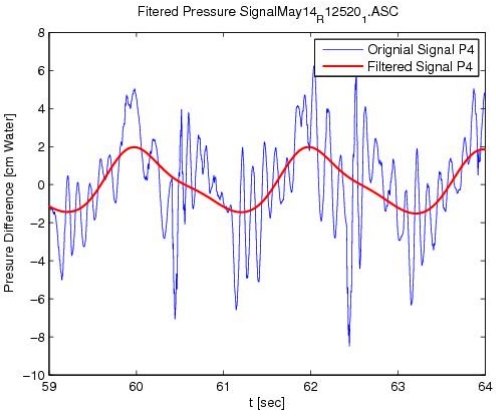

Figure 4.8: Filter comparison sensor 4

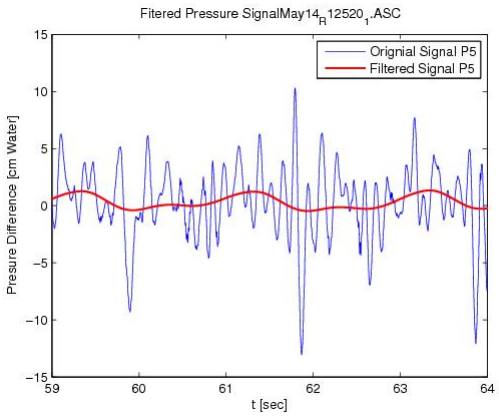

Figure 4.9: Filter comparison sensor 5

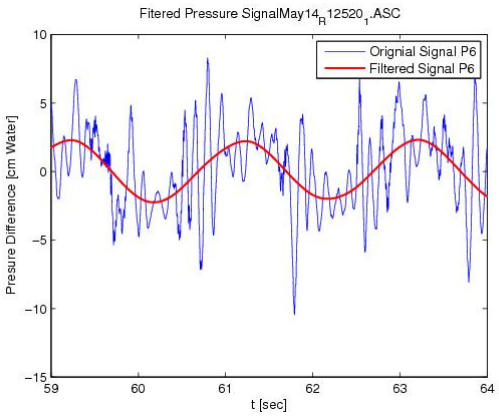

Figure 4.10: Filter comparison sensor 6

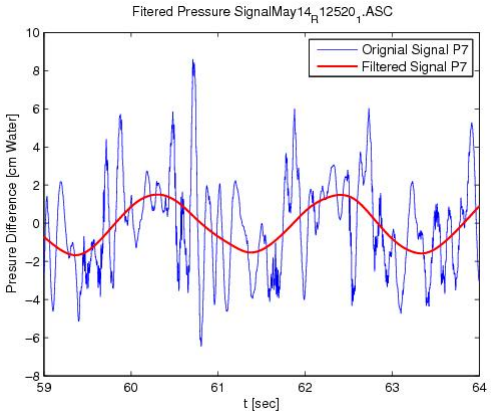

Figure 4.11: Filter comparison sensor 7

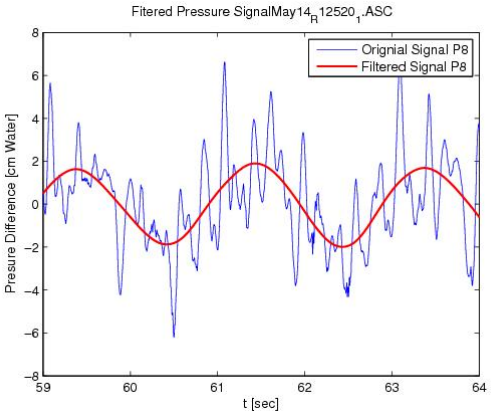

Figure 4.12: Filter comparison sensor 8

4.2.3 Absolute Pressures

The next step is to add the pressure differences and reconstruct the absolute pressures at certain points. In Figures 4.13 and 4.14 the results are plotted for block 5. One would expect a sort of exponential decay of the pressure further inside the block. However, from these pictures it seems that the pressure decay is very irregular. Figure 4.13 shows that the largest pressures are at 16 cm (front of the block), followed by respectively 8 cm, 12 cm and 4 cm.

Figure 4.14 shows a similar irregular picture. Here the pressure at 8 cm is largest while the pressure at 12 cm and 4 cm is smaller.

When looking at the results for block2 (Figures 4.15 and 4.16), the results seem more logical. There is a logical pressure decay throughout the block. Pressures do not seem to vary much between the different depths. Though, the pressures measured at a deeper location are a bit smaller

Looking at the circuit used for these measurements (Appendix D.1) it is possible to cal-

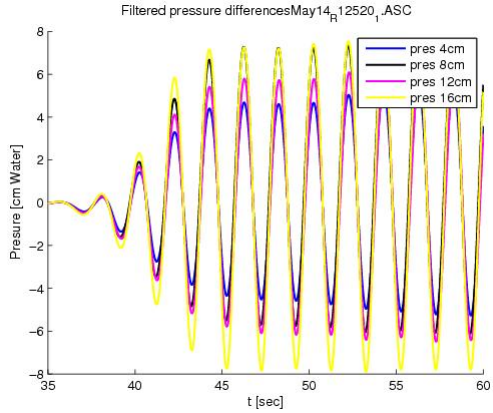

Figure 4.13: Absolute pressures on different points (16cm is front of block, 0cm is back of block), depth is 50cm. Results for block5

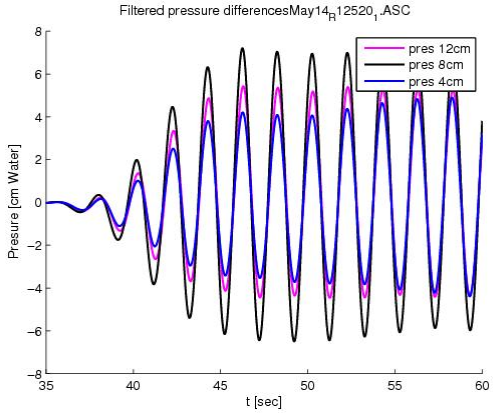

Figure 4.14: Absolute pressures on different points (16cm is front of block, 0cm is back of block), depth is 43cm. Results for block5

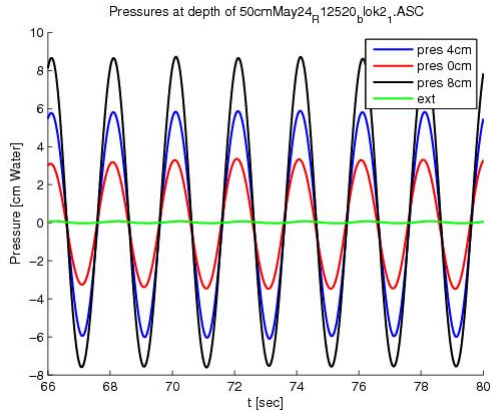

Figure 4.15: Pressures block2, depth 50cm

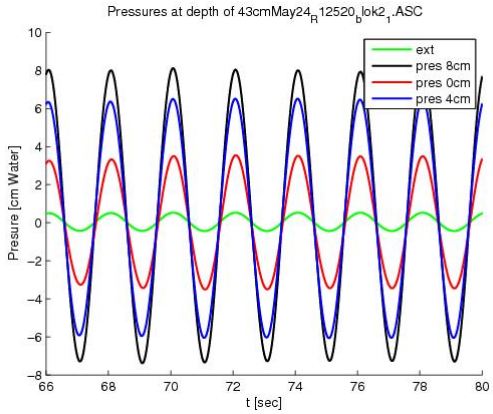

Figure 4.16: Pressures block2, depth 43cm

culate the measuring error. When adding all pressures from a reference point till the next reference point the only difference is a measuring error. This is probably the result of a slightly wrong calibration. These measuring errors are indicated with the green lines in Figure 4.15 and 4.16.

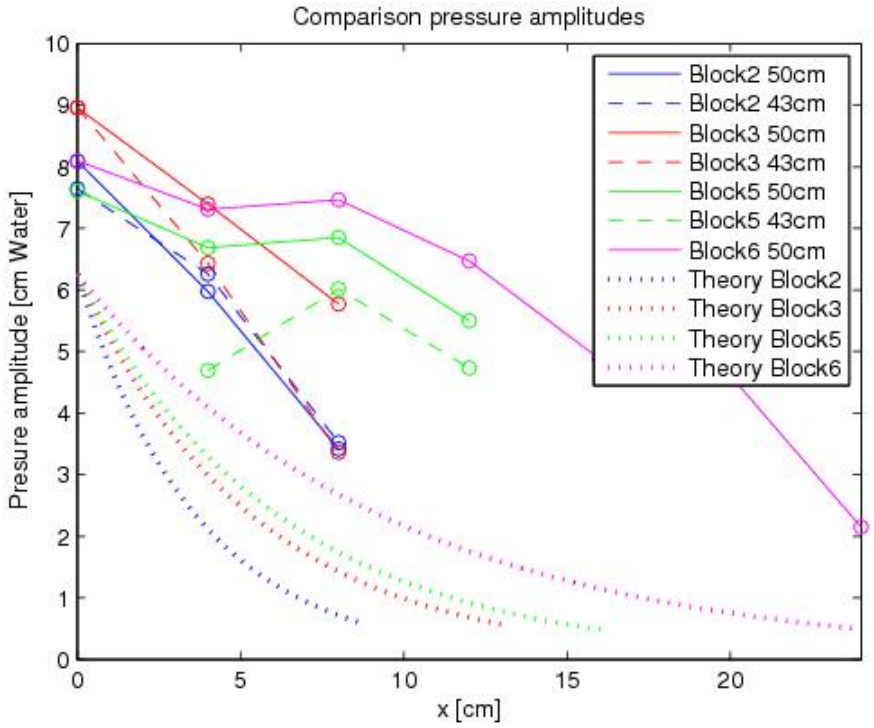

Figure 4.17: Comparison of measured amplitudes of different blocks (solid and dashed line) for the case of H=0.125 and T=2s with the theoretical pressure decay (dots) calculated with eq. 2.48 and eq. 2.50, assuming a reference pressure according to eq. 2.51

In Figure 4.17 the different amplitudes are plotted against the distance inside the block. It must be noted that individual results can have an error up to 20%. As said before, the pressure decay for the blocks with an irregular placement of the sensors (block5 and 6) generate less logical results than the blocks with the drilled holes and the uniform direction (block2 and 3). However it becomes evident that the longer structures in general generate a higher starting pressure, see block3 vs block2 and block6 vs block5. Overall, there is also a clear tendency of longer blocks having a less steep decay.

The pressure decay doesn't give an exponential decay as expected from the theory. In Figure 4.17 the theoretical decay is computed for the different blocks which shows that the reference pressure is in the measured case higher. The trend is quite different from the experimental results however, it doesn't look like an exponential decay. Overall, it can be stated that the theoretical pressure distribution underestimates the pressures. This could be due to the fact that the theory is developed for core materials while this is an armour layer.

In Figure 4.18 the pressures are normalized for the distance in the block. This shows that the trend for all blocks is roughly the same with a linear pressure decay.

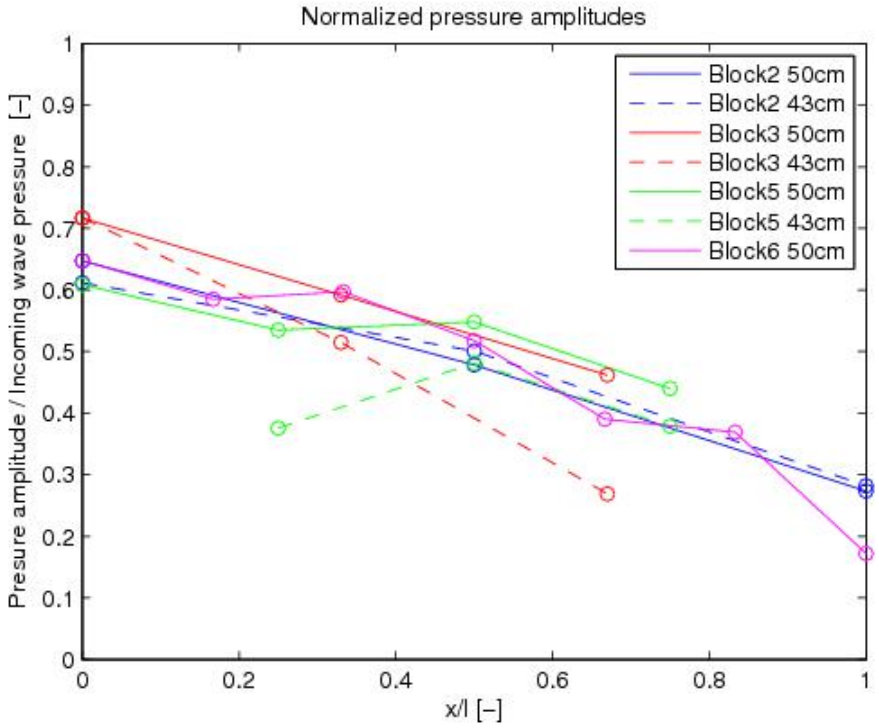

Figure 4.18: Pressure amplitude normalized with incoming wave pressure plotted against the normalized distance in the block x/l

4.2.4 Conclusion Pressure Measurements

Looking at the total results of the pressure measurements there are three problems:

- There is probably still a rather large measuring error, in the order of 10-20 %. The system is very sensitive to tiny air bubbles and calibrations are difficult. Some results show an unlogical pressure amplitude increase over small sections.
- Local geometry has a strong effect on the outcome. The shape of the pore plus the direction of the sensor and surrounding of the sensor determines locally the pressure more than the theoretical pressure decay. Taking into account the total result, there is no clear exponential decay visible.
- The total pressures are of the correct magnitude but slightly higher than the theory prescribes. They show a different trend (no exponential decay). It would be convenient for a proper comparison to measure only dynamic or static pressures. This way it is easier to relate the pressures to the Forchheimer flow formula.

Because of these points the pressure data has not proven to be sufficiently reliable to use for calibrating a numerical model. There are simply too many random effects.

4.3 Transmission and Reflection

Reflection and transmission data can be obtained by using the results of the wave gauges. As they are placed in groups with a fixed distance, it is possible from the time series to decompose the signal into an incoming wave and a reflected wave. This section will discuss the results of the case with a wave height of 0.125m and 2s unless mentioned otherwise.

4.3.1 Explanation method and error analysis

The raw data consists of time series of surface elevations. Contra-dictionary to the raw data of the pressure sensors the raw data of the wave gauges shows hardly any noise and can be used for analysis. They were sampled on the same frequency as the pressure sensors, 2000 Hz.

Reflection and transmission can be evaluated with the help of a Matlab script called refreg. This script is based on the method of Goda and Suzuki (1976). A summary of the method can be found in Appendix F. The script analyses two time signals with a fixed distance and the script can decompose the incoming wave and reflected wave amplitudes.

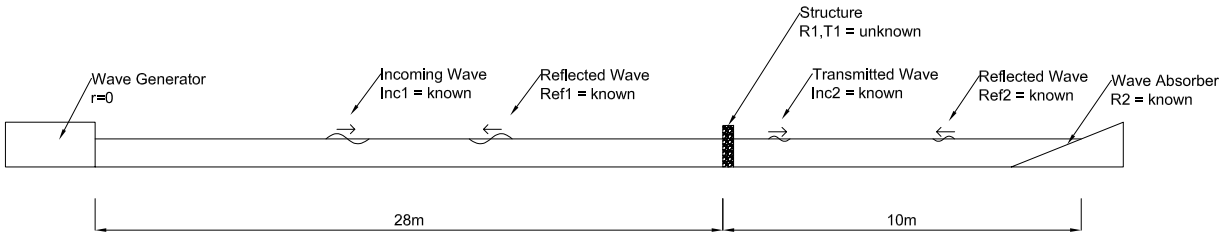

Figure 4.19: Definition skecth of incoming and reflecting waves per section

In Figure 4.19 the situation is sketched. Based on the incoming and reflected wave signals in front and at the back of the structure, three different variables are defined:

$$R_1 = \frac{H_{ref,1}}{H_{inc,1}} \tag{4.1}$$

$$T_1 = \frac{H_{inc,2}}{H_{inc,1}} \tag{4.2}$$

$$Dissipation = 1 - \left(R_1^2 + T_1^2\right) \tag{4.3}$$

4.3.2 Discussion of reflection from wave absorber

In Table 4.1 the results for block 5 are presented. What is remarkable is that the reflected wave in the second section ($H_{ref,2}$) still has a significant height. Only for the cases with a period of 1 s it is acceptable low. For other cases the reflection at the end of the flume

Wave Height (m)	**Period** (s)	$\boldsymbol{H_{inc,1}}$ (m)	$\boldsymbol{H_{ref,1}}$ (m)	$\boldsymbol{H_{inc,2}}$ (m)	$\boldsymbol{H_{ref,2}}$ (m)
0.075	1	0.0337	0.0204	0.0109	0.0003
0.075	1.5	0.0354	0.0179	0.0142	0.0059
0.075	2	0.0353	0.0199	0.0216	0.0087
0.075	3	0.0371	0.0220	0.0235	0.0113
0.100	1	0.0425	0.0252	0.0131	0.0014
0.100	1.5	0.0470	0.0253	0.0171	0.0072
0.100	2	0.0472	0.0272	0.0263	0.0102
0.100	3	0.0498	0.0315	0.0294	0.0152
0.125	1	0.0541	0.0283	0.0145	0.0011
0.125	1.5	0.0580	0.0322	0.0194	0.0079
0.125	2	0.0583	0.0351	0.0311	0.0122
0.125	3	0.0615	0.0401	0.0331	0.0158
0.150	1	0.0640	0.0251	0.0154	0.0024
0.150	1.5	0.0684	0.0392	0.0216	0.0085
0.150	2	0.0698	0.0435	0.0366	0.0147
0.150	3	0.0713	0.0474	0.0390	0.0208

Table 4.1: Example of measured wave heights for block 5. Note the relatively high $H_{ref,2}$

(R_2) varies between 38 % and 53 %. This wave will travel back to the structure and will interact with the incoming waves creating an increased reflection and transmission.

Another note is the measured incoming wave height in comparison to the wave height given to the wavemaker. On average the analysed results show an incoming wave height of roughly 0.5 cm lower than the intended wave height.
Extra tests were carried out with single wave groups. There were two kind of tests:

- With structure
- Without a structure

The tests were performed with the wave gauges spread out over the flume in order to capture the wavetrain at different places. See Figure 4.20 for the setup.

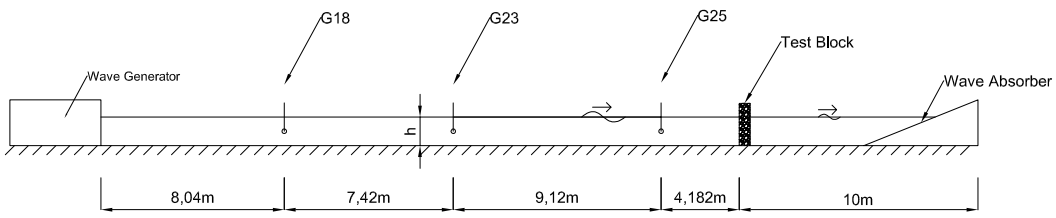

Figure 4.20: Setup of test with a single wave train, note that the wave gauges are spread out over the flume

In Figure 4.21 the result of the experiment without a structure is shown. Analysis of the travel times shows that the wavetrain travels with group velocities till the absorber at the end of the wave flume. The reflections are decomposed in higher harmonics which each travel with their own group velocity. So for the case with waves with a period of 1.5s the first reflection has a period of 1.5s, the second reflection has a period of 0.75s and the third reflection has a period of 0.5s. In Table 4.2 the peaks of the different wave trains are compared.

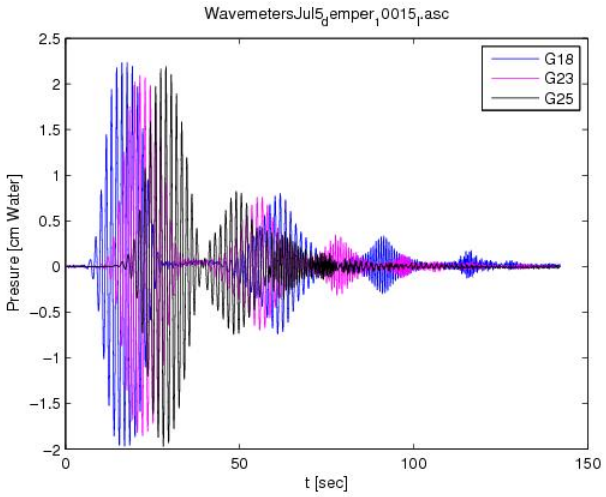

Figure 4.21: Small wave train of waves with height of 0.1m and period of 1.5s interacting with absorber at end of flume.

Period	**1st Reflection** (%)	**2nd Reflection** (%)	**3rd Reflection** (%)	**4th Reflection** (%)
1.0s	14.7	6.1	-	-
1.5s	34.9	14.6	7.7	3.0
2.0s	38.3	19.9	9.2	4.3
3.0s	43.9	8.6	4.2	-

Table 4.2: Measured reflection from the wave train tests performed without a structure in the flume

Based on the total reflections it can be concluded that the reflections measured before are accurate. In Figure 4.22 the results of the tests with a structure are plotted. For the tests performed with a structure the reflection returns much faster to the wave gauges. As it is impossible to create short enough wave trains, the flume is physically not long enough in order to separate the different reflections from the wave train. The first incoming wave seems to have a shorter time span than the 1st reflecting signal. The explanation for this is that the reflection from the end of the flume and the reflection from the structure overlap. Consequently it is impossible to separate the signals and quantify the different effects.

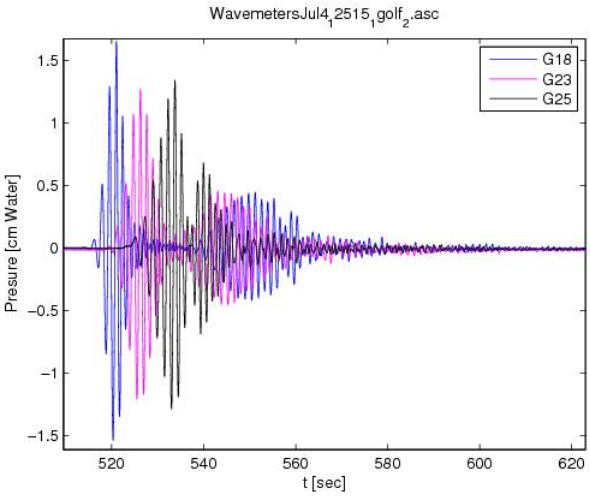

Figure 4.22: Small wave train of waves with height of 0.125m and period of 1.5s interacting with block3 and end of flume.

The conclusion from the different tests with the wave train is that the reflection at the end of the flume is significant and does influence the experiment. Therefore it is decided to correct that reflection on a theoretical basis.

4.3.3 Correction Method

Based on the situation drawn in Figure 4.19, the four incoming and reflected waves can be calculated from the data analysis. However, the definition of reflection and transmission in Equations 4.1 and 4.2 are not valid if there is a reflection coming from the end of the flume. The following assumptions have been applied:

- The wave generator has no reflection for all waves
- The porous structure has an unknown reflection r1 for all waves
- The porous structure has an unknown transmission t1 for all waves
- The wave absorber has a known reflection r2 for all waves
- The wave absorber has no transmission for all waves.

And by adding the additional reflected and transmitted waves from the reflection at the end of the flume the following equations can be derived:

$$H_{ref,1} = R_1 H_{inc,1} + T_1 H_{ref,2} \tag{4.4}$$

$$H_{inc,2} = T_1 H_{inc,1} + R_1 H_{ref,2} \tag{4.5}$$

$$H_{ref,2} = R_2 H_{inc,2} \tag{4.6}$$

The system comes down to a system of two equations and two unknowns.

$$\begin{pmatrix} H_{inc,1} & R_2 H_{inc,2} \\ R_2 H_{inc,2} & H_{inc,1} \end{pmatrix} \begin{pmatrix} R_1 \\ T_1 \end{pmatrix} = \begin{pmatrix} H_{ref,1} \\ H_{inc,2} \end{pmatrix}$$

By solving the equation the transmission and reflection coefficients (R1,T1) could be found without reflection from the end of the flume. This will result in a lower reflection and transmission coefficient. These will be used in the rest of this thesis.

4.3.4 Corrected experimental results

The experimental results are plotted in Figures 4.23 and 4.24. The data is plotted against the wave steepness. The results with a similar period are grouped together. When comparing the results to Figures 2.11 and 2.12 a similar trend as measured by Keulegan is identified. The steeper the waves, the more reflection and less transmission. Keulegans graphs show an intersection between the reflection and transmission at a wave steepness of roughly 0.01. This is roughly comparable to this dataset. Nevertheless, there is not a direct relation between wave steepness and reflection/transmission, a different combination of wave height and period will give different results.

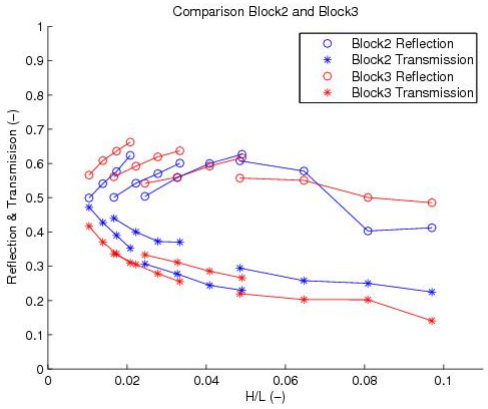

Figure 4.23: Comparison Reflection and Transmission for block 2 and 3

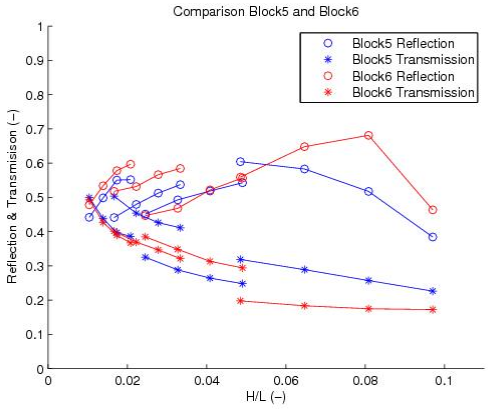

Figure 4.24: Comparison Reflection and Transmission for block 5 and 6

Comparing the longer blocks (6 vs 5 and 3 vs 2) it appears that when the length of the block increases the reflection is larger and the transmission gets smaller which is in line with the theory. Though not all data are consistent with this theory, in general the data for the waves with a smaller steepness show more consistency with that pattern.

The data for a period of 1s, which has the largest steepness, has the largest deviations. Especially the reflection for very steep cases shows a different pattern than the rest of the dataset. This could have two reasons:

- Very steep waves had the largest problem with the asymmetry of the structure as can be seen in Figure 3.4. This resulted sometimes in a standing wave pattern perpendicular to the main wave direction.
- The waves showed some beginning breaking processes along the edges of the flume.

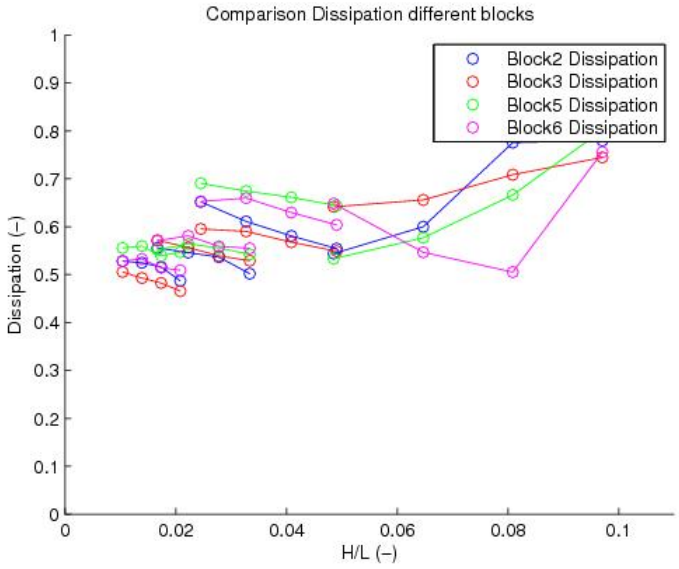

Figure 4.25: Comparison of dissipation of different tests grouped per block

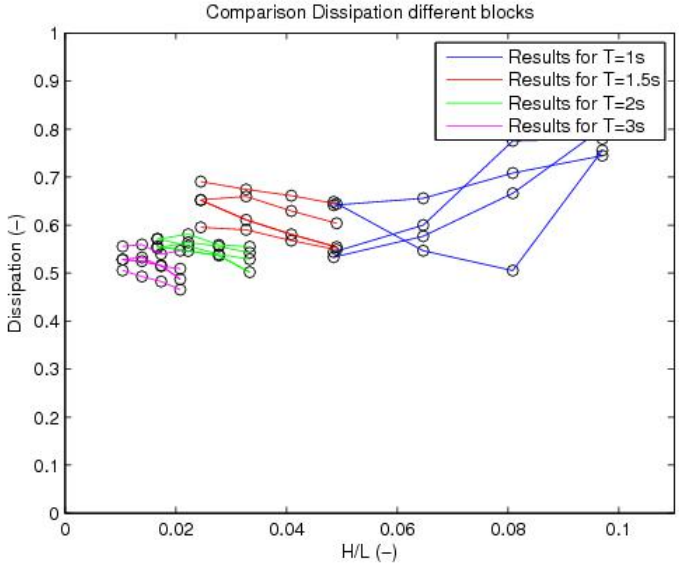

Figure 4.26: Comparison of dissipation of different tests grouped per period

In Figure 4.25 the dissipation for all different blocks are plotted against the wave steepness. The results are grouped per block and results with a similar period are connected with solids. In Figure 4.26 the same results are grouped per period which clearly shows that

the dissipation is mostly depending on the period and is almost independent of the wave height.

4.3.5 Conclusion Reflection and Transmission analysis

The data from the wave gauges is the most reliable because they can be compared with earlier experiments and they are independent of the local geometry. The main issues are the reflection at the end of the flume and the partial blocking of the flume due to the setup. The correction method for wave reflection from the end of the flume makes the data suitable to compare with analytical and numerical results. The data shows similar patterns as expected from the theory and earlier experiments.

Measuring the reflection and transmission seems a reliable way to judge the wave interaction with a porous structure as the sensors are placed far outside the structure and do not influence the measurements. In addition, it cancels out the local effects in the pores because the result is a reflection and transmission coefficient which is a more global result of the wave interaction. For these reasons, it is decided to use the reflection and transmission data for the further analysis of this study.

Chapter 5

Analytical Model

This chapter discusses the analytical model described in section 2.3. The analytical solution and the experimental are compared in this chapter

5.1 Usage of the Analytical Model

The analytical solution described by Madsen and White (1976) is explained in Section 2.3. The usage of the analytical model is simple, it returns the reflection and transmission coefficient for the case designed by the user. The following variables need to be defined.

Variable	**Symbol**	**Unit**
Incident Wave Amplitude	a_i	(m)
Period	T	(s)
Length of Porous Structure	l	(m)
Water depth	h_0	(m)
Stone size	d_{n50}	(m)
Porosity	n	(-)
Laminar Forchheimer Constant	α	(-)
Turbulent Forchheimer Constant	β	(-)

Table 5.1: Input variables for the analytical model

All these variables are experimentally derived and can be found in Section 3.2. This makes it possible to obtain an analytical solution for all 72 wave cases.

5.2 Comparison with Experimental Data

In Figures 5.1 to 5.4 the results of the analytical model are plotted against the experimental derived values. For all simulations, the RMSE and the Bias are also given. A positive bias means an overestimation of the analytical model and vice versa. It can be concluded that the analytical model is fairly close to the experimental results but shows for all cases an overestimation of the reflection and transmission. This seems to be an issue with a lack of dissipation in the analytical model.
In general, the transmission seems to be quite accurate for the wave cases of 2.0s and 3.0s while it analytically overestimates for the cases of 1.5s and 1.0s. The reflection for very

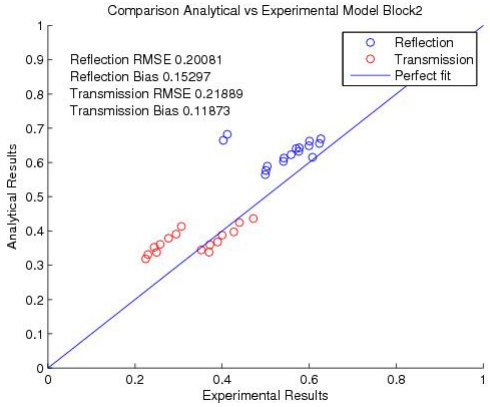

Figure 5.1: Analytical results vs Experimental Results Block2

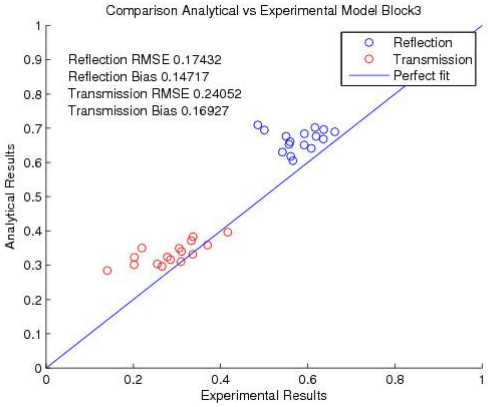

Figure 5.2: Analytical results vs Experimental Results Block3

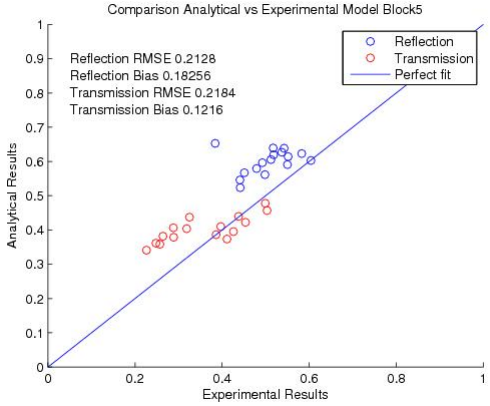

Figure 5.3: Analytical results vs Experimental Results Block5

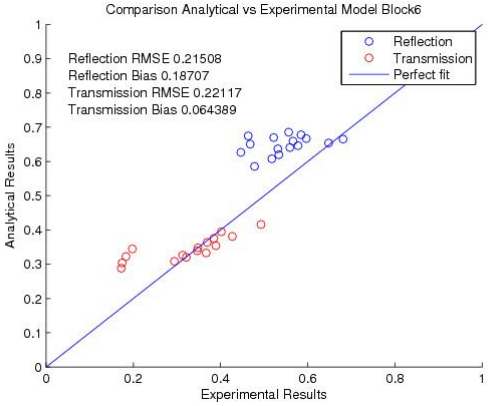

Figure 5.4: Analytical results vs Experimental Results Block6

steep cases (period of 1.0s) show also the biggest offset with the analytical model.

In Figure 5.5 the analytical and experimental dissipation for all cases is plotted. This indicates that for the steeper wave cases the dissipation of the analytical model is underestimated. Moreover, it indicates that for almost all cases the analytical model gives a dissipation of 0.5. This explains the bias for reflection as well as transmission for the steeper wave cases.

The lack of dissipation can be explained as well, by taking into account the equations. The advective term is neglected in the analytical model. For very steep waves the $u\frac{\partial u}{\partial x}$ starts becoming important.

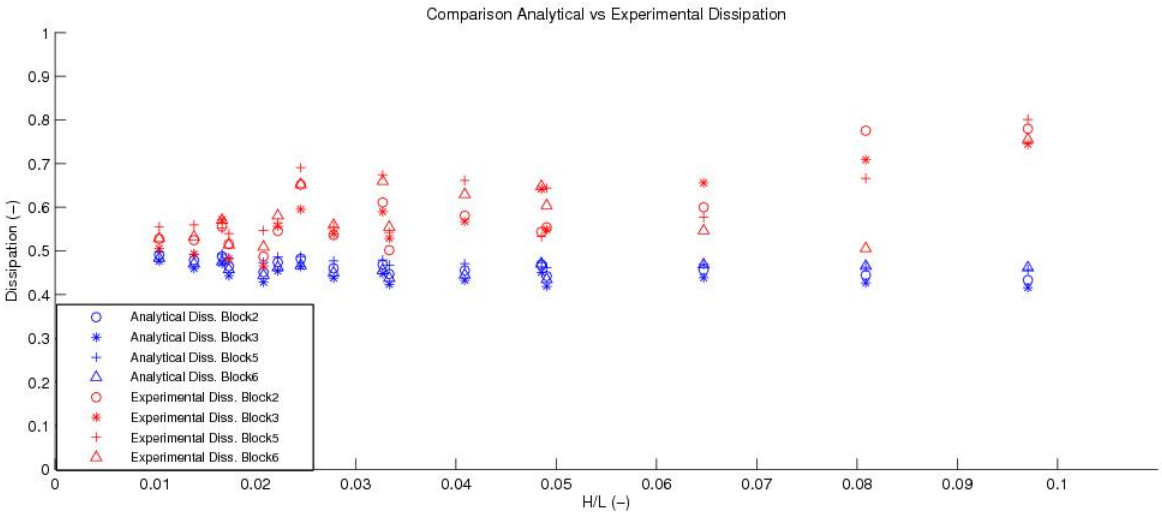

Figure 5.5: Comparison of analytical and experimental dissipation

5.3 Conclusion regarding analytical model

The analytical model performs fairly well. Without any tweaking it is possible to give a proper estimation of the reflection and transmission for all cases. The strange thing is that it gives an overestimation for both the reflection and transmission. It performs best for the waves with a lower steepness. This is due to the dissipation which is not correct for the steeper wave cases as shown in Figure 5.5. Overall the analytical model gives a quite accurate prediction.

Therefore the model could be used to determine some important variables for the numerical model. It is for example possible to calculate a characteristic velocity amplitude and therefore possible to determine a KC and Re_d number for the different wave cases. With these values it is also possible to determine the non-static β_{NS} according to Equation 2.41. Table 5.2 below gives the range in which these tests are done according to the analytical model.

Note that this Re number is determined with $\hat{u_f}$ instead of an averaged u_{char} which explains the higher Reynolds numbers. The range of the Reynolds numbers is comparable to the range for which the experiments were done by Zeelenberg and Koote (2012).

Experiment	**KC Range** (-)	$\boldsymbol{Re_d}$ (-) **Range**
Block2	14-73	2300-4100
Block3	12-64	2000-3600
Block5	6-37	4500-8800
Block6	5-33	3800-7600
Total Experiments	5-73	2000-8800

Table 5.2: Total range of KC and Re_d numbers according to the analytical model

Chapter 6

Numerical modeling

This chapter discusses the numerical modelling with the SWASH model. The experimental and analytical results are compared with the numerical solution. Also a numerical approach to investigate P values is described. In this chapter the default case will be a wave height of 0.125m and a period of 3.0s unless mentioned otherwise.

6.1 The SWASH model

SWASH is a recently developed numerical package by the TU Delft. It can be downloaded from http://swash.sourceforge.net/ and is constant under development. The name SWASH is an acronym of Simulating WAves till SHore. This report used version 1.10 of SWASH. From the website:

"SWASH is a non-hydrostatic wave-flow model and is intended to be used for predicting transformation of surface waves from offshore to the beach for studying the surf zone and swash zone dynamics, wave propagation and agitation in ports and harbours, and rapidly varied shallow water flows in coastal waters."

SWASH uses the nonlinear shallow water equations including non-hydrostatic pressures as described in Section 2.1.2. The model recently got extended into covering porous flow and the ability to predict partial reflection and transmission. The Forchheimer relation is included in the porous momentum equations by means of two extra friction terms f_l and f_t. Every grid cell has a porosity ranging from n=0 (wall) till n=1 (pure water). The governing equations are:

$$\frac{\partial \eta}{\partial t} = -\frac{\partial \left(\frac{q}{n}\right)}{\partial x} \tag{6.1}$$

$$\frac{1}{n}\frac{\partial u}{\partial t} + \frac{\frac{u}{n}\partial \frac{u}{n}}{\partial x} + g\frac{\partial \eta}{\partial x} + \cdots + f_l u + f_t u\,|u| = 0 \tag{6.2}$$

$$f_l = \alpha_E \frac{(1-n)^3}{n^2}\frac{\nu}{d^2},\ f_t = \beta\frac{1-n}{n^3}\frac{1}{d} \tag{6.3}$$

where η denotes surface elevation, ν the kinematic viscosity, and u the horizontal flow velocity, d is the grain size and g is the gravitational constant. The default value from

SWASH for $\alpha_0 = 1000$ and for $\beta_0 = 2.8$. However, the experimental obtained values will be used. Note that the Forchheimer equation is written in the form of Engelund (1953) which is slightly different than the form of (Burcharth & Andersen, 1995), see Equation 2.38.

$$\alpha = \alpha_E n\,(1 - n) \tag{6.4}$$

For typical porosities (n = 0.4) this means the alpha value entered in SWASH needs to be divided by roughly 4. The partial reflection and transmission were validated with the test case of Madsen and Warren (1984) described in Section 2.6

6.2 Numerical Setup

The numerical setup is made as close as possible to the experimental setup. In Figure 6.1 the setup is sketched. The choices made are explained in this section.

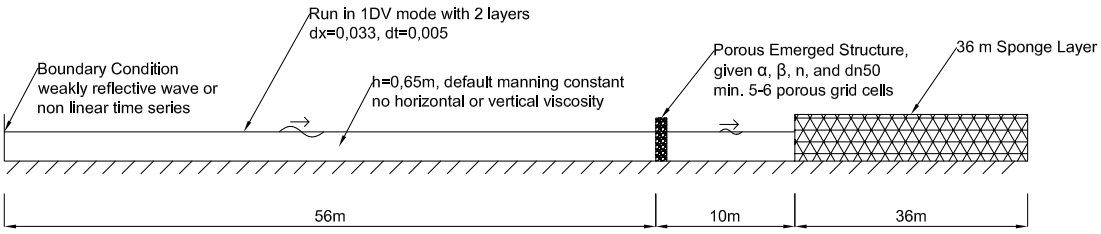

Figure 6.1: Numerical Setup used

6.2.1 Input

The outcome of the simulation depends on the period and wave height of the boundary condition and the variables of the porous part:

1. Laminar Friction constant (α)
2. Non Stationary Turbulent Friction constant (β_{NS})
3. Grain size (d_{n50})
4. Porosity (n)
5. Length of structure (l)

The domain consists out of two vertical layers, has no turbulent viscosity model and the default setting for the bottom friction constant. The initial conditions are set as stagnant water. The kh values for the different cases vary from 0.57 till 2.64.

As described earlier the α value has to be corrected with Equation 6.4. The biggest uncertainty is the turbulent β term. The β constant is corrected according to Equation

H_{inc} (m)	T (s)	KC (-)	β (-)	β_{NS} (-)
0.075	1	5.46	1.44	3.44
0.075	1.5	9.09	1.44	2.65
0.075	2	12.79	1.44	2.30
0.075	3	20.25	1.44	1.99
0.1	1	6.82	1.44	3.05
0.1	1.5	11.23	1.44	2.42
0.1	2	15.70	1.44	2.14
0.1	3	24.72	1.44	1.89
0.125	1	8.05	1.44	2.80
0.125	1.5	13.16	1.44	2.28
0.125	2	18.33	1.44	2.04
0.125	3	28.73	1.44	1.83
0.15	1	9.20	1.44	2.63
0.15	1.5	14.93	1.44	2.18
0.15	2	20.74	1.44	1.97
0.15	3	32.37	1.44	1.79

Table 6.1: Example of conversion of β to the non-stationary β_{NS} for block 6

2.41 for non stationary flow. For example, for block number 6 the $\beta = 1.45$. But by correcting the stationary beta with (1+7.5/KC) the equivalent beta for non-stationary cases could be derived. The Keuler Carpenter Number is calculated with the help of the analytical model.

6.2.2 Grid Resolution

The time integration method of SWASH is explicit, which means that in order to end up with a stable computation the CFL condition has to be fullfilled.

$$\frac{c\Delta t}{\Delta x} < 1 \tag{6.5}$$

Where c is the celerity of the signal which is the wave speed in this case. SWASH automatically adjusts the time step if the CFL condition is not fullfilled. For determining an accurate spatial resolution, different plots for a test case on block 6 are made with H=0.125 m and T=2s. In Figure 6.2 the results are shown for resolutions ranging from 45 points/wave till 225 points/wave. This is a very zoomed result, only the peaks show a significant difference. The results do not show a clear convergence pattern, but the errors between dx=0.02 and dx=0.05 are considerably smaller than compared to dx=0.10m. Based on this a resolution of dx=0.033 is chosen, since this gives a sufficient number of points/wave for the whole range of cases. As base timestep dt=0.005 is used, as stated before, timestep can be changed for individual cases in order to fullfill the CFL condition.

Porosity is imposed at the corners of the grid cells. The grid cell gets a porosity by interpolating the porosity of the corners. Because the structures are very small, it is computationally necessary to have enough porous grid cells in order to solve the porous

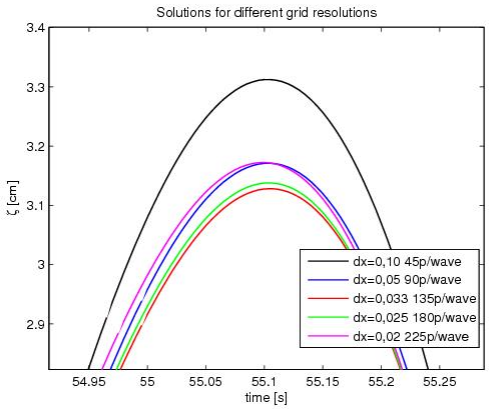

Figure 6.2: Water levels from gauge 1 compared for different spatial grids

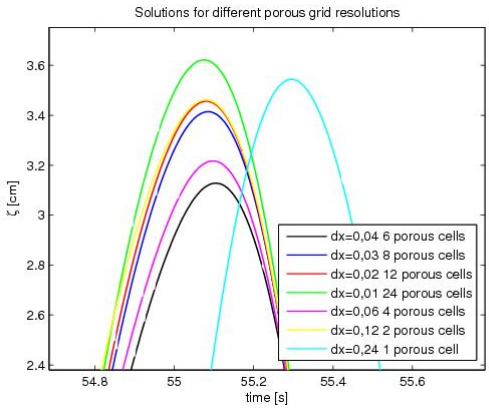

Figure 6.3: Water levels from gauge 1 compared for different porous grids

equations accurately. Recommended is a minimum of 4-5 porous grid cells. In Figure 6.3 different configurations are compared. The figure is very zoomed, only the peaks show a difference between the different cases.It can be concluded that at least two grid cells are needed for a correct phase. Looking at the amplitude, it can be concluded that the error between the different results is roughly twice as large as for the spatial grid computations in Figure 6.2. The numerical results do not show a clear convergence pattern but rather a general trend of a higher amplitude for a higher resolution. Therefore, it is decided to use a porous grid resolution of Δx =0.02 for all computations. This means a minimum of 4-5 porous grid cells for the smallest block (block2).

6.2.3 Output

The output consists out of three tables.

- The wave height H_{rms} is recorded for every section of the flume with intervals of 0.1 m.
- The 6 wave gauges record every 0.005 s the water level at the same location as the experimental wave gauges.
- The water level is stored in a table every 0.05s for every 0.1 m of flume.

This way it is possible to produce a total envelope of the recorded wave data conform Figure 6.4 and 6.5. But it is also possible to compare experimental wave series with numerical wave series since they are both recorded at the same locations.

6.2.4 Boundary conditions and Initial Conditions

The 1D model has two boundaries, one at the end of the flume and one at the start of the flume. The boundary condition at the start of the flume needs to be a wavemaker. Based

on Figure 3.6 it was concluded that the linear wave theory is not applicable for this case. That is why two different boundary conditions are examined.

- A weakly reflective regular linear wave boundary condition
- Timeseries of discharges for 2 layers of a non-linear incoming wave.

In Figure 6.4 and 6.5 the two different boundary conditions are plotted for a domain without a structure (n=1). It can be concluded that for the given circumstances the time series of a cnoidal wave show a more constant wave amplitude. There is a strange oscillation for the case with the linear forcing which might be caused by instabilities. For the very steep waves (cases with period of 1.0 and 1.5s) the weakly reflective boundary condition shows better results. However, there is still a significant amplitude loss. One big downside of the cnoidal wave is that it does not posess a weakly reflective characteristic. Therefore simulations have to be done in a short time to prevent wave reflection from the start of the flume returning into the domain. This is why the experimental flume length of 28 m is doubled till 56 m for the numerical computations. This allows simulations of 1 min for all waves without reflections from the wavemaker influencing the results.

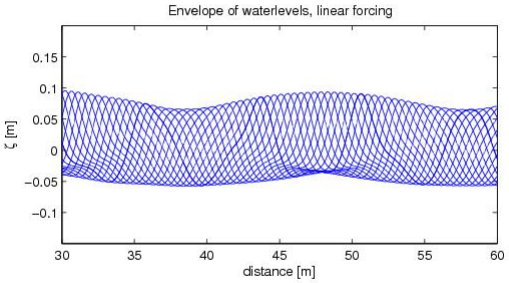

Figure 6.4: Envelope results for regular a weakly reflective boundary condition. H=0.125 m, T=3 s.

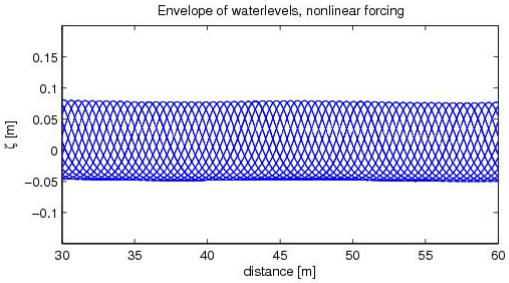

Figure 6.5: Envelope results for time series of a cnoidal wave as boundary condition. H=0.125 m, T=3 s.

The boundary condition at the end of the flume is not entered into SWASH. SWASH uses sponge layers at the end of the domain to absorb the waves. For good damping characteristics sponge layers of 3-5 times the wave length are recommended. Based on the longest waves which has a period of 3s and a length of 7.2m, a sponge layer of 35m is determined. The sponge layer will therefore absorb the waves much better than the experimental absorber and this simplifies the analysis afterwards.

6.2.5 Test Case: Reflection from impermeable wall

In order to find the best way to analyze the results, a test case was created where the structure has 0 porosity, which equals a vertical wall. Therefore conform the theory, a

wave which reflects from a vertical wall needs to have 100% reflection. There are 2 possible methods for determining the partial reflection and transmission:

1. The Healy formula
2. Method of Goda and Suzuki (1976) based on time signals

The formula of Healy is derived from a theoretical analysis based on two linear waves interacting. It is denoted as:

$$R_H = \frac{H_{max} - H_{min}}{H_{max} + H_{min}} \tag{6.6}$$

Where H_{max} and H_{min} represent the highest and lowest wave height from a partial standing wave pattern. Madsen and White (1976) show that the Healy formula is quite sensitive for errors in H_{min}. In addition, H_{min} is the most difficult to determine, especially if the waves are non-linear. Take for example Figure 6.6, the troughs of the waves are much longer than the peaks so the minimum wave height has an overlap between both. When the minimum and maximum of the envelope are taken and calculated according to Equation 6.6 the result is a reflection R_H of 0.65.

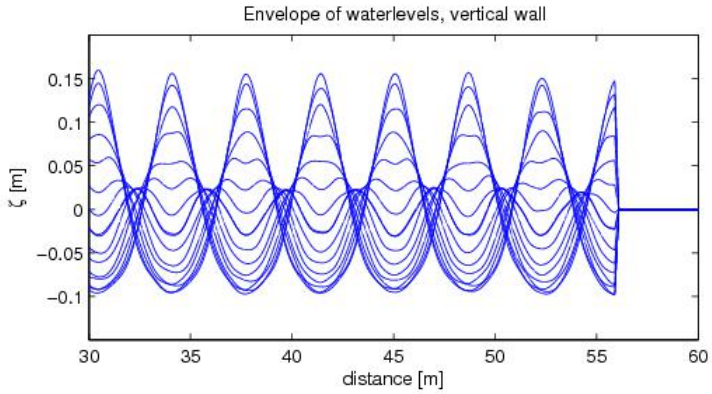

Figure 6.6: Envelope of water levels for case with interaction with a vertical wall

The alternative to calculate the reflection is using two time signals with a fixed distance and the method of Goda and Suzuki (1976). By placing the numerical wave gauges at the same location as the experimental wave gauges the signals can be analysed identically. Analysing the results for the similar cases resulted in a reflection of 0.99. This method has three advantages:

- The results are more accurate for non-linear waves

- It is a more objective method as one can treat every signal in the same way. The Healy formula needs the user to pick a wave and the minimal wave height is highly influenced by the judgement of the user.
- The method is completely similar to the experimental analysis.

6.3 Uncalibrated results

Next step is using the settings described in Section 6.2 for all the wave cases of block6. However, the very steep wave cases with a period of 1.0 s did not provide a stable computation. Because these series also gave lots of problems with the experimental measurements, it is decided to leave them out for the rest of the numerical analysis.

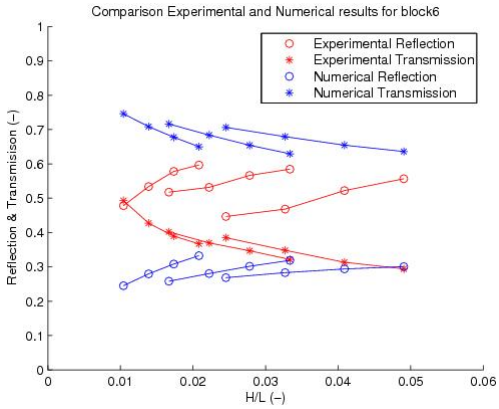

Figure 6.7: Comparison of experimental results with numerical results without any form of calibration

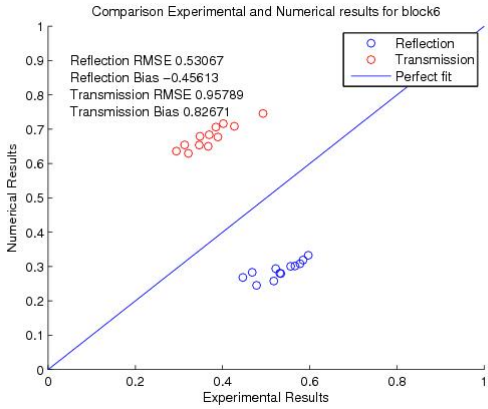

Figure 6.8: Comparison of experimental results with numerical results without any form of calibration

In Figure 6.7 and 6.8 the results are plotted for block6. The results are not very satisfactory, the reflection is greatly underestimated and the transmission is greatly overestimated. A positive remark is that the results show a somehow similar trend with increasing reflection for steeper waves and decrease of transmission.

The obvious conclusion is that the uncalibrated results do not posses enough resistance for the flow in the porous part. Wave energy is too easily transmitted.

In Figure 6.9 and 6.10 the direct timeseries of the numerical and experimental wave gauges are plotted. Two things are really clear, wave gauges 4,5 and 6 (behind the structure) have a way lower amplitude experimentally than numerically which means that the numerical transmission is too high. Also the wave sensors 1, 2 and 3 (in front of the structure) have numerically a lower amplitude and differ in amplitude less from each other than experimentally, which suggests that the numerical reflection is too low.

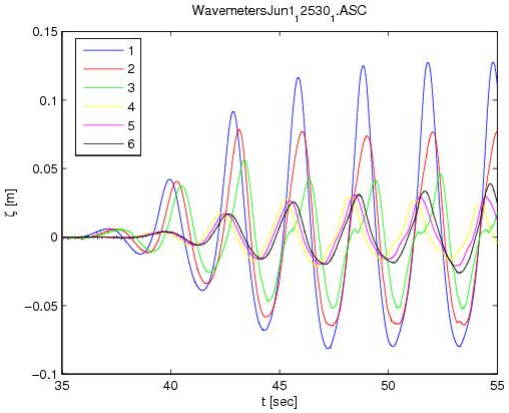

Figure 6.9: Results from experimental wave gauges. The numbers are ordered in the direction of the wave. Gauges 1,2,3 are in front of the block and 4,5,6 are at the back of the block.

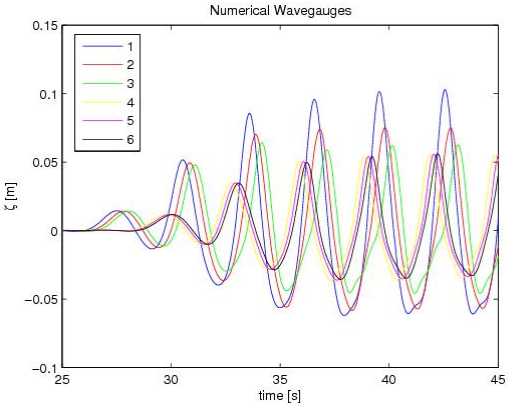

Figure 6.10: Results from numerical wave gauges in similar location

6.4 Calibration

Because of the large difference between experimental and numerical results some sort of calibration is needed. As first step a sensitivity analysis is done on the results in order to see which parameters influence the results most. The results of the sensitivity analysis are shown in Table 6.2.

	% change in Reflection	**% change in Transmission**
10% lower n	10.62	-4.16
10% higher n	-10.01	4.05
10% lower d_{n50}	5.98	-2.27
10% higher d_{n50}	-5.25	2.16
10% lower α	-0.19	0.27
10% higher α	0.19	0
10% higher β_{NS}	5.02	-1.72
20% higher β_{NS}	9.67	-3.62

Table 6.2: Results of sensitivity analysis on block 5

The sensitivity analysis shows that by far the most sensitive variables are the porosity followed by the β_{NS} and d_{n50}. Because the determination of the porosity and d_{n50} is far more accurate than the determination of the β_{NS} constant, the β_{NS} constant will be used to calibrate the results. Calibration is done by trial and error and the reflection is used to judge the calibration. For the default case (H=0.125m , T=3.0s) the best fit was found when multiplying the β_{NS} constant with a factor 6.80.

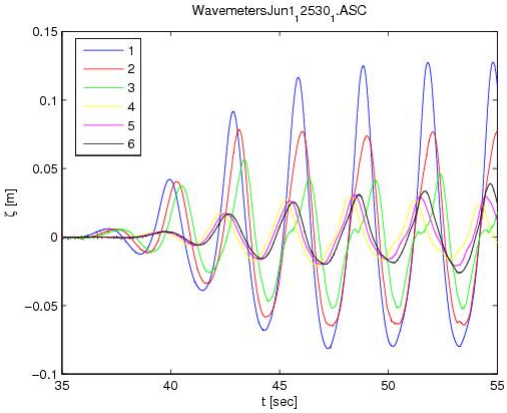

Figure 6.11: Results from experimental wave gauges. The numbers are ordered in the direction of the wave. Gauges 1,2,3 are in front of the block and 4,5,6 are at the back of the block.

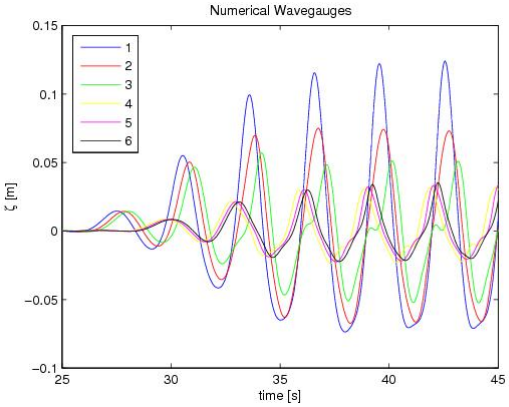

Figure 6.12: Results from numerical wave gauges with the Beta constant multiplied by 6.80.

The results after calibration are plotted in Figure 6.12. Comparing them to Figure 6.11 shows that the results are far more similar. Though, it must be mentioned that these results cannot be compared one on one because the numerical part is calibrated on the corrected experimental results while these plots show the uncorrected raw data. However, the graphs look fairly similar which is promising.

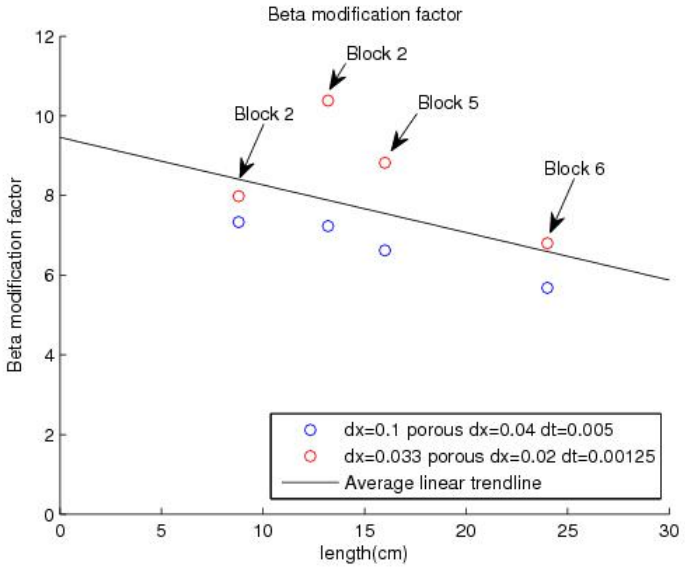

Figure 6.13: Comparison of beta modification factor for different block sizes and different resolutions

In Figure 6.13 the different modification factors are plotted against the block lengths for

the calibration of two different resolutions. The results show that for an increasing block length the modification factor tends to get smaller. Besides, for a higher resolution a higher β_{NS} modification factor is needed in general.

6.5 Verification

The verification is done by using the same multiplication factor per block for all β_{NS} constants over the whole range of cases. This way the predictive skills can be examined. For all blocks a RMSE and BIAS is computed.

6.5.1 Block5 and Block6

These 2 blocks are made out of the same material with the only difference that the length of block6 is longer (24cm) than block5 (16cm).

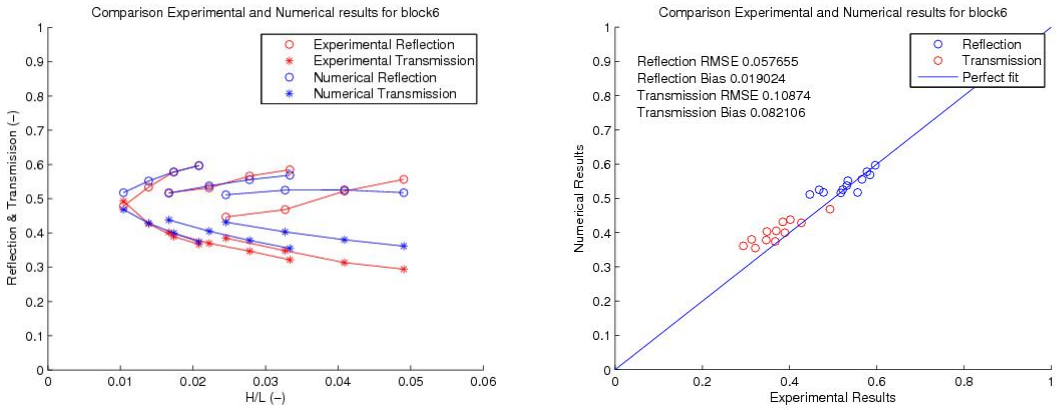

Figure 6.14: Block6, Reflection and Transmission of SWASH in comparison to experimental results, using a nonstationary β_{NS} multiplied by 6.80

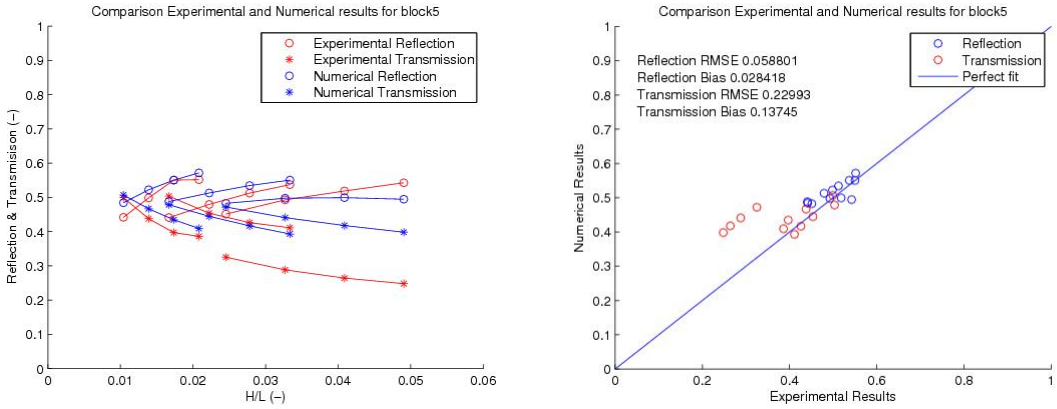

Figure 6.15: Block5, Reflection and Transmission of SWASH in comparison to experimental results, using a nonstationary β_{NS} multiplied by 8.82

Figure 6.14 and 6.15 show that the computations with a higher β_{NS} make a very decent fit. It only seems to seriously overestimate the transmission for the wave periods of 1.5 s for block5. It is strange is that a similar trend of higher transmissions for the steeper waves is not seen in the results of block6. This might be caused by an experimental error as in Figure 4.24 a similar strange pattern has been identified for these wave cases.

6.5.2 Block2 and Block3

Block2 and block3 differ also only in length (13.2 cm vs 8.8 cm). For block3 an extended range of data has been measured. However, analysing the data gave some problems as the first harmonic was not clearly recognizable from the time series. A larger distance between the wave gauges should be used because for waves with a period of 6s and wave length of 15m the gauges are placed too close together.

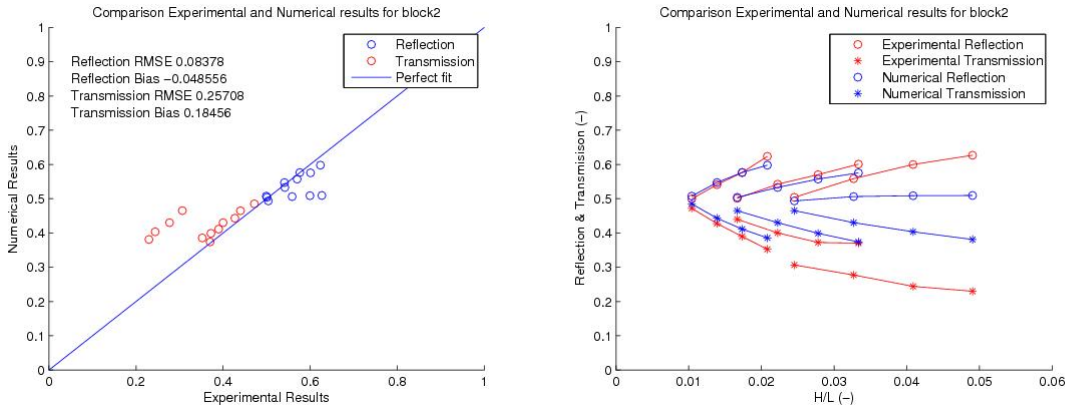

Figure 6.16: Block2, Reflection and Transmission of SWASH in comparison to experimental results, using a nonstationary β_{NS} multiplied by 7.98

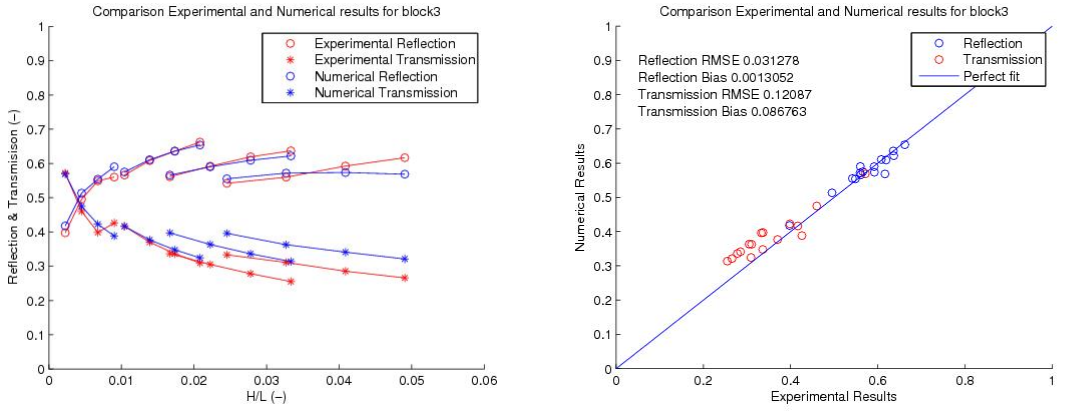

Figure 6.17: Block3, Reflection and Transmission of SWASH in comparison to experimental results, using a nonstationary β_{NS} multiplied by 10,38

In Figure 6.16 and 6.17 the results are shown for block 2 and block3. Both figures show again a very decent fit where the results get less accurate for the steeper waves (Period 1.5s).

6.6 Comparison Analytical and Numerical model

In Table 6.3 all values for the RMSE and Bias are shown for the numerical and analytical comparison with the experimental data. All cases higher than 0.20 are shown in red. Overall it becomes clear that the numerical model performs significantly better than the analytical model. The only two cases higher than 0.20 are for block 2 and 5 which can be explained by the transmission results for a wave periods of 1.5s being completely off.

Statistic	**Numerical Result**	**Analytical Result**
Block2 Reflection Bias	-0.05	0.20
Block2 Reflection RMSE	0.08	0.15
Block2 Transmission Bias	0.18	0.11
Block2 Transmission RMSE	0.26	0.22
Block3 Reflection Bias	0.001	0.15
Block3 Reflection RMSE	0.03	0.17
Block3 Transmission Bias	0.09	0.17
Block3 Transmission RMSE	0.12	0.24
Block5 Reflection Bias	0.03	0.18
Block5 Reflection RMSE	0.06	0.21
Block5 Transmission Bias	0.14	0.12
Block5 Transmission RMSE	0.23	0.22
Block6 Reflection Bias	0.02	0.19
Block6 Reflection RMSE	0.06	0.22
Block6 Transmission Bias	0.08	0.06
Block6 Transmission RMSE	0.11	0.22

Table 6.3: Comparison of the RMSE and Bias of the analytical and numerical model

Comparing the equations of the analytical model (Equations 2.55, 2.56, 2.57 and 2.58) and SWASH model (Equations 6.1, 6.2) it can be seen that the main differences are:

- Analytical model has no advection terms.
- Analytical model uses linearised friction instead of Forchheimer formula with α and β.
- Analytical model uses an hydrostatic approach

In order to understand the differences between the two approaches attempts are made to make the SWASH model similar to the analytical model. The advection terms can be taken out and the friction can be linearised. Unfortunately it is not possible to take out the non-hydrostatic part since that will make the computation unstable for short waves.

Setup	**Reflection** (%)	**Transmission** (%)
Analytical model	65	35
Measured	58	39
Calibrated SWASH	58	40
Uncalibrated SWASH	28.2	70.8
Uncalibrated SWASH without advection	28.0	70.4
Uncalibrated SWASH without advection and linearised friction	46.0	52.3

Table 6.4: Comparison of different SWASH settings for the case of H=0.125m and T=3s for block6

Table 6.4 shows that the linearised friction has a big influence on the outcome. Apparently the linearised friction is an overestimation of the friction which corrects the results just like in the modified SWASH computations. There is still a significant difference between the analytical model and the SWASH computations without advection and with a linearised friction. This can be due to:

- The non-hydrostatic calculation
- The factor S for unsteady motion in the analytical model
- The influence of the grid size

6.7 Discussion of calibrated SWASH results

The results for a modified β_{NS} factor show a good fit with the experimental data.
The β_{NS} modification factor showed in Figure 6.13 a high dependency on the grid resolution. This might suggest it is a numerical problem.

Overall the static β values measured are quite low as discussed in Section 2.2.3. In Table 6.5 an overview is given of the different β values. The non-static β_{NS} factors used in SWASH are ranging from 12-18. This is 6-10 times higher than the experimentally derived values. An average value on basis of literature based on Appendix A can also be calculated. The β_{NS} used in SWASH is still roughly three times as high (12-18 divided by 5) as the average of literature .

	Stationary β	**Non-Stationary β_{NS}**
β values experimentally derived	1.1-1.7	1.4-3.5
β values based on average of literature	3.4	$\sim$5
β values used in SWASH	-	12-18

Table 6.5: Comparison of different β values

A likely explanation for the need of higher β values in SWASH is suggested by Van Gent (2012). He argues that besides the correct representation of porous flow also a good numerical solution is needed for the interface between water and porous medium. Vertical accelerations near the water surface behave differently in a porous medium. The porous resistance will also hinder the vertical motion of the water level which results in the internal water table being unable to follow the external water table. This results in a discontinuity between the both water levels. In Figure 6.18 this is graphically explained. SWASH only uses horizontal porous resistance terms and calculates the vertical accelerations per layer which is a very rough estimate for waves in a porous medium.

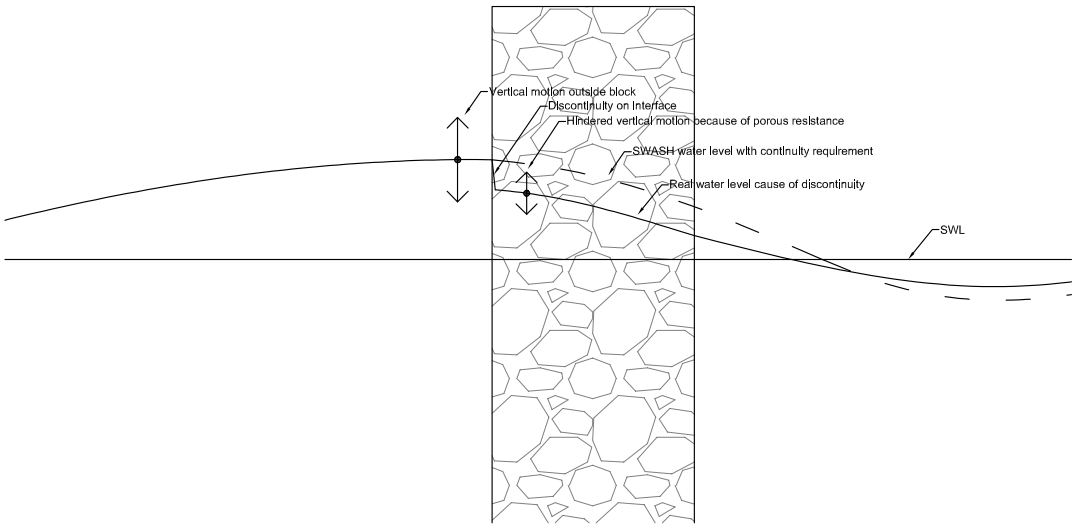

Figure 6.18: Hypothesis of Van Gent (2012), for explaining the deficit between the uncalibrated SWASH results and the experimental measurements

For the transition to a porous medium, SWASH uses a continuity formulation. This results in a higher incoming wave in the porous part and therefore a higher transmission and a lower reflection then reality. Instead of a modification of the β term splitting up the transition effect and the internal propagation leads to a better formulation of the problem. With the modification of the β_{NS} constant an error in the first part is solved by adjusting the second part. The observation of a declining modification factor with longer blocks is also in line with this theory. For longer blocks the transition effect is relatively lower so the correction is lower.

6.8 Multilayered Structure

In the introduction the method of Van der Meer was discussed in order to numerically compute a P value. It is therefore interesting to test that hypothesis numerically with a simple multi-layered setup and to combine the knowledge obtained from measuring the

individual blocks. SWASH still has some limitations for multi-layered structures:

- It is only possible to enter one value for α and β for the whole domain
- Different layers with different porosities and grain sizes can only be entered in horizontal direction. Therefore it is not possible to create multiple layers under a slope with differences in the vertical.

For these reasons a vertical layered structure will be used as test case. It should be noted that the P value is defined by Van der Meer for sloped structures and is not valid for a vertical structure, however, a similar approach will be used in order to determine a "vertical P". The objective is to determine a P value for two configurations of the blocks tested earlier. Structure A consists out of block5 as armour layer with block2 as filter layer and block1 as core material. Structure B consists out of block6 as armour layer, block3 as filter layer and block1 as core material. In Figure 6.19 the different configurations are sketched.

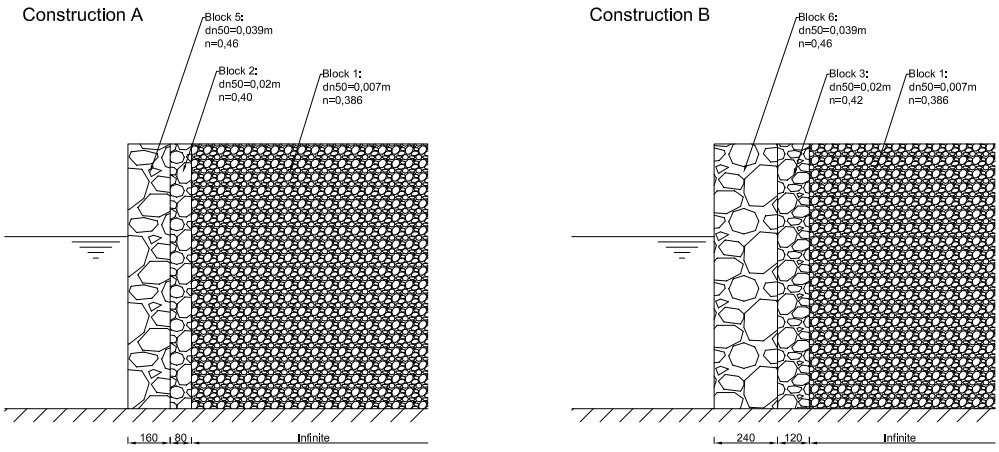

Figure 6.19: Sketch of setup for the numerical structures A and B

In order to determine the P value first of all the relative discharges for known structures should be computed. The structure described by Van der Meer (1988) as P=0.1, P=0.43, P=0.5 and P=0.6 are transformed in similar structures with the same armour layer stone size. In Table 6.6 a summary of the structures is given.

	Armour layer d_{n50}	**Armour thickness**	**Filter layer d_{n50}**	**Filter thickness**	**Core d_{n50}**	**Core thickness**
P=0.1	0.039 m	8 cm	impermeable wall	∞	-	-
P=0.43	0.039 m	8 cm	0.02 m	6 cm	0.005 m	∞
P=0.5	0.039 m	8 cm	-	-	0.0122 m	∞
P=0.6	0.039	∞	-	-	-	-

Table 6.6: Description of the tested structures and their build up

The α and β value of the armour layer will be used for the whole domain. The different porosities layers and grain size layers need separate input files.

The method of Van der Meer dictates that one should use the dissipation in the core per wave cycle. One of the output possibilities of SWASH is a discharge on a certain place in the domain. By specifying this output at the boundary between filter/armour layer and the core layer it is possible to calculate the discharge entering the core of the structure. By integrating the results over one wave cycle the total discharge into the core per wave cycle can be calculated. The relative dissipation is then obtained by stating that the dissipation for the P=0.6 structure is equal to 100% and calculating the other dissipations relatively to that value. This is done for three wave cases with a wave height of 0.125 m and periods of 1.5s , 2.0s and 3.0s.

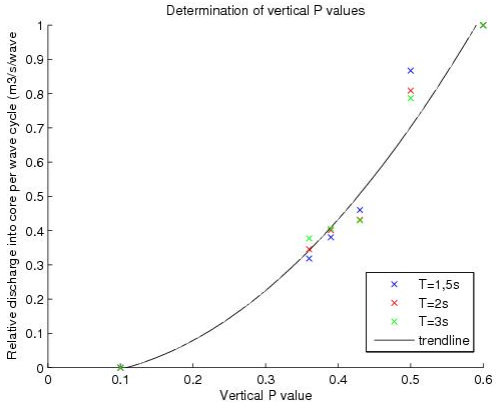

Figure 6.20: Relative dissipation into the core as a function of the vertical P value

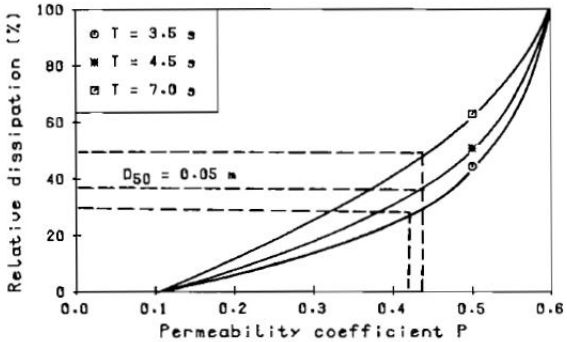

Figure 6.21: Relative dissipation into the core as a function of notional permeability, Van der Meer (1988)

In Figure 6.20 the result is plotted. First of all a trendline for the known cases has been determined, later on the new cases of structure A and B have been fitted on this trendline.

Based on this method, structure A has a "vertical P" value of 0.39 and structure B has a "vertical P" value of 0.36.

Comparing Figure 6.20 to Figure 6.21 from Van der Meer quite some differences can be seen. First of all the relative dissipation for all wave periods is quite similar while Van der Meer suggests a higher relative dissipation for larger periods. Also the values for P=0.5 are much lower than Van der Meer computes (45-63% against 79-87 %). The values for P=0.43 are quite similar though (29-43% against 43-46%). The combination of these two facts causes quite some problems in creating the trendline, especially the P=0.5 case has a large offset. The usage of P=0.43 for constructing the figure can be argued as it is a computed result by Van der Meer and not experimentally verified. Excluding the case of P=0.43 will result in a more linear trendline and therefore a lower P value for structure A and B.

The usage of P=0.43 can be justified by the tests performed by Kluwen (2012). The P=0.43 structure was experimentally tested and Kluwen (2012) measured a P value of P=0.45. The structure described by Kluwen (2012) was calculated in a similar way and the outcome showed hardly any difference with the structure used in this research. Other cases can not be compared due to the usage of an impermeable core.

The method shows the possibility to determine a P value numerically. The determined values for the structures A and B seem logical because they are almost the same case as P=0.43 but with thicker layers which causes a lower discharge.

Chapter 7

Conclusion and Recommendations

7.1 Conclusions

The main objective was validating a numerical model for a simplified setup with porous flow. This has been partially realized. It turned out not to be possible to directly use measured constants from the Forchheimer formula into the numeric model, but after a calibration the results show a good match.

The main research question of this study is:

Is it possible to numerically simulate the wave interaction with a simplified setup of a breakwater?

If one compares the experimental data to the numerical data from the SWASH model, large deviations are discovered. The cases examined in this research showed that the experimental determined Forchheimer constants for SWASH gave an severe underestimation for the reflection and an overestimation of the transmission in comparison to both experimental and analytical data. In order to "fit" the data the β_{NS} constants need to be calibrated. The calibrated value for the β_{NS} factor is 6-10 times as high as experimental determined. However with these settings the SWASH model shows a good fit with the experimental data. The fit showed that SWASH is capable of simulating the reflection and transmission for a wide range of cases. In most cases the model is able to predict only for some steep waves this is not possible.

The reason behind the need for an increased β_{NS} is still unknown. One possible explanation is a numerical problem, as the analytical model did not need any calibration of beta values in order to give reasonable data. Another explanations is that the experimentally derived values for β_{NS} were a bit low compared to earlier measurements in literature. However the values used in SWASH are unrealistic high.

The most plausible explanation is the hypothesis of Van Gent (2012). Discontinuities on the transition to the porous medium might not be modelled correctly by SWASH. So the higher β_{NS} is needed to correct for an error in the transition. This hypothesis is in line with the observation of the modification factor decreasing for increasing block length. Future research is needed to test this.

In addition, the first formulated sub questions is:

Looking at the options of pressure sensors and wave gauges for collecting data from the experiment, what is the most reliable method for validating a numerical model?

In order to answer this subquestion, data is collected from differential pressure sensors and wave gauges. It can be concluded that the data from the wave gauges are more reliable. The data was comparable with similar experiments from literature and the method was less vulnerable for measuring errors. The results from the pressure sensors showed a large randomness depending on the placement of the exact sensorpoint in combination with the mean flow direction and the geometry of the pores.

In addition, the experiments carried out in the large wave flume showed two main problems. First of all, the setup was limited because of the full blocking of the flow at one side. Secondly, the wave absorber installed at the end of the flume showed really bad characteristics for longer waves. The experimentally derived data needed to be corrected to account for the second problem.

The second subquestion is:

Are classical theoretical relationships valid to describe porous flow for this case?

The main conclusion is that the pressure attenuation theory is not valid for this case, as it is derived for core material and not for armour layers. As a result the decay of pressures showed a different pattern and different magnitude. The results of the pressure measurement show a linear pressure decay with the distance inside the block.

However, the Forchheimer relations seems valid if one uses unrealistic high β constants for the numerical computations. The theory of Van Gent, relating the β_{NS} value to the KC number, helped in realising a sufficient fit with the experimental data.

The analytical model gave a reasonable fit with the experimental data without any form of calibration. This may partly be caused by the artificial high friction caused by the linearised friction. However, the analytical model showed to be a very reliable way for a first estimate and suitable to predict KC values and the order of magnitude of velocities.

The third and final subquestion is:

Does this method have potential to grow into a P value predicting model?

Section 6.8 showed that the method described by Van der Meer has capabilities of determining P values for unknown structures. However, the P value is defined for sloped cases with a far more complex flow pattern. This fact combined with the results of the SWASH model show that the model has potential to predict porous flow and therefore the notional permeability P. Though the adjustment of β_{NC} constants for calibrating is the wrong approach. Other downside is that this method is only capable of calculating P

values for structures with a permeable core.

7.2 Recommendations

The following recommendations are provided for future experimental research:

- Further attempts to measure pore pressures should be done on a normalized grid with fixed spherical grain sizes and fixed pore sizes. This prevents a lot of randomness coming from the geometry in the results.
- Further research into porosities should not be carried out on small samples with relatively large effects of the borders. The magnitude of the stone size over the size of the mould should be limited for porous measurements. It is wise to use the larger blocks to measure the porosity for the bigger stone sizes.
- For analysing the results it would be help full if it is possible to separate the dynamic pressure from the hydrostatic pressure. This way it is easier to relate the measured pressures to the Forchheimer formula.
- Furthermore it is advisable to include the sensors in the blocks prior of construction.
- Further experimental research should be done with a wave absorber with better damping characteristics for long waves. This way the uncertainty relating to the correction of the data is excluded.
- An experiment where the block is placed directly to the window with fixed video positions and rulers. This way the discontinuity effect can be observed and quantified. This makes it possible to separate the transition effect and wave propagation in the porous domain.

Further development of the SWASH model is required to take the next numerical steps:

- The hypothesis of Van Gent (2012) should be verified. A possible solution could be of adding a vertical porous friction to the vertical momentum balance. Also a finer vertical grid with more layers in the top section is needed. This should be validated with experimental research.
- The cnoidal time series used for the boundary conditions need to be converted into a non-reflective boundary condition in order to allow for longer computations. This could also improve the computation time, as a smaller grid could be used.
- A method to give an input grid for the α and β values in order to impose correct values throughout the whole domain. At the moment only one α and β variable for all porous parts can be imposed.
- A method needs to be developed to model different porous vertical layers, to create a sloped multi-layered structure.

As for calibration and validation the following models need further investigation:

- A vertical multi-layered structure with regular waves. This can be done with the same blocks as used in this setup.
- A sloped multi-layered structure with regular and irregular waves.

Finally, it is advisable to compare the numerical computed values with higher scale breakwaters. It is crucial to investigate what the influence is of far higher Reynolds number and effects as air entrainment on the results.

Appendices

Appendix A

Measured Forchheimer constants in Literature

Material	Packing	$d_{85}/\ d_{15}$	α	β	Re	Source
Spheres	Cubic	1.0	900-6000	1.0-1.3	630-14000	Sm
	Rhomb	1.0	640-900	0.47-1.1	630-14000	Sm
	Random	1.0	410-1700	1.1-1.5	180-9000	D
	Random	1.8	3100	1.6	3700-7700	D
	Random	1.0	220	1.5	120-410	F
	Random	2.0	240	1.6	120-410	F
		1	2070	0.69		G
Round rock	Random	1.4	∼10000	2.2	<2100-8050	B
		1.7	1400-15000	2.2-2.9	500-3600	D
		?	160-9800	1.7-2.2	?	H
		1.3	?	1.9	750-7500	W
Very round rock	Random	1.3	1066	0.29		G
		1.4	10070	2.15	?	T
Semi-round rock	Random	1.9	∼3000	2.7	800-2100	B
		1.3	?	2.4	750-7500	W
		1.3	0	0.88		G
		1.4-1.9	3000	2.45	?	T
Irregular rock	Random	1.4-1.8	1400-13000	2.4-3.0	600-10300	B
		1.6	270-1400	4.1-11	400-8200	D
		?	90-540	3.0-3.7	?	H
		1.3-1.4	980-2100	2.5-2.9	300-5700	Sh
		1.3	?	3.7	750-7500	W
		1.0-1.7	1000-1800	0.55-1.07	?	G
		1.4-1.8	1400-13000	2.45-3.45	?	T
		1.3	**700-1900**	**1.1-1.7**	**220-8400**	**Z**
Equant rock	Random	1.2	?	3.6	750-7500	W
Tabular rock	Random	1.4	3000	1.5	1500-18000	Sm
		1.2	?	3.7	750-7500	W

B: Burcharth and Christensen (1991); D: Dudgeon (1966); F: Fand et al. (1987); G: Van Gent (1993); H: Hannoura and Mc-Corquodale (1978); Sh: Shih (1990); Sm: Smith (1991); T: Troch (2000); W: Williams (1992); Z: Zeelenberg and Koote (2012).

Appendix B

Theory of Biesel

In the model of Biésel (1950) an incompressible and perfect fluid is described. According to this the Navier Stokes equation can be reduced to the Euler equation.

$$\nabla \frac{p}{\rho_w} + \frac{\partial \overrightarrow{u}}{\partial t} + (\overrightarrow{u}\nabla)\,\overrightarrow{u} - \overrightarrow{G} = 0 \tag{B.1}$$

Where G is the gravity vector: $\overrightarrow{G} = -\nabla U$. If there is only a vertical component of G it can also be written as

$$g = -\frac{\partial u}{\partial y} \tag{B.2}$$

Integration of equation B.2 gives:

$$U = -gy \tag{B.3}$$

Besides the gravity also a linearized gravitational force is added:

$$\overrightarrow{W} = c_f \nabla \varphi \tag{B.4}$$

Where $c_f$is a constant friction term which is always positive. φ is an velocity potential function:

$$\overrightarrow{u} = \nabla \varphi \tag{B.5}$$

Combining all these terms results in:

$$\nabla \frac{p}{\rho_w} + \nabla \frac{\partial \varphi}{\partial t} + (\overrightarrow{u}\nabla)\,\overrightarrow{u} + \nabla\,(gy) + c_f \nabla \varphi = 0 \tag{B.6}$$

The term $(\overrightarrow{u}\nabla)\,\overrightarrow{u}$ can be neglected since the local accelerations in a breakwater are normally far more important than the advective accelerations. This results in:

$$\nabla \left(\frac{p}{\rho_w} + \frac{\partial \varphi}{\partial t} + gy + c_f \varphi \right) = 0 \tag{B.7}$$

And after integration:

$$\frac{p}{\rho_w} + \frac{\partial \varphi}{\partial t} + gy + c_f \varphi = cte \tag{B.8}$$

Le Mehauté (1957) used this equation for porous flow by adding an extra term:

$$k_v = \frac{D}{n} \tag{B.9}$$

Where n is the porosity and D must account for inertia effects. D is empirically determined at D=1.4.

$$\frac{p}{\rho_w} + k_v \frac{\partial \varphi}{\partial t} + gy + c_f \varphi = cte \tag{B.10}$$

This equation describes a 2D wave through a porous structure with porosity n and a linearized friction constant.

By adding boundary conditions it is possible to generate solutions. First the laplace equation for continuity:

$$\nabla^2 \varphi = 0 \tag{B.11}$$

The dynamical boundary condition for the free surface:

$$p = cte \ for \ y = \eta(x,t) \tag{B.12}$$

The kinematic boundary condition for the bottom:

$$v = \frac{\partial \varphi}{\partial y} = 0 \ for \ y = 0 \tag{B.13}$$

Le Mehauté (1957) determined a particular solution for equation B.10 with boundary conditions B.11, B.12 and B.13.

$$\varphi(x,y,t) = a_o e^{-\delta k' x} \left[cos\left(\delta k' y\right) cosh\left(k' y\right) \sin\left(\omega t - k' x\right) + sin\left(\delta k' y\right) sinh\left(k' y\right) \cos\left(\omega t - k' x\right) \right] \tag{B.14}$$

The wave number is, where L' is the wave length inside the porous medium:

$$k' = \frac{2\pi}{L'} \tag{B.15}$$

Based on equation B.14 the exponential pressure decay is derived:

$$p(x) = p_0 e^{-\delta \frac{2\pi}{L'} x} \tag{B.16}$$

Appendix C

Sensor Reference Sheets

Pressure Sensors
Gage and Differential/Unamplified-Noncompensated

24PC Series

Basic Sensors

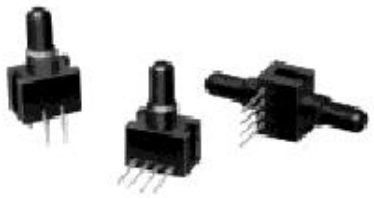

FEATURES

- Lowest priced pressure sensor
- Miniature package
- Variety of gage pressure port configurations - easily and quickly modified for your special needs
- Choice of termination for gage sensors
- 2 mA constant current excitation significantly reduces sensitivity shift over temperature *
- Can be used to measure with vacuum or positive pressure

24PC SERIES PERFORMANCE CHARACTERISTICS at 10.0 ±0.01 VDC Excitation, 25°C

	Min.	Typ.	Max.	Units
Excitation	---	10	12	VDC
Null Offset	–30	0	+30	mV
Null Shift, 25° to 0°, 25° to 50°C	---	±2.0	---	mV
Linearity, P2 > P1, BFSL	---	±0.25	±1.0	%Span
Sensitivity Shift, 25° to 0°, 25° to 50°C	---	±5.0*	---	%Span
Repeatability & Hysteresis	---	±0.15	---	%Span
Response Time	---	---	1.0	msec
Input Resistance	---	5.0 K	---	ohms
Output Resistance	---	5.0 K	---	ohms
Stability over One Year	---	±0.5	---	%Span
Weight	---	2	---	grams

ENVIRONMENTAL SPECIFICATIONS

Operating Temperature	–40° to +85°C (–40° to +185°F)
Storage Temperature	–55° to +100°C (–67° to +212°F)
Shock	Qualification tested to 150 g
Vibration	Qualification tested to 0 to 2 kHz, 20 g sine
Media (P1 & P2)	Limited only to those media which will not attack polyetherimide, silicon and fluorosilicone seal

24PC SERIES ORDER GUIDE

Catalog Listing	Pressure Range psi	Span, mV			Sensitivity mV/psi Typ.	Overpressure psi Max.
		Min.	Typ.	Max.		
24PCE Type	0.5	24	35	46	70	20
24PCA Type	1.0	30	45	60	45	20
24PCB Type	5.0	85	115	145	23	20
24PCC Type	15	165	225	285	15	45
24PCD Type	30	240	330	420	11	60
24PCF Type	100	156	225	294	2.25	200
24PCG Type	250	145	212	280	0.85	500

* Non-compensated pressure sensors, excited by constant current instead of voltage, exhibit temperature compensation of Span. Application Note # 1 briefly discusses current excitation.

Constant current excitation has an additional benefit of temperature measurement. When driven by a constant current source, a silicon pressure sensor's terminal voltage will rise with increased temperature. The rise in voltage not only compensates the Span, but is also an indication of die temperature.

Constant Current Excitation Schematic

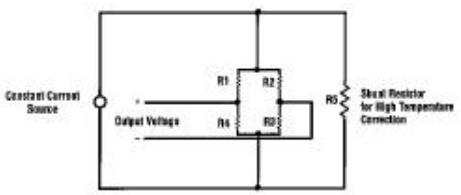

Pressure Sensors
Gage and Differential/Unamplified-Noncompensated

24PC Series

SENSOR SELECTION GUIDE

2 Product Family	4 Circuit Type	PC Pressure Transducer	A Pressure Range	F* Type of Seal	A Type of Port	2 Termination Style	G Pressure Measurement
2 20PC family	4 Noncompensated		A 1 psi B 5 psi C 15 psi D 30 psi E 0.5 psi F 100 psi G 250 psi	F Fluorosilicone	A Straight B Barbed C Luer D Modular H M5 Thread I 90° Port J Needle M ¼ - 28 UNF Thread	1 1 x 4 2 2 x 2	G Gage D Differential

Example: 24PCAFA2G
Standard, non-compensated 1 psi sensor with fluorosilicone seal, straight port, 2 x 2 terminals, and Gage pressure measurement.
*Other media seal materials may be available.

ACCESSORIES SELECTION GUIDE

Catalog Listing	Description
PC10182	Steel lockring (Included with Port Style A, 1 x 4 terminals only)
PC10949	Single hole plastic bracket (Must be separately ordered)

Not all combinations are established. Contact 800 number before final design. The following listings are typically stocked in small quantities.

Unamplified

1. Application.

The Wave-Height meter has been designed for dynamic fluid level measurements, e.g. wave-height measurements in hydraulic models.

2. Principle.

The instrument is composed of two parts:
- a gauge with integral pre-amplifier, and
- a separate main-amplifier (Figure 1).

The gauge consists of two parallel stainless steel rods, mounted underneath a small box, containing the pre-amplifier and the dc-dc converter.
The rods act as the electrodes of an electric resistance meter.
To eliminate the effect of the conductivity variations of the fluid, a platinum electrode is part of the system.
The main-amplifier contains a power-supply, a variable gain amplifier, a zero-shift and a panel-meter, indicating the instanteneous wave-height.
An analog output is available.

3. Features.

Wide range
Ranges of 5, 10, 20 and 50 cm can be selected at the main-amplifier.

Linearity.
Better than +/- 0.5% of the range selected.

Dynamic responce.
The frequency characteristics of the system permit measurements from 0 up to 10 Hz..

Input/Output isolation.
The gauge circuit is powered by an isolating dc-dc coupled power-supply, minimizing electric interference problems when grounding the floating output.

4. Specifications.

a. Probe.

Level-electrodes	: rods, stainless steel, type 316, 4 mm. diam., electrode spacing 23 mm, electrode length 59 cm.
Ref. electrode	: platinum, 5 x 2 mm diam..
Non-linearity	: 0.5% of selected range, b.s.l..
Liquid medium	: all liquids compatible with above-mentioned materials.
Conductivity-influence	: - minimum required conductivity 0.08 mS - sensitivity change <1% for variations between 0.1 and 2 mS.
Dimensions	: incl. electronics 70 x 8 x 9 cm.
Weight	: 0.7 kg. in container (12 x 73 x 14 cm), 3 kg.
Output	: 0.05 VDC/cm level-variation.
Power	: +/- 15 VDC, +/- 100 mA.

b. Control-unit.

Input	: 0.05 VDC/cm. (+/- 15 VDC for probe electronics is supplied via input-connector.).
Ranges	: 5, 10, 20 and 50 cm.
Output-shift	: between + and - 10 VDC, within the limits of the standard output-voltage.
Freq. responce	: 0 to 10 Hz.
Output	: +/- 10 VDC, 2 mA max. for the range selected.
Power	: 220 VAC, 50-60 Hz., 20 VA, incl. probe.
Dimensions	: portable case, 26 x 15 x 32 cm, (for 2 plug-in units Euro-frame)
Weight	: portable case 5 kg nett shipping weight per set 10 kg.

Appendix D

Pressure Sensor Setup

D.1 Block2

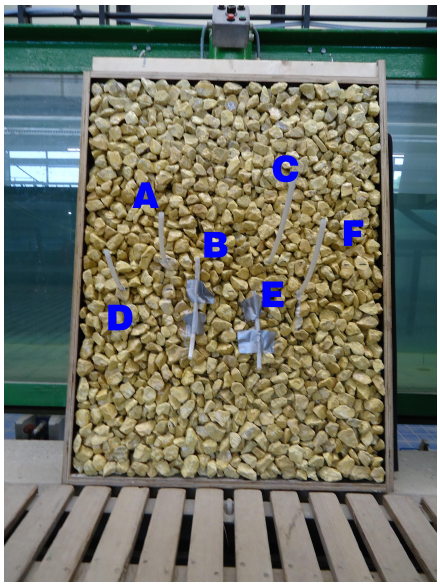

Sensorlocations for block 2

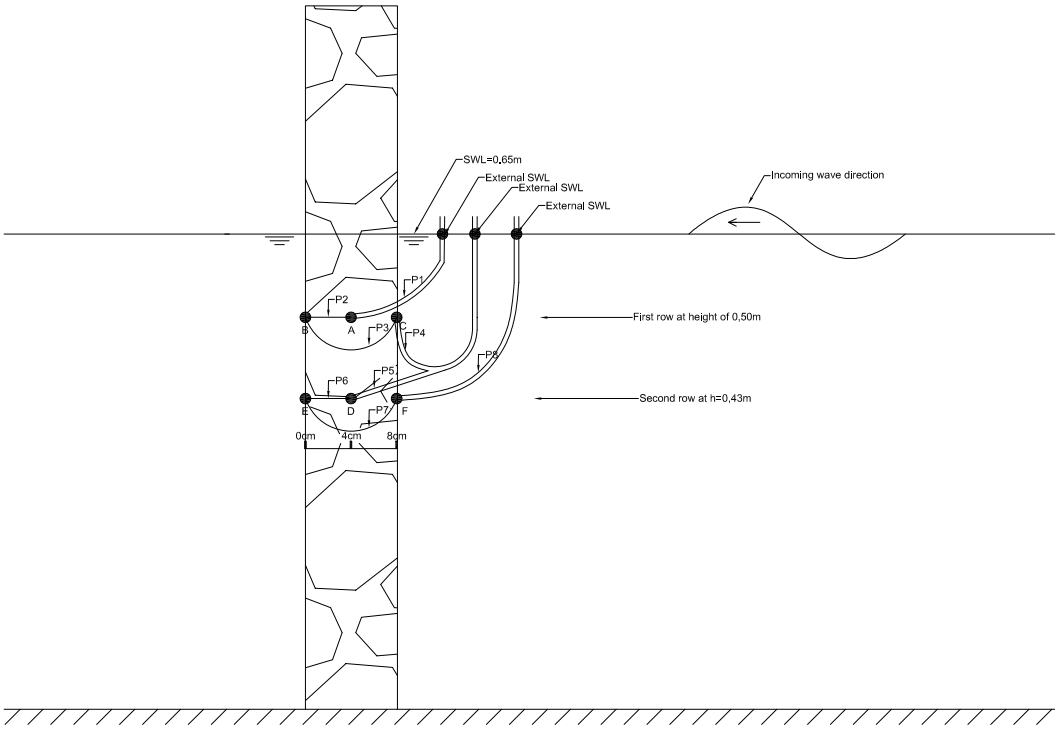

Sketch of setup circuit

D.2 Block3

Sensorlocations for block 3

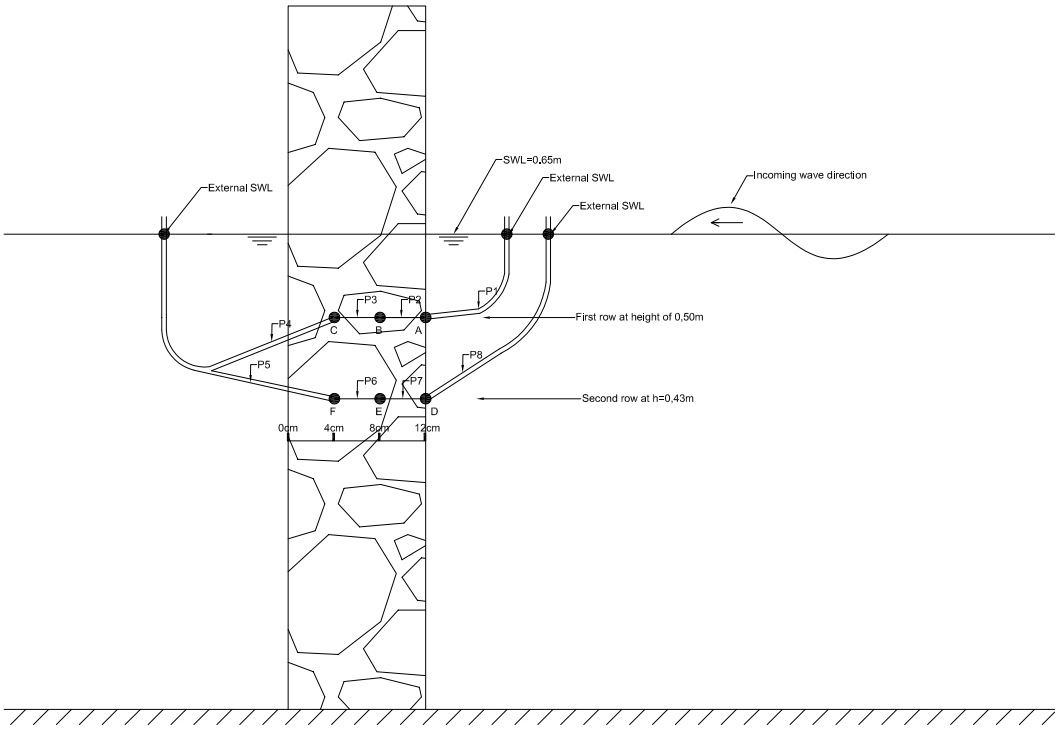

Sketch of setup circuit

D.3 Block5

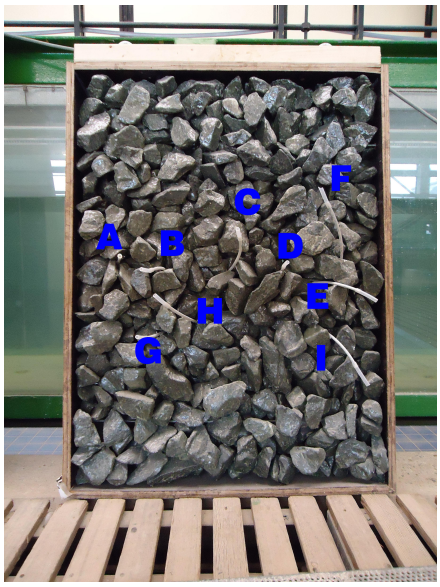

Sensorlocations for block 5

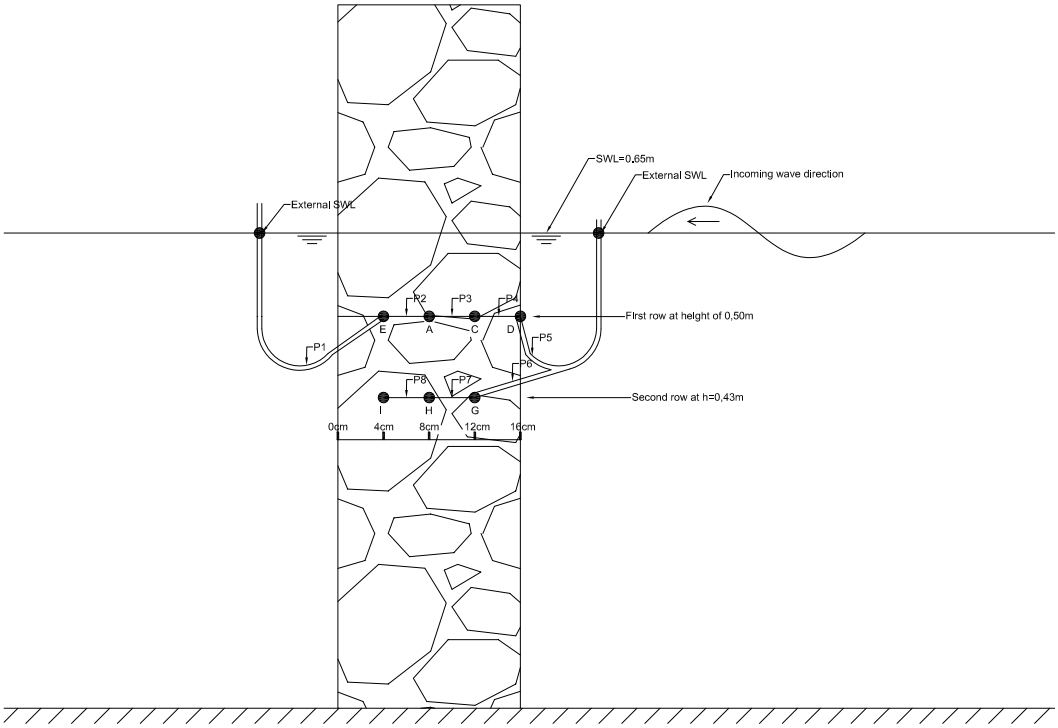

Sketch of setup circuit

D.4 Block6

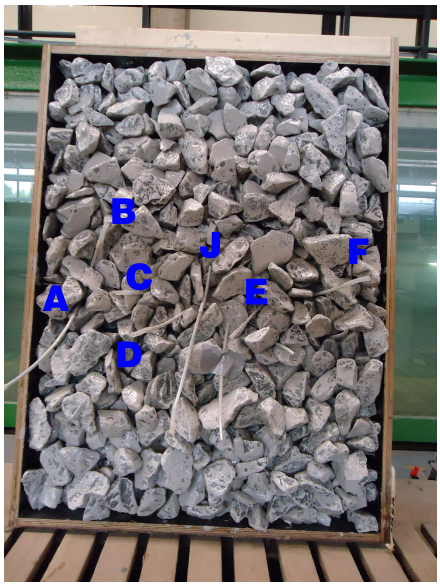

Sensorlocations for block 6

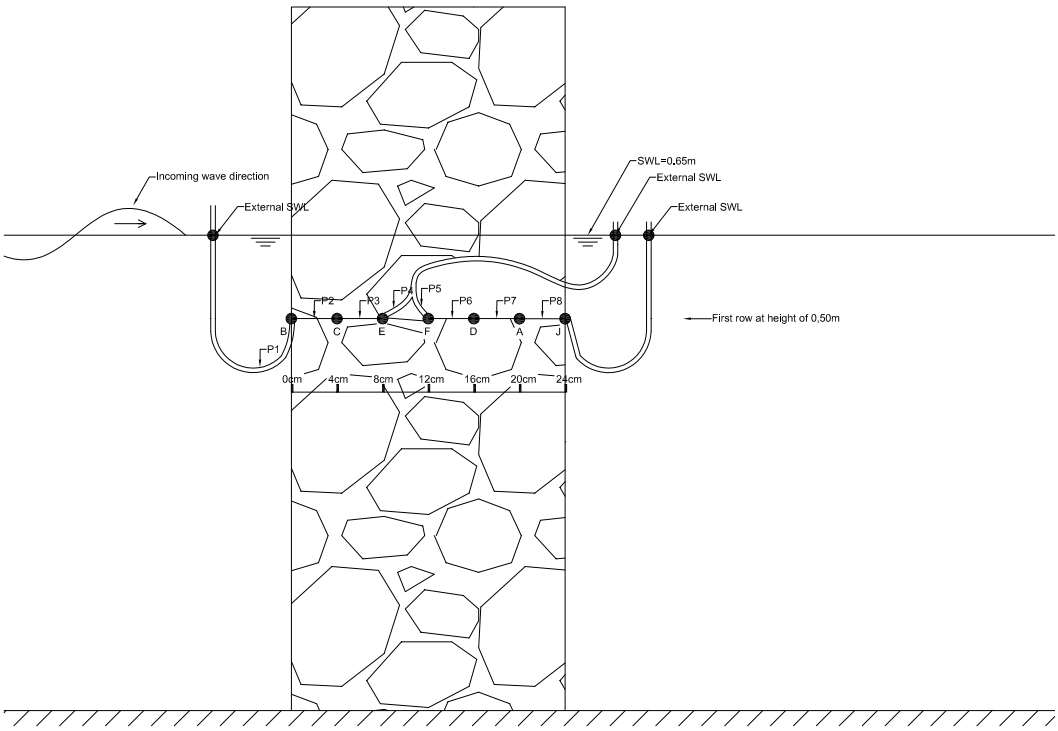

Sketch of setup circuit

Appendix E

Total Measurement Table

Test Nr	Block	Thickness	h (m)	Hs (m)	Tp (s)
1	2	80 mm	0.65	0.075	1.0
2	2	80 mm	0.65	0.075	1.5
3	2	80 mm	0.65	0.075	2.0
4	2	80 mm	0.65	0.075	3.0
5	2	80 mm	0.65	0.100	1.0
6	2	80 mm	0.65	0.100	1.5
7	2	80 mm	0.65	0.100	2.0
8	2	80 mm	0.65	0.100	3.0
9	2	80 mm	0.65	0.125	1.0
10	2	80 mm	0.65	0.125	1.5
11	2	80 mm	0.65	0.125	2.0
12	2	80 mm	0.65	0.125	3.0
13	2	80 mm	0.65	0.150	1.0
14	2	80 mm	0.65	0.150	1.5
15	2	80 mm	0.65	0.150	2.0
16	2	80 mm	0.65	0.150	3.0
17	3	132 mm	0.65	0.075	1.0
18	3	132 mm	0.65	0.075	1.5
19	3	132 mm	0.65	0.075	2.0
20	3	132 mm	0.65	0.075	3.0
21	3	132 mm	0.65	0.100	1.0
22	3	132 mm	0.65	0.100	1.5
23	3	132 mm	0.65	0.100	2.0
24	3	132 mm	0.65	0.100	3.0
25	3	132 mm	0.65	0.125	1.0
26	3	132 mm	0.65	0.125	1.5
27	3	132 mm	0.65	0.125	2.0
28	3	132 mm	0.65	0.125	3.0
29	3	132 mm	0.65	0.150	1.0
30	3	132 mm	0.65	0.150	1.5
31	3	132 mm	0.65	0.150	2.0
32	3	132 mm	0.65	0.150	3.0

Test Nr	Block	Thickness	h (m)	Hs (m)	Tp (s)
33	5	160 mm	0.65	0.075	1.0
34	5	160 mm	0.65	0.075	1.5
35	5	160 mm	0.65	0.075	2.0
36	5	160 mm	0.65	0.075	3.0
37	5	160 mm	0.65	0.100	1.0
38	5	160 mm	0.65	0.100	1.5
39	5	160 mm	0.65	0.100	2.0
40	5	160 mm	0.65	0.100	3.0
41	5	160 mm	0.65	0.125	1.0
42	5	160 mm	0.65	0.125	1.5
43	5	160 mm	0.65	0.125	2.0
44	5	160 mm	0.65	0.125	3.0
45	5	160 mm	0.65	0.150	1.0
46	5	160 mm	0.65	0.150	1.5
47	5	160 mm	0.65	0.150	2.0
48	5	160 mm	0.65	0.150	3.0
49	6	240 mm	0.65	0.075	1.0
50	6	240 mm	0.65	0.075	1.5
51	6	240 mm	0.65	0.075	2.0
52	6	240 mm	0.65	0.075	3.0
53	6	240 mm	0.65	0.100	1.0
54	6	240 mm	0.65	0.100	1.5
55	6	240 mm	0.65	0.100	2.0
56	6	240 mm	0.65	0.100	3.0
57	6	240 mm	0.65	0.125	1.0
58	6	240 mm	0.65	0.125	1.5
59	6	240 mm	0.65	0.125	2.0
60	6	240 mm	0.65	0.125	3.0
61	6	240 mm	0.65	0.150	1.0
62	6	240 mm	0.65	0.150	1.5
63	6	240 mm	0.65	0.150	2.0
64	6	240 mm	0.65	0.150	3.0
65	3	132 mm	0.65	0.025	4.5
66	3	132 mm	0.65	0.050	4.5
67	3	132 mm	0.65	0.075	4.5
68	3	132 mm	0.65	0.100	4.5
69	3	132 mm	0.65	0.025	6.0
70	3	132 mm	0.65	0.050	6.0
71	3	132 mm	0.65	0.075	6.0
72	3	132 mm	0.65	0.100	6.0

Appendix F

Method of Goda and Suzuki

This part is copied from the documentation of the matlab scripts used in the Environmental Fluid Mechanics Laboratory of the TU Delft written by Klaasman (2005).

To calculate the reflection of a regular wave, a Matlab program Refreg has been written in the Laboratory of Fluid Mechanics. The method used has been described by Goda and Suzuki (1976), see Goda (1985). In this method two wave gauges are used at a distance of about one fourth of the wave length.

Basic equations in the case of a regular wave with wave gauges at positions x=x_1 en x=x_2 are:

$$\eta(x_1,t) = \sum_{n=1}^{N} a_{i,n}\cos(k_n x_1 - \omega_n t + \phi_{i,n}) + \sum_{n=1}^{N} a_{r,n}\cos(k_n x_1 + \omega_n t + \phi_{r,n}) \qquad \text{(F.1)}$$

$$\eta(x_2,t) = \sum_{n=1}^{N} a_{i,n}\cos(k_n x_2 - \omega_n t + \phi_{i,n}) + \sum_{n=1}^{N} a_{r,n}\cos(k_n x_2 + \omega_n t + \phi_{r,n}) \qquad \text{(F.2)}$$

Where:

- η is the water-surface elevation relative to the mean water level
- t is the time
- $a_{i,n}$, $a_{r,n}$ the amplitude of the n-th harmonic of the incoming and the reflected wave
- k_n the wave number of the n-th harmonic
- ω_n the angular wave frequency of the n-th harmonic
- $\phi_{i,n}$,$\phi_{r,n}$ the phase of the n-th harmonic of the incoming and the reflected wave.

In the Refreg program, the first harmonic is used only. Higher harmonic components and free or bound harmonics are not taken into account.

Equations F.1 and F.2 for the first harmonic are

$$\eta\left(x_1,t\right)=a_i\cos\left(kx_1-\omega t+\phi_\iota\right)+a_r\cos\left(kx_1+\omega t+\phi_r\right) \tag{F.3}$$

$$\eta\left(x_2,t\right)=a_i\cos\left(kx_2-\omega t+\phi_\iota\right)+a_r\cos\left(kx_2+\omega t+\phi_r\right) \tag{F.4}$$

F.3 can be written as:

$$\eta\left(x_1,t\right)=a_i\ \left\{\cos\left(kx_1+\phi_i\right)\cos\left(\omega t\right)+\sin\left(kx_1+\phi_i\right)\sin\left(\omega t\right)\right\}+$$

$$+ar\left\{\cos\left(kx_1+\phi_r\right)\cos\left(\omega t\right)-\sin\left(kx_1+\phi_r\right)\sin\left(\omega t\right)\right\}$$

or

$$\eta\left(x_1,t\right)=A_1\cos\left(\omega t\right)+B_1\sin\left(\omega t\right) \tag{F.5}$$

In the same way, F.4 can be written as:

$$\eta\left(x_2,t\right)=A_2\cos\left(\omega t\right)+B_2\sin\left(\omega t\right) \tag{F.6}$$

where:

$$A_1=a_i\cos\left(kx_1+\phi_i\right)+a_r\cos\left(kx_1+\phi_r\right) \tag{F.7}$$

$$B_1=a_i\sin\left(kx_1+\phi_i\right)-a_r\sin\left(kx_1+\phi_r\right) \tag{F.8}$$

$$A_2=a_i\cos\left(kx_2+\phi_i\right)+a_r\cos\left(kx_2+\phi_r\right) \tag{F.9}$$

$$B_2=a_i\sin\left(kx_2+\phi_i\right)-a_r\sin\left(kx_2+\phi_r\right) \tag{F.10}$$

F.7 through F.10 lead to the complex equations:

$$A_1+\mathrm{i}B_1=a_ie^{\mathrm{i}kx_1}e^{\mathrm{i}\phi_i}+a_re^{-\mathrm{i}kx_1}e^{-\mathrm{i}\phi_r} \tag{F.11}$$

$$A_2+\mathrm{i}B_2=a_ie^{\mathrm{i}kx_2}e^{\mathrm{i}\phi_i}+a_re^{-\mathrm{i}kx_2}e^{-\mathrm{i}\phi_r} \tag{F.12}$$

where $i^2=-1$.

F.11 and F.12 can be written as matrices:

$$\left(\begin{array}{cc}e^{\mathrm{i}kx_1} & e^{-\mathrm{i}kx_1}\\ e^{\mathrm{i}kx_2} & e^{-\mathrm{i}kx_2}\end{array}\right)\left(\begin{array}{c}a_ie^{\mathrm{i}\phi_i}\\ a_re^{-\mathrm{i}\phi_r}\end{array}\right)=\left(\begin{array}{c}A_1+\ \mathrm{i}B_1\\ A_2+\ \mathrm{i}B_2\end{array}\right) \tag{F.13}$$

The A and B in the right hand side of (F.13) can be found from a harmonic analysis of $\eta(x_1,t)$ and $\eta(x_2,t)$ in F.5 and F.6, e.g. by using a Fast Fourier Transform (FFT). In the program Refreg two zero crossings with the same sign, one at the begin and one at the end of the first data series, are used to determine the length of the series to be analysed. In that case the data series can be regarded as cyclic. The only error is a cut off error

if the wave period does not fit on the time step. The FFT of Matlab is used on the two data series from the wave gauges under consideration, where the number of points used fits to the time between the zero crossings as meant above. The period with the maximum modulus of the FFT-coefficients is used as the base period.

Appendix G

Tables of Results

Block 2 Reflection						
Case nr	H (m)	T (s)	R (measured)	R (corrected)	R (analytical)	R (SWASH)
1	0.075	1	0.62	0.61	0.62	
2	0.075	1.5	0.56	0.50	0.59	0.49
3	0.075	2	0,62	0.50	0.58	0.50
4	0.075	3	0.65	0.50	0.56	0.51
5	0.100	1	0.59	0.58	0.64	
6	0.100	1.5	0.60	0.56	0.62	0.51
7	0.100	2	0.64	0.54	0.61	0.53
8	0.100	3	0.68	0.54	0.60	0.55
9	0.125	1	0.41	0.40	0.66	
10	0.125	1.5	0.64	0.60	0.65	0.51
11	0.125	2	0.65	0.57	0.64	0.56
12	0.125	3	0.69	0.58	0.63	0.58
13	0.150	1	0.42	0.41	0.68	
14	0.150	1.5	0.66	0.63	0.67	0.51
15	0.150	2	0.68	0.60	0.66	0.58
16	0.150	3	0.73	0.62	0.66	0.60

Block 2 Transmission						
Case nr	H (m)	T (s)	R (measured)	R (corrected)	R (analytical)	R (SWASH)
1	0.075	1	0.32	0.29	0.39	
2	0.075	1.5	0.39	0.31	0.41	0.47
3	0.075	2	0.57	0.44	0.42	0.46
4	0.075	3	0.63	0.47	0.44	0.48
5	0.100	1	0.28	0.26	0.36	
6	0.100	1.5	0.36	0.28	0.38	0.43
7	0.100	2	0.53	0.40	0.39	0.43
8	0.100	3	0.60	0.43	0.40	0.44
9	0.125	1	0.26	0.25	0.34	
10	0.125	1.5	0.33	0.24	0.35	0.40
11	0.125	2	0.50	0.37	0.36	0.40
12	0.125	3	0.56	0.39	0.37	0.41
13	0.150	1	0.24	0.22	0.32	
14	0.150	1.5	0.32	0.23	0.33	0.38
15	0.150	2	0.50	0.37	0.34	0.37
16	0.150	3	0.53	0.35	0.34	0.39

Block 3 Reflection						
Case nr	H (m)	T (s)	R (measured)	R (corrected)	R (analytical)	R (SWASH)
17	0.075	1	0.64	0.56	0.65	
18	0.075	1.5	0.60	0.54	0.63	0.56
19	0.075	2	0.63	0.56	0.62	0.57
20	0.075	3	0.68	0.57	0.61	0.58
21	0.100	1	0.56	0.55	0.68	
22	0.100	1.5	0.61	0.56	0.66	0.57
23	0.100	2	0.65	0.59	0.65	0.59
24	0.100	3	0.71	0.61	0.64	0.61
25	0.125	1	0.50	0.50	0.69	
26	0.125	1.5	0.64	0.59	0.68	0.57
27	0.125	2	0.67	0.62	0.68	0.61
28	0.125	3	0.72	0.64	0.67	0.64
29	0.150	1	0.49	0.49	0.71	
30	0.150	1.5	0.65	0.62	0.70	0.57
31	0.150	2	0.68	0.64	0.70	0.62
32	0.150	3	0.74	0.66	0.69	0.65
65	0.025	4.5	0.51	0.40	0.45	0.42
66	0.050	4.5	0.61	0.50	0.54	0.51
67	0.075	4.5	0.66	0.55	0.60	0.55
68	0.100	4.5	0.68	0.53	0.63	0.59
69	0.025	6	0.35	0.29	0.44	0.41
70	0.050	6			0.54	0.51
71	0.075	6			0.59	0.56
72	0.100	6			0.63	0.60

Block 3 Transmission						
Case nr	H (m)	T (s)	R (measured)	R (corrected)	R (analytical)	R (SWASH)
17	0.075	1	0.25	0.22	0.35	
18	0.075	1.5	0.43	0.33	0.37	0.40
19	0.075	2	0.45	0.34	0.38	0.40
20	0.075	3	0.57	0.42	0.40	0.42
21	0.100	1	0.23	0.20	0.32	
22	0.100	1.5	0.41	0.31	0.34	0.36
23	0.100	2	0.41	0.31	0.35	0.36
24	0.100	3	0.53	0.37	0.36	0.38
25	0.125	1	0.20	0.20	0.30	
26	0.125	1.5	0.38	0.29	0.32	0.34
27	0.125	2	0.38	0.28	0.32	0.34
28	0.125	3	0.50	0.34	0.33	0.35
29	0.150	1	0.15	0.14	0.28	
30	0.150	1.5	0.35	0.27	0.30	0.32
31	0.150	2	0.36	0.26	0.30	0.31
32	0.150	3	0.48	0.31	0.31	0.32
65	0.025	4.5	0.65	0.57	0.55	0.57
66	0.050	4.5	0.58	0.46	0.46	0.47
67	0.075	4.5	0.55	0.40	0.40	0.42
68	0.100	4.5	0.61	0.43	0.37	0.39
69	0.025	6	0.48	0.44	0.56	0.58
70	0.050	6			0.46	0.48
71	0.075	6			0.41	0.43
72	0.100	6			0.37	0.39

Block 5 Reflection						
Case nr	H (m)	T (s)	R (measured)	R (corrected)	R (analytical)	R (SWASH)
33	0.075	1	0.61	0.60	0.60	
34	0.075	1.5	0.51	0.45	0.57	0.48
35	0.075	2	0.56	0.44	0.55	0.49
36	0.075	3	0.59	0.44	0.52	0.48
37	0.100	1	0.59	0.58	0.62	
38	0.100	1.5	0.54	0.49	0.60	0.50
39	0.100	2	0.58	0.48	0.58	0.51
40	0.100	3	0.63	0.50	0.56	0.52
41	0.125	1	0.52	0.52	0.64	
42	0.125	1.5	0.55	0.52	0.62	0.50
43	0.125	2	0.60	0.51	0.61	0.53
44	0.125	3	0.65	0.55	0.59	0.55
45	0.150	1	0.39	0.38	0.65	
46	0.150	1.5	0.57	0.54	0.64	0.49
47	0.150	2	0.62	0.54	0.63	0.55
48	0.150	3	0.66	0.55	0.61	0.57

Block 5 Transmission						
Case nr	H (m)	T (s)	R (measured)	R (corrected)	R (analytical)	R (SWASH)
33	0.075	1	0.32	0.32	0.40	
34	0.075	1.5	0.40	0.33	0.44	0.47
35	0.075	2	0.61	0.50	0.46	0.48
36	0.075	3	0.63	0.50	0.48	0.51
37	0.100	1	0.31	0.29	0.38	
38	0.100	1.5	0.36	0.29	0.41	0.44
39	0.100	2	0.56	0.45	0.42	0.44
40	0.100	3	0.59	0.44	0.44	0.47
41	0.125	1	0.27	0.26	0.36	
42	0.125	1.5	0.33	0.26	0.38	0.42
43	0.125	2	0.53	0.43	0.40	0.42
44	0.125	3	0.54	0.40	0.41	0.43
45	0.150	1	0.24	0.23	0.34	
46	0.150	1.5	0.32	0.25	0.36	0.40
47	0.150	2	0.52	0.41	0.37	0.39
48	0.150	3	0.55	0.39	0.39	0.41

Block 6 Reflection						
Case nr	H (m)	T (s)	R (measured)	R (corrected)	R (analytical)	R (SWASH)
49	0.075	1	0.57	0.56	0.64	
50	0.075	1.5	0.51	0.45	0.63	0.51
51	0.075	2	0.61	0.52	0.61	0.52
52	0.075	3	0.64	0.48	0.59	0.52
53	0.100	1	0.65	0.65	0.65	
54	0.100	1.5	0.53	0.47	0.65	0.53
55	0.100	2	0.61	0.53	0.64	0.54
56	0.100	3	0.66	0.53	0.62	0.55
57	0.125	1	0.68	0.68	0.67	
58	0.125	1.5	0.57	0.52	0.67	0.53
59	0.125	2	0.64	0.57	0.66	0.56
60	0.125	3	0.68	0.58	0.65	0.58
61	0.150	1	0.47	0.46	0.67	
62	0.150	1.5	0.60	0.56	0.69	0.52
63	0.150	2	0.65	0.58	0.68	0.57
64	0.150	3	0.70	0.60	0.67	0.60

Block 6 Transmission						
Case nr	H (m)	T (s)	R (measured)	R (corrected)	R (analytical)	R (SWASH)
49	0.075	1	0.22	0.20	0.34	
50	0.075	1.5	0.46	0.38	0.38	0.43
51	0.075	2	0.53	0.40	0.39	0.44
52	0.075	3	0.65	0.49	0.42	0.47
53	0.100	1	0.20	0.18	0.32	
54	0.100	1.5	0.43	0.35	0.35	0.40
55	0.100	2	0.49	0.37	0.36	0.41
56	0.100	3	0.58	0.43	0.38	0.43
57	0.125	1	0.18	0.17	0.30	
58	0.125	1.5	0.40	0.31	0.33	0.38
59	0.125	2	0.47	0.35	0.34	0.38
60	0.125	3	0.54	0.39	0.35	0.40
61	0.150	1	0.19	0.17	0.29	
62	0.150	1.5	0.38	0.29	0.31	0.36
63	0.150	2	0.43	0.32	0.32	0.35
64	0.150	3	0.53	0.37	0.33	0.37

Bibliography

O. Anderson. *Flow in porous media with special reference to breakwater structures.* PhD thesis, Dept. of Civil Engineering, Aalborg University, Denmark, 1994.

K. Bakker. Klassieke theorie leidt tot kostbare filterconstructies. *Land + Water nu*, 10: 35–47, 1989.

F. Biésel. Equations de l'écoulement non lent en milieu perméable. *La Houille Blanche*, No2:157–160, Mars Avril 1950.

G. Bullock, P. Hewson, M. Walkden, and P. Bird. The influence of air and scale on wave impact pressures. *Coastal Engineering*, (42):291–312, 2001.

H. Burcharth and O. Andersen. On the one-dimensional steady and unsteady porous flow equations. *Coastal Engineering*, (No. 24):p. 233–257, 1995.

H. Burcharth, Z. Liu, and P. Troch. Scaling of core material in rubble mound breakwater model tests. In *Proc. 5th COPEDEC*, pages 1518–1528, Cape Town(South Africa), 1999.

A. Dybbs and R. Edwards. *Fundamentals of Transport Phenomena in Porous Media*, chapter A new look at porous media fluid mechanics - Darcy to turbulent. Nijhoff Publishers, 1984.

P. Forchheimer. Wasserbewegung durch boden. *Zeitschrift des Vereines Deutscher Ingenieuer*, 45th edtition, 1901.

Y. Goda and Y. Suzuki. Estimation of incident and reflected waves in random wave experiments. In *Proceedings of the International Conference on Coastal Engeneering*, number 15, pages 828–845, Honolulu, Hawai, 1976.

Z. Gu and H. Wang. Gravity waves over porous bottoms. *Coastal Engineering*, 15:695–524, 1991.

R. Hudson. Wave forces on breakwaters. In *Proceedings-Separate ASCE*, number 113, pages 653–674.

S. Hughes. Physical models and laboratory techniques in coastal engineering. advanced series on ocean engineering. *Coastal Engineering*, 1993.

H. D. Jumelet. The influence of core permeability on armour layer stability. Master's thesis, Delft University of Technology, 2010.

G. H. Keulegan. Wave transmission through rock structures : hydraulic model investigation. Technical report, United States Army Corps of Engineers, Vicksburg, Missisipi, 1973.

R. Kik. The notional permeability of breakwaters: experimental research on the permeability factor p. Master's thesis, Delft University of Technology, 2011.

B. Klaasman. *Manual Matlab scripts Laboratory of Fluid Mechanics*. Delft University of Technology, 2005.

J. Kluwen. Physical model tests of the notional permeability on breakwaters. Master's thesis, Delft University of Technology, 2012.

B. Le Mehauté. Perméabilité des digues en enrochements aux ondes de gravité periodiques. *La Houille Blanche*, 1957.

B. Le Mehauté. *An Introduction to Hydrodynamics and Water Waves*. Springer, 1976.

O. Madsen and I. Warren. Performance of a numerical short-wave model. *Coastal Engineering*, 8:73–93, 1984.

O. Madsen and S. White. Reflection and transmission characteristics of porous rubble-mound breakwaters. Technical Report 76-5, U.S. Army Corps of Engineers, Coastal Engineering Research Center, Fort Belvoir, March 1976.

H. Oumeraci and H. Partenscky. Wave-induced pore pressures in rubble mound breakwaters. In *Proc. 22th International Conference on Coastal Engineering*, 1990.

O. Polubarinova-Kocina. *Theory of motion of ground water*. Gosudarstv. Izdat. Tehn.-Teor., Moscow, 1952. translated as Polubarinova-Kochina, P. Ya. (1962). Theory of ground water movement. Princeton, NJ: Princeton University Press.

G. Schiereck. *Introduction to Bed, Bank and Shoreline Protection*. VSSD, 2004.

D. Slauenwhite and B. Johnson. Bubble shattering: Differences in bubble formation in fresh water and seawater. *Journal of Geophysical Research*, 104, 1999.

G. Stelling and M. Zijlema. An accurate and efficient finite-difference algorithm for non-hydrostatic free-surface flow with application to wave propagation. *International Journal for Numerical Methods in Fluids*, 43:1–23, 2003.

M. Tirindelli and A. Lamberti. Wave action on rubble mound breakwaters: the problem of scale effects. Technical report, DELOS project, 2000.

P. Troch. *Experimentele studie en numerieke modellering van golfinteracitie met stort-steengolfbrekers*. PhD thesis, Gent: Dept. Civiele techniek, Ghent University, 2000.

P. van Broekhoven. The influence of armour layer and core permeability on the wave run-up. Master's thesis, Delft University of Technology, 2011.

J. Van der Meer. *Rock slopes and gravel beaches under wave attack*. PhD thesis, Delft University of technology, 1988.

M. Van Gent. Formulae to describe porous flow. Communications on Hydraulic and Geotechnical Engineering 92-2, Delft University of Technology, February 1992.

M. Van Gent. Stationary and oscillatory flow through course porous media. Communications on Hydraulic and Geotechnical Engineering 93-9, Delft University of Technology, June 1993.

M. Van Gent. Personal communication, 2012.

C. Vreugdenhil. *Numerical Methods for Shallow-Water Flow*. Kluwer Academic Publishers, Dordrecht, 1994.

W. Zeelenberg and M. Koote. The use of elastocoast in breakwater research. Technical report, Delft University of Technology, 2012.

M. Zijlema, G. Stelling, and P. Smit. Swash: An operational public domain code for simulating wave fields and rapidly varied flows in coastal waters. *Coastal Engineering*, 58:992–1012, 2011.